Master's thesis

2020

Henrik Nyholm

NTNU
Norwegian University of Science and Technology
Faculty of Information Technology and Electrical Engineering
Department of Electronic Systems

Henrik Nyholm

Localizing Sheep using a Bluetooth Low Energy enabled Unmanned Aerial Vehicle for Round-trip Time of Arrival-based Multilateriation

July 2020

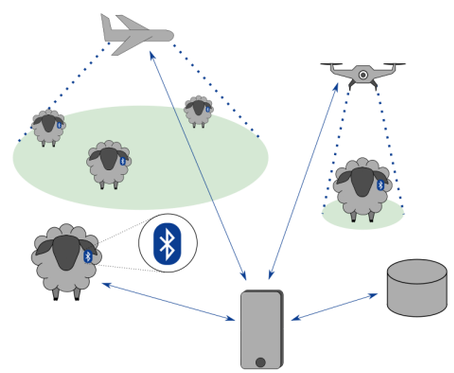

NTNU
Norwegian University of Science and Technology

NTNU
Norwegian University of Science and Technology

Abstract

Locating the position of free ranging sheep over wide geographical areas is a difficult endeavour that requires significant resources in terms of time and effort. However, this effort can be significantly reduced by using modern tracking and localization technology. A significant barrier for the wide adoption of such systems is that the cost of commercially available systems today is disproportionally high compared to the economic value of the sheep while requiring the deployment of expensive infrastructure.

In this thesis, a novel low-cost and power-efficient system for locating sheep using Bluetooth Low Energy (BLE) and an Unmanned Aerial Vehicle (UAV) is proposed. The solution consists of mounting small form factor BLE long range enabled ear tags on the sheep to perform round-trip time of arrival (ToA) measurements and estimate the distance between the location of the sheep and the UAV. Exploiting the movement of the UAV, the distance measurements are used to perform a relatively high precision multilateration-based localization technique. A less precise and more energy efficient localization scheme is also presented, where the inherent short range of BLE is used to perform proximity-based localization. Both methods eliminate the necessity of equipping each animal with a GPS receiver and requires no additional infrastructure – significantly reducing both energy consumption and costs for each ear tag.

A review of previously suggested animal tracking and localization solutions in in the literature was conducted. Herein, several wireless technology solutions and localization techniques were evaluated. The performance of the proposed system was assessed by conducting several field experiments. The accuracy of the implemented round-trip ToA scheme was compared to a received signal strength indicator (RSSI) distance estimation implementation. It was found that the ToA approach significantly outperformed the RSSI-based system, with achieving a root mean square error of approximately 6.5 m. It was concluded that the proposed round trip ToA implementation can reliably be used for a multilateration-based localization scheme. Finally, estimations of the expected battery lifetime of the ear tag was conducted, indicating that a single ear tag can remain operational for several years depending on the implementation.

Keywords: Radio Localization, Bluetooth Low Energy, Time of Arrival, Multilateration, Unmanned Aerial Vehicle, Animal Tracking

Sammendrag

Lokalisering av frittgående sau i vidstrakte kulturlandskap er en tidkrevende og vanskelig oppgave. Innsatsen som kreves kan imidlertid reduseres ved å ta i bruk moderne sporing- og lokaliseringsteknikker. Det største hinderet for utstrakt implementering av slike systemer i dag er den disproporsjonalt store kostnaden av kommersielt tilgjengelige løsninger sammenliknet med den økonomiske verdien av en sau, samt behovet for utbygging av kostbar infrastruktur.

Denne masteroppgaven legger frem et kostnads- og energieffektivt system for lokalisering av sau basert på bruk av Bluetooth Low Energy (BLE) og et ubemannet luftfartøy, også kalt drone. Den foreslåtte løsningen involverer å øremerke sauene med en lang-distanse BLE enhet, og gjennomføre round-trip time of arrival (ToA) målinger som så kan brukes til å estimere avstanden mellom sauene og dronen. Basert på dronens bevegelsesmønster kan sauens posisjon bestemmes med relativt høy presisjon ved hjelp av multilaterasjonsteknikk. En annen mindre presis men mer energieffektiv lokaliseringsmetode basert på BLEs korte rekkevidde og nærhetsbasert lokalisering er også presentert. Begge metodene eliminerer behovet for å utstyre hvert enkelt dyr med en kostbar GPS mottaker og krever ikke utbygging av omfattende infrastruktur, noe som reduserer både energibehovet og kostnaden til hvert enkelt øremerke betraktelig.

En litteraturstudie på tidligere foreslåtte løsninger for sporing og lokalisering av dyr er også inkludert sammen med en evaluering av en rekke trådløse teknologier og lokaliseringsteknikker. Ytelsen til det foreslåtte systemet ble evaluert på bakgrunn av en rekke felt eksperimenter. Nøyaktigheten av round-trip ToA målingene ble sammenliknet med en indikator på mottatt signal styrke (RSSI) basesert avstandsestimeringsteknikk. Det ble vist at ToA tilnærmingen med en kvadratisk gjennomsnittsfeil på omtrent 6.5 m utkonkurrerte det RSSI-baserte systemet. På bakgrunn av dette ble det konkludert med at round-drip ToA fint kan brukes til multilaterasjonsbasert lokalisering. En vurdering av forventet batterilevetid indikerte at et enkelt øremerke kan forbli operativt i opptil flere år avhengig av implementasjonens natur.

Preface

This Master's thesis is the result of work performed during the spring of 2020 in the final semester of a 5-year Master's degree program called Electronic Systems Design and Innovation in the course called TFE4580 at the Department of Electronic Systems, Faculty of Information Technology and Electrical Engineering, Norwegian University of Science and Technology (NTNU). The project is a result of a collaboration between the Department of Electronic Systems, the Department of Computer Science and Nordic Semiconductor ASA.

Associate Professor Egil Eide from the Department of Electronic Systems acted as the main supervisor for this project. The project was also co-supervised by Professor Svein-Olaf Hvasshovd from the Department of Computer Science and was the initiator and main stakeholder in the project. Torstein Heggebø and Carsten Wulff from Nordic Semiconductor acted as external co-supervisors.

The project was conducted in collaboration with fellow student Ole Alexander Hole from the Department of Computer Science. However, it was decided that separate contributions were to be presented in our respective master theses. This division of labour was mainly achieved by assigning Hole the task of managing the UAV, the GPS receiver and data storage while the author managed the radio and BLE specific tasks and the implementation of the source code for the different field investigations. Moreover, it was decided that Holes thesis should mainly focus on determining the feasibility of using a multilateration-based localization scheme given a certain accuracy or uncertainty of the distance measurements, while this thesis is mainly focused on determining the performance of the distance measurement schemes themselves.

The project was also conducted in collaboration with Jonathan Nilsen and Grzegorz Swidenski who worked as interns in a 20 % position at Nordic Semiconductor during the duration of the project. They were assigned the task of developing the round trip time of arrival scheme which is a continuation of work conducted by fellow student Martin Aalien, Department of Electronic Systems, during a course at NTNU in collaboration with Nordic Semiconductor.

Trondheim, 16.07.2020

Henrik Nyholm

Acknowledgements

The work this semester has been a challenging endeavour. As radio communication is not my main field of expertise, it has been both demanding and stimulating to undertake such a task. Despite several setbacks and dark days during the duration of the project, especially with the emergence of the COVID-19 pandemic, it was fulfilling to finally work on a larger project that ultimately could be useful in a real world application. I have learned much through the work of this project and it has made me more resilient to stress and handling setbacks.

With this, I would like to thank Egil Eide for helping me navigate the difficult world of radio systems. I would also like to thank Svein-Olaf Hvasshovd for advertising the project in the first place and his continuous excitement at each weekly status meeting while lending me his expertise concerning tracking and relocating of sheep. I would also like to thank Torstein Heggebø for following up on the project and enabling the collaboration between me, Nordic Semiconductor, Jonathan Nilsen and Grzegorz Swidenski while going out of his way to ensure that the necessary equipment was made available. I would also like to thank Carsten Wulff who gave feedback on the project and valuable advice. I would also like to thank Nordic Semiconductor for allowing me to work at their offices and borrow equipment. I would also like to thank Jonathan Nilsen and Grzegorz Swidenski for going the extra mile to ensure that the system could be tested in time. Sharing their expertise was an invaluable resource that was appreciated very much. I would also like to thank Martin Aalien for sharing his experience and source code from his previous work. Lastly, I would like to thank Ole Alexander Hole for sharing the pain of conducting field experiments and an overall fruitful collaboration.

On a more personal note, I would like to thank Herman Dieset for friendly discussions, suggestions and allowing be to vent my frustration when things did not work as expected. I would like to thank Pauline Hardeberg for reading through some of my chapters and correcting grammar. Last, but not least, I would like to thank my best friend and love of my life Nora Jansson for helping me through the difficult days such as when the drone crashed or nothing seemed to make sense. Moreover, I would like to thank her for helping me think through my experiments and results. Most importantly, I would like to thank her for the immense work she put into proofreading and improving this thesis.

Table of Contents

List of Figures xvii

List of Tables xxiii

List of Symbols xxv

List of Abbreviations xxvii

1 Introduction 1

1.1 Motivation 1

1.2 Contributions 2

1.3 Outline 3

2 Previous Work 5

2.1 Vision Based Solutions 5

2.2 Radio Based Solutions 6

2.2.1 Global Positioning System 6

2.2.2 Long-range Radio 7

2.2.3 Short-range Radio 11

2.2.4 Bluetooth Low Energy 15

2.3 UAV Data Collection 18

3 Localization Using BLE 19

3.1 Radio Fundamentals 19

3.1.1 Basic Principles . . . 19
3.1.2 Polarization . . . 22
3.1.3 Radio Propagation Models . . . 25
3.2 Radio Localization Techniques . . . 29
3.2.1 Triangulation . . . 29
3.2.2 Multilateration . . . 30
3.2.3 Proximity Based Localization . . . 35
3.2.4 Scene Analysis . . . 36
3.3 BLE Protocol Stack . . . 36
3.3.1 Controller Layers . . . 37
3.3.2 Host Layers . . . 41
3.4 UAV-Enabled BLE Localization . . . 43
3.4.1 Transmission Range . . . 43
3.4.2 UAV Search Pattern . . . 44
3.4.3 Advertising Interval . . . 46

4 System Architecture **49**

4.1 Wireless Communication Technology . . . 49
4.2 Localization Method . . . 50
4.3 System on Sheep . . . 54

5 Implementation **57**

5.1 Preliminary Investigation . . . 57
5.1.1 Methodology . . . 58
5.1.2 Results . . . 63
5.2 Aerial Investigation . . . 71

5.2.1 Methodology 72
5.2.2 Results 76
5.3 Round Trip Timing Accuracy 86
5.3.1 Methodology 86
5.3.2 Results 90
5.4 Multilateration Performance 93
5.4.1 Methodology 93
5.4.2 Results 96

6 Results and Discussion **103**
6.1 System Performance 103
6.2 Advertising Interval and Battery Lifetime 111

7 Conclusion **115**

8 Future Work **119**

References **121**

A Preliminary Investigation **129**

B Aerial Investigation **135**

C Multilateration **139**

List of Figures

2.1 Three models for a LoRa-based mesh network 10

3.1 Radiation pattern of an isotropic antenna 21
3.2 Radiation pattern of a monopole antenna 22
3.3 Decomposition of an E-field vector 23
3.4 Antenna polarization relative to the ground 23
3.5 Common EM-wave polarization states 24
3.6 Illustration of the Two-ray ground reflection model 27
3.7 The four fundamental radio positioning techniques 29
3.8 Triangulation with AoA measurement uncertainty 30
3.9 Illustration of a trilateration problem 31
3.10 Geometric Dilution of Precision principle 32
3.11 One way and round trip timing 34
3.12 Delay in round trip timing 34
3.13 Overview of the BLE protocol stack 37
3.14 Format of a BLE packet 38
3.15 Effective transmission range with UAV heights 44
3.16 Parallel search pattern considerations I 45
3.17 Parallel search pattern considerations II 45
3.18 Parallel search pattern considerations III 46

4.1 System on Sheep use-case. 54

5.1 nRF52840 Development Kit with highlighted antenna 58
5.2 Test set-up for the preliminary investigation 60
5.3 Topographic cross-section of preliminary investigation field (600 m) . 62
5.4 Topographic cross-section of preliminary investigation field (1 km) . 63
5.5 PDR per transmit power using LE PHY 64
5.6 PDR per transmit power using coded PHY 65
5.7 Performance of LE versus coded PHY 65
5.8 Current consumption of an LE PHY advertisement 66
5.9 Current consumption of a coded PHY advertisement 67
5.10 PDR for three different angles 67
5.11 PDR for the different heights 68
5.12 Boxplot of measured RSSI values 69
5.13 Distribution of RSSI values 69
5.14 Measured RSSI versus free space and log distance propagation models I 70
5.15 Measured RSSI versus free space and log distance propagation models II 71
5.16 Vertical versus horizontal polarization on a UAV 74
5.17 Illustration of peripheral orientations 75
5.18 PDR with horizontal polarization, best case orientation and LP receiver 77
5.19 PDR with vertical polarization, best case orientation and LP receiver 77
5.20 PDR with horizontal polarization, worst case orientation and LP receiver 78
5.21 PDR with vertical polarization, worst case orientation and LP receiver 78
5.22 RSSI with horizontal polarization, best case orientation and LP receiver 79

5.23 RSSI with horizontal polarization, worst case orientation and LP receiver . . . 79

5.24 PDR with horizontal polarization, best case orientation and CP receiver . . . 80

5.25 PDR with vertical polarization, best case orientation and CP receiver 80

5.26 PDR with horizontal polarization, worst case orientation and CP receiver . . . 80

5.27 PDR with vertical polarization, worst case orientation and CP receiver 81

5.28 PDR compared to the two ray ground reflection model I 81

5.29 PDR compared to the two ray ground reflection model II 82

5.30 PDR compared to the two ray ground reflection model III 82

5.31 Measured RSSI values compared to propagation models I 83

5.32 Measured RSSI values compared to propagation models II 83

5.33 Measured RSSI values compared to propagation models III 84

5.34 Measured RSSI values compared to propagation models IV 84

5.35 Measured RSSI values compared to propagation models V 85

5.36 PCB size of a vertically and horizontally polarized PCB antenna . . 86

5.37 Boxplot of the RTT error for different distances 91

5.38 Mean RTT error for for different numbers of RTT packets 91

5.39 Boxplot of the RTT error for different numbers of RTT packets . . . 92

5.40 RMS error for each test number using different statistical methods . 97

5.41 RMS error for several distance bins 98

5.42 Boxplot of the error for each test number 98

5.43 Sequence of errors for test number 3 99

5.44 Sequence of errors for test number 5 99

5.45 RMS error for RSSI-based distance measurements using different offsets 100

5.46 Multilateration using RSSI-based distance measurement 7 101
5.47 Multilateration using RTT-based distance measurement 7 102
5.48 Multilateration using RTT-based distance measurement 5 102

A.1 Photograph of the tripod test setup 129
A.2 Aerial photo of the initial investigation measurement field (600 m) . 130
A.3 Aerial photo of the initial investigation measurement field (1 km) . . 131
A.4 Photograph of initial investigation field 132
A.5 Measured RSSI versus free space and log distance propagation models132
A.6 Measured RSSI versus free space and log distance propagation models133
A.7 Measured RSSI versus free space and log distance propagation models133

B.1 Photograph of quadcopter drone 135
B.2 Photograph of the cloverleaf antenna 136
B.3 Photograph of cloverleaf antenna on the UAV. 137

C.1 Drone path in the multilateration investigation 140
C.2 Multilateration using RSSI-based distance measurement 6 141
C.3 Multilateration using RSSI-based distance measurement 2 142
C.4 Multilateration using RSSI-based distance measurement 3 143
C.5 Multilateration using RSSI-based distance measurement 4 144
C.6 Multilateration using RSSI-based distance measurement 5 145
C.7 Multilateration using RSSI-based distance measurement 6 146
C.8 Multilateration using RTT-based distance measurement 1 147
C.9 Multilateration using RTT-based distance measurement 2 148
C.10 Multilateration using RTT-based distance measurement 3 149
C.11 Multilateration using RTT-based distance measurement 4 150

C.12 Multilateration using RTT-based distance measurement 6 151

List of Tables

3.1 BLE advertising packet types. 39

5.1 Combinations of parameter values in the preliminary investigation . 61

5.2 Maximum theoretical transmission range using the nRF52840 DK. . 64

5.3 Combinations of parameter values in the aerial investigation 73

5.4 Combinations of parameter values in the round trip timing accuracy investigation. 87

5.5 Combinations of parameter values in the multilateration investigation. 94

5.6 Test set-up for the different multilateration tests. 95

6.1 Different advertising intervals depending on drone speed and parallel search pattern distance with a given effective transmission range. . . 111

6.2 Estimated battery lifetime of the ear tag using a 225 mAh coin cell battery and different advertising intervals. 113

List of Symbols

d	Distance.
λ	Wavelength of an electromagnetic wave.
G	Antenna gain.
G_t	Antenna gain of a receiving antenna.
G_r	Antenna gain of a receiving antenna.
$\vec{E}$	Vector describing an electric field.
$\vec{H}$	Vector describing a magnetic field.
ϕ	Relative rotational angle between two lineraly polarized antennas in radians.
P_t	Transmitted power of an antenna.
P_r	Received power of an antenna.
n	Path loss exponent.
$\overline{P_0}$	Average received power in the log-normal propagation model.
P_0	Received power at a short reference distance d_0.
d_0	A (short) reference distance for measuring P_0.
h_r	Height of a receiving antenna.
h_t	Height of a transmitting antenna.
θ	Angle of reflection given by h_t and h_r.
Γ	Ground reflection coefficient.
ϵ_r	Relative permittivity of the ground.
d_{los}	Distance traveled by a received signal in a LOS scenario.
d_{ref}	Distance traveled by a reflected signal in free space.
$\Delta\phi$	Phase difference between a LOS signal and a reflected signal.
G_{los}	Product of the antenna gain with a LOS ray.
G_{ref}	Product of the antenna gain with a reflected ray.
j	Imaginary or complex number unit, also known as i, where $j = \sqrt{-1}$.
f	Frequency.
MPT	Meters Per Tick, the maximum resolution of a round trip ToA measurement.
f_{clk}	Clock frequency of a timer.
c	Speed of ligth in air, approximatley equal to $299\,704\,645\,\mathrm{m/s}$.
T_{start}	Delay between starting a timer and transmitting an RTT packet.
T_{stop}	Delay between starting a timer and transmitting an RTT packet.

T_D	Dwell time, time delay between receiving an RTT packet and transmitting a response.
T_{tot}	Total measured time for a single RTT measurement.
T_J	Total hardware jitter in delay values when performing a RTT measurement in number of clock ticks.
N_r	Number of received data packets.
N_t	Number of transmitted data packets.
r_t	Transmission range/radius.
r_{eff}	The effective transmission range when projecting the LOS transmission range to a 2D surface given a height difference between the antenna.
Δh	Height difference between a transmitting antenna and receiving antenna.
d_s	Distance between the pararell lines in a paralell search pattern.
d_{wc}	Distance that a UAV can travel before leaving the transmission range of a peripheral in a worst case position relative to the UAV path
s_{uav}	Speed of a UAV.
T_{Amin}	Minimum advertising perioid.
T_{wc}	Advertising period with a worst case position of peripherals
V_{BC}	Vertically polarized antenna best case orientation.
H_{BC}	Horizontally polarized antenna best case orientation.
V_{WC}	Vertically polarized antenna worst case orientation.
H_{WC}	Horizontally polarized antenna worst case orientation.
N_{RTT}	Number of RTT packets used in a single distance measurement.
Δt	Time difference between a received GPS location and an RTT measurement beeing performed.

List of Abbreviations

AoA Angle of Arrival

AoI Age of Information

API Application Programming Interface

ATT Attribute Protocol

BLE Bluetooth Low Energy

Bluetooth SIG Bluetooth Special Interrest Group

CEP Circular Error Propability

CP Circular Polarization

CPU Central Processing Unit

CRC Cyclic Redudancy Check

DK Development Kit

DoA Direction of Arrival (synonymous with AoA)

EM Electromagnetic (wave)

FFT Fast Fourier Transform

FSM Finite State Machine

GAP Generic Access Profile

GATT Generic Attribute Profile

GDoP Geometric Dillution of Precision

GFSK Gaussian Frequency Shift Keying

GPS Global Positioning System

GSM Global System for Mobile Communications – 2G cellular network

HCI Host Controller Inferface

I2C Inter-Integrated Circuit – communication protocol

ID Identification

IoT Internet of Things

IR Infrared

ISM Industrial, Scientific and Medical radio band

L2CAP Logical Link Control and Adaption Protocol

LE Low Energy

LE PHY Low Energy Physical Layer

LED Light Emitting Diode

LHC Left-Hand-Circular (polarization sense)

LHS Left-Hand Side

LL Link Layer

LoRa Long Range – sub-gigahertz LPWAN radio technology

LoRaWAN Long Range Wide Area Network

LOS Line-of-sight

LP Linear Polarization

LPWAN Low Power Wide Area Network

LTE Long-Term Evolution

LTE-M LTE-MTC (Machine Type Communication)

MASL Meters Above Sea Level

NB-IoT Narrowband Internet of Things – a LPWAN radio technology

OS Operating System

PAN Personal Area Network

PCB Printed Circuit Board

PD Pseudo Doppler

PDR Packet Delivery Ratio

PDU Protocol Data Unit

PHY Physical Layer

PLF Polarization Loss Factor

PPK Power Profiling Kit

PPM Parts Per Million

R/W Read and Write

RAM Random-Access Memory

RC Resistor-Capacitor (circuit)

RDF Radio Direction Finding

RF Radio Frequency

RFID Radio Frequency Identification

RHC Right-Hand-Circular (polarization sense)

RHS Reft-Hand Side

RMS Root Mean Square

RP-SMA Reverse Polarity SubMiniature version A – coaxial RF connector

RSSI Received Signal Strength Indicator [dbm]

RTT Round Trip Time

SD Card Secure Digital Card – proprietary non-volatile memory card

SDK Software Development Kit

SDR Software Defined Radio

SIM Subscriber Identification Module (card)

SiP System-in-Package

SMA SubMiniature version A – coaxial RF connector

SMP Security Manager Protocol

SoC System-On-Chip

SoS System on Sheep

SPI Serial Peripheral Interface

TDoA Time Difference of Arrival

ToA Time of Arrival

ToF Time of Flight

ToT Time Of Transmission

UART Universal Asynchronous Receiver-Transmitter

UAV Unmanned Aerial Vehicle

UHF Ultra High Frequency – radio frequencies from 300 MHz to 3 GHz

URE User Range Error

USB Universal Serial Bus

VHF Very High Frequency – radio frequencies from 30 to 300 Mhz

WAN Wide Area Network

WPAN Wireless Personal Area Network

WSN Wireless Sensor Nodes/Network

YR Yagi Rotation – an RDF technique

1 Introduction

1.1 Motivation

The husbandry of free range grazing livestock have been part of the human endeavour for millennia [1]. An especially old tradition is the domestication of sheep for nutrition and other secondary resources. In some countries, like Norway, the rearing of sheep is often practiced by allowing the animals to graze freely in unfenced rangelands during the summer. However, a challenge with this practice is keeping track of their position, as sheep tend to travel in smaller flocks over large geographical areas. This poses as a significant problem when farmers set out to relocate their sheep in the fall. Even though most of the animals are easily found, a lot of tine and resources are spent locating the remaining 10% of the population [2]. This effort is not only carried out for economical reasons, but is more importantly an issue of animal welfare, as the sheep will suffer in the outdoors during the winter. Indeed, awareness regarding animal welfare in farming has steadily increased in the last decades and has consequently led to stronger legislation and increased pressure to optimize husbandry systems in domestic animal production [3]. Even the localization of deceased sheep is of economic interest in countries which subsidizes or compensates for predator attacks.

While the tracking of sheep is the main focus of this thesis, several other factors point to the necessity of a cost effective tracking system for animals in general. Many animal-borne diseases are transmitted via meat products [4]. Tracing the origins of such a disease back to the source animal may help to prevent similar outbreaks in the future. Indeed, observing the spatial and temporal interactions between wild and domestic animals is crucial for understanding how diseases are transferred among them [5]. This effort could be accomplished more easily with a less intrusive and cost effective animal tracking system [6]. Such a system could also aid biologists with understanding and protecting wildlife which are spread over vast areas or located in remote locations, while reducing invasiveness of animal habitats. This could also help combat poaching activities that are rapidly causing the extinction of several species today [7].

Tracking a large amount of animals necessitates the implementation of identification systems. Traditional livestock identification methods include ear tags, collars, branding or tattooing [6]. Tracking is traditionally accomplished by individuals who monitor and record the animals. However, such methods are labour intensive and prone to human recording error, while the identification systems are vulnerable to duplications, fading and fraud [8].

A modern solution to the ancient problem of tracking livestock is to utilize positioning technology such as GPS or other radio enabled mechanisms. However, equipping every animal with a module capable of both finding its geographical position and conveying this information to the farmer can be a challenge for several reasons. Such a module may be very expensive relative to the economic value of the animal, making the solution economically unfeasible. The module must also not hinder the animal by being too large or impractical, which could set restrictions on the battery life and might further drive up the manufacturing costs. While such expenses are sometimes justifiable with larger and more valuable livestock, such as reindeer, it is often not the case for smaller animals, such as sheep. For this reason, farmers only equip a fraction of the livestock with the implemented tracking technology, thus only partly solving the problem. Another challenge is the lack of infrastructure and coverage of wireless networks solutions in these uncultivated highland areas, making long distance communication with the farmers either difficult or expensive.

1.2 Contributions

This thesis include the following contributions:

- An exhaustive investigation of previous work with animal tracking and localization, both in literature and some excising commercial solutions, is presented and evaluated.
- Proposal of a novel cost-effective bluetooth low energy (BLE) and unmanned aerial vehicle (UAV) based localization system, intended for finding the geographical location of sheep. The system uses two localization schemes. The first scheme is a simple proximity based solution, which can be used for coarse localization and is very cheap in terms of ear tag energy consumption. The second scheme is a multilateration solution where distances are measured using round-trip time of arrival (ToA), which can be used for precision localization at the cost of larger ear tag energy consumption.
- Several field experiments were conducted where the possible transmission range of both the normal and long range BLE mode were investigated with different transmission parameters.
- The effects of antenna directivity and polarization mismatch on both the transmission range and packet delivery ratio (PDR) of the system were investigated, where the effect of using a linearly and circularly polarized antenna was examined.
- The accuracy and performance of the round-trip ToA distance measurements scheme was tested and evaluated against a received signal strength indicator (RSSI) distance measurement approach.

- An estimation of the expected battery lifetime of the ear tags was conducted.
- Finally, it is shown that a round-trip ToA distance measurement scheme can reliably be used for multilateration localization using a UAV and BLE, although an exact estimation of the accuracy is considered out of scope for this thesis.

1.3 Outline

Chapter 2 presents previous work of animal tracking solutions proposed in the literature. Here, both visual and radio based solutions are explored and discussed in terms of accuracy and cost in Section 2.1 and 2.2. For radio based solutions, both long- and short-range radio implementations are evaluated and some commercially available solutions for sheep tracking is presented. Finally, a motivation for using a UAV-assisted BLE-based system for tracking sheep along with a short introduction to recent advancements in UAV-based data collection system is presented.

Chapter 3 presents the necessary background theory for understanding the proposed solution, the conducted experiments and their results. This is accomplished by introducing fundamental radio communication principles in Section 3.1 and the four principal radio-based localization techniques in Section 3.2. Moreover, a short introduction to the BLE protocol stack is presented in Section 3.3 while a few considerations related to a UAV-enabled BLE localization scheme is finally presented in Section 3.4.

Chapter 4 presents the system architecture of the proposed solution. Here, a discussion and motivation of which wireless communication technology should be deployed is provided in Section 4.1. Section 4.2 discusses and provides a motivation for the radio localization techniques used in the system. Finally, a complete overview of the proposed system is provided with an envisioned typical use-case.

Chapter 5 presents how the proposed system was implemented and evaluated by conducting several field experiments and investigations. Each section presents both methodology and results of the four main experiments conducted. As methodology of subsequent experiments are affected by the results of the prior investigation, the results are also discussed as they are presented. Section 5.1 presents a preliminary investigation that mainly evaluated the performance of the normal and long range BLE modes on the ground. Section 5.2 presents an aerial investigation where the effective transmission range of the system when using a UAV is established. Section 5.3 presents an investigation into the accuracy of using round-trip ToA measurements to estimate the distance between two devices. Finally, the performance of using both a round-trip ToA and RSSI-based scheme for distance measurements in a multilateration localization scheme is evaluated and compared in Section 5.4.

Chapter 6 provides a summary of the results and discusses limitations with the implementation and the overall performance of the proposed system. An estimation of the expected battery lifetime of the ear tags is also provided. Chapter 7 presents the conclusion of the thesis while future work is discussed in Chapter 8.

2 Previous Work

This chapter presents and evaluates previous work of animal tracking and localization solutions proposed in the literature and some commercially available solutions. Modern animal tracking solutions can be broadly categorized into vision and radio based systems and is presented in Section 2.1 and 2.2 respectively. Finally, a short overview of recent advancements in UAV data collection schemes is presented in Section 2.3.

2.1 Vision Based Solutions

While radio based tracking solutions have been proposed since the early 1960s [9], several vision based solutions have been proposed more recently.

In [7], an autonomous camera-based aerial system for tracking wildlife is presented. Here, the proposed system autonomously tracks animals as well as poachers using a visual algorithm. However, the authors note that significant animal appearance changes, variation in illumination, partial animal occlusion in terrain, blur motion, rapid pose variation, cluttered background environments and onboard mechanical vibration from the UAV, are significant challenges that must be addressed and overcome in such systems. There is also a tradeoff between using a high camera resolution with high zooming levels, affecting the maximum altitude of the UAV and tracking accuracy, and the onboard energy consumption stemming from heavy payloads or an increase in required computational power due to more advanced hardware.

Other visual approaches include using infrared (IR) sensors, either active or thermal. In [10], a UAV equipped with a low cost thermal camera identified the heat signature of a target animal from a predetermined height. The UAV could then follow the animal in real-time. However, the system required low UAV altitudes of approximately 10 m and could only track a single animal. Requiring low UAV altitudes for a tracking system could potentially agitate or scare the animals [3].

In [11], a UAV equipped with a miniaturized thermal camera was used to prerecord footage of wildlife of altitudes up to 60 m, where an artificial intelligence algorithm was used to classify and count different species in post-processing. While an impressive feat, this approach, in addition to other IR sensor-based implementations, has several limitations. IR-based sensors are sensitive to environmental temperature and become less reliable when used outdoors, especially during day-time in the

summer [12]. In addition to requiring full or partial line of sight (LOS) to properly track animals, the greatest drawback for vision based systems is the inability to differentiate between individual animals based on appearance alone [13].

Kim *et al.* [14] proposed an system for tracking multiple animals with a single thermal sensor as part of an intelligent livestock breeding applications. Similar colors and shapes between animals often lead to the failure when tracking multiple objects, while the background further clutters and complicates the problem. Here, the authors propose a novel method that separate the foreground (i.e animals) from the background by using a simple threshold in a thermal frame as a topographic surface, to more easily find the boundary of each object, even when overlapping. From here, an efficient refinement scheme was applied to consistently find the center position of each animal, despite abrupt motion of the animals. Experiments show promising and robust results for tracking animals, compared to previous solutions proposed in the literature. Even though this solution was proposed for tracking livestock kept indoors, it is possible that this scheme can be further applied to a drone or UAV equipped with a thermal sensor, to track animals outdoors over large areas. However, the thermal sensor used in their research would likely not be effective at higher altitudes.

In conclusion, vision based UAV tracking systems have the potential to become an effective and non-intrusive solution, either by itself or as part of a larger radio based system. However, the current underlying technology is either too expensive in terms of power and economic cost, or too inaccurate for tracking multiple animals over large areas.

2.2 Radio Based Solutions

Several radio based solutions for tracking animals have been proposed or are already commercially available. The most popular solutions include using the global positioning system (GPS), very high frequency (VHF) radio telemetry, radio-frequency identification (RFID) tags or long-range radio such as cellular, satellite or the emerging sub-GHz standards. Some solutions utilize a combination of these alternatives.

2.2.1 Global Positioning System

The most obvious approach for tracking animals is to utilize the global positioning system or GPS. GPS is a tried and tested technology that is widely used for localization and tracking in many applications. GPS provides geolocation and time information to a GPS receiver by using 24 satellites that continuously broadcast a signal down to earth [15]. Whenever four or more satellites are within the LOS

of a GPS receiver, a geolocation and time measurement can be performed. The receiver accomplishes this conceptually by measuring the time of arrival (ToA) of the incoming signals according to its own clock, while recording the precise and calibrated time of transmission (ToT) included in each satellite signal. These values are in turn used to calculate the time of flight (ToF) for each signal, which can be further converted to a distance that closely corresponds to each satellite-receiver distance. Finally, the receiver calculates an estimated three-dimensional geolocation and timestamp based on the computed ToF values using a technique called multilateration.

The accuracy of GPS is generally considered high, with a committed global average user range error (URE) of $\leq$7.8 m with 95 % probability [16]. However, this accuracy can vary widely depending on satellite geometry and local factors such as signal blockage, multipath propagation, atmospheric conditions and receiver design and quality. While some precise systems achieve an accuracy within 30 cm under open sky [17], a typical GPS-enabled smartphone is generally accurate within 5 m in the same conditions. Moreover, the GPS accuracy tends to deteriorate in areas with obstacles such as trees and mountains in landscape settings, or buildings in urban environments. This is often due to the obstacles blocking the relatively weak GPS signals or causing multipath propagation (changing the ToA measurements and distorting ToT calculations). Despite this, GPS can generally be considered more than adequate when used in the context of livestock tracking.

There are generally two types of GPS technologies available for animal monitoring: passive and real-time [18]. Passive GPS tracking consists of either equipping or implanting an animal with a GPS receiver, which then proceeds to record the position and time-stamp of the animal at certain intervals. To retrieve this historical data, the animal must first be located by other means, where the device is typically removed for analysis. This implementation has traditionally been deployed to monitor wildlife in research situations, but is not useful for locating the current position of the animal. Real-time GPS tracking similarly consists of equipping or implanting a GPS receiver on the animal. However, as the name suggests, instead of logging the positions for later retrieval, the data is transmitted in real-time using another radio technology. This solution is the most common implementation used for tracking livestock over wide areas today [19].

2.2.2 Long-range Radio

Several real-time GPS tracking solutions utilize long-range radio technologies to periodically transmit the current position and other sensor data of the animal being monitored. Long-range radio has the obvious advantage of greater coverage compared to short-range radio solutions. While utilizing the existing infrastructure for cellular networks (like 2G, 3G and 4G) seems promising at first glance, the coverage is often not sufficient for real-time tracking in rangelands or pastures with

existing infrastructure in many countries. Such implementations might also require expensive subscription models. Moreover, the standard cellular network technologies prioritize high data rates over low power consumption [20]. While this is a reasonable approach to enable high resolution video streaming for instance, the radio design requirements for animal tracking applications are often reversed. This is because such applications generally transmit small data packets fairly infrequently since prolonging the battery life is crucial to drive down economic costs.

An alternative is to utilize the emerging low power wide area network (LPWAN) wireless technologies. LPWAN has seen a massive increase in popularity in recent years, driven by the requirements of several new IoT applications [20]. It generally provides long-range communication of up to 10-40 km in rural areas and is additionally highly energy efficient and inexpensive, with the tradeoff of low data-rates. Several LPWAN standards have been developed, both in the licensed and unlicensed frequency bandwidth, where Sigfox, LoRa and NB-IoT has gained the most traction. While a comprehensive comparison between different LPWAN technologies is considered out of scope for this thesis, a short summary of the main differences is given in the following paragraph, based on this excellent comparative study by Mekki *et al.* [20].

The development of both Sigfox and LoRa started around the same time frame, at the beginning of the last decade, where a standardized communication protocol based on LoRa technology called LoRaWAN was introduced in 2015. NB-IoT is the youngest of the three with specifications published in 2016. As the name suggest, it is based on utilizing narrow band radio technology. Both Sigfox and LoRa utilize the unlicensed sub-GHz ISM bands, whereas NB-IoT uses the licensed LTE frequency bands. This makes the latter more susceptible to interference compared to the two former. Neither Sigfox nor NB-IoT allows for establishing private networks and require fees to utilize them. This gives LoRaWAN an advantage in terms of early adoptability, while the others might eventually reach better coverage due to the economic interest related to developing the infrastructure. Sigfox can generally be seen as a more lightweight LPWAN, with significantly lower bandwidth, data rates and maximum payload size with the advantage of longer range compared to the others. Sigfox additionally enforces a fixed maximum messages per day. Finally, LoRaWAN seems to be the middle ground in terms of capabilities, where NB-IoT generally has higher performance – with the tradeoff of lower ranges (up to 10 km) in rural areas and overall higher energy consumption.

Several commercial solutions for long-range radio enabled GPS trackers exist or are in development today. The Finnish startup Anicare has developed an autonomous IoT-enabled herding livestock management solution called the *Healtag*, which is mainly intended for reindeer [21, 22]. The small form-factor device contains an onboard GPS and uses NB-IoT to wirelessly convey the activity of a herding animal, using an accelerometer and thermal sensor, once every hour. The Healtag reportedly has a battery lifetime of up to 5 years, while only weighing 25 g and can be mounted as an ear tag. These impressive features are made possible in part by uti-

lizing the nRF9160 System-in-Package (SiP) LTE-M/NB-IoT cellular IoT module from Nordic Semiconductor, reducing cost and size. According to Anicare themselves, the latest NB-IoT technology deployed throughout Northern Europe ensures sufficient cellular coverage even in areas with no 2G cellphone coverage [22]. The product is not yet commercially available, but ongoing testing seems promising for NB-IoT utilization for animal farming in general [23]. However, while using a dedicated GPS and long-range radio on each reindeer is probably economically feasible, it is likely not the case for sheep, since the worth of each animal is significantly smaller.

Other tracking solutions for sheep in particular are also available from some Norwegian companies. *Shiip*, developed by Nortrace [24], *Radiobjella* from Telespor [25] and *E-bjella* from FindMy [26] are some of the alternatives. Shiip uses an onboard GPS to transmit positional and other sensor data via NB-IoT. The device is equipped with a thermal sensor, battery surveillance and death alarm. The interval between updates can range between 1 and 24 hours, which in turn results in an estimated battery lifetime of 1.5 to 17 years respectively [27]. These features do, however, require the device to be mounted as a collar, as opposed to an ear tag, with its rather large form factor and weight of 140 g. The currently listed price is also rather large relative to the economic worth of a single sheep, while also requiring yearly licensing fees to utilize the NB-IoT infrastructure. As a result, it would be economically unfeasible to equip each sheep in the herd with a tracker. According to [2], there are also limitations with the NB-IoT coverage in several important locations for sheep farming in Norway – requiring further development of the NB-IoT infrastructure in order to become viable.

Radiobjella is a very similar device equipped with an onboard GPS, motion sensor and also utilizes LTE-M/NB-IoT for long-range communication. It also features a Bluetooth radio for direct communication with the device in the terrain. However, with a comparable weight, form factor, battery lifetime and price point to Shiip, the same drawbacks as mentioned above apply for this system.

E-bjella is yet another similar collar device with GPS, sensors and Bluetooth communication. The Bluetooth radio is used to communicate directly with smartphones in range. However, the main means of transmitting the sensor data is by using satellite communication instead of NB-IoT technology. This results in superior wireless coverage, compared to the other solutions mentioned, but at the cost of lower battery lifetime (2–3 seasons depending on communication intervals) and a steep increase in price. Thus, the viable ratio of tracked and untracked sheep is comparatively lower. The need for a simpler and more cost effective system for localizing sheep is evident.

While the above solutions utilize real-time GPS tracking, as opposed to a static solution, a hybrid between the two is also possible. Panicker *et al.* [19] proposed a novel design of a mesh network formed by LoRa based animal collars or tags for both conveying positional information using GPS and other sensor data over

very wide areas. The authors point out that the inherent one-hop star topology of conventional LoRa networks might be a weakness in an animal tracking applications over large areas with uneven terrain and obstacles such as trees. The resulting data loss and low coverage can be mitigated by installing several LoRaWAN gateways in the area, but could prove to be economically unfeasible in many situations. Instead, the authors propose three different mesh network models, which could be implemented depending on factors such as the geographic area under consideration, the migration and movement patterns of the animals in question and their density or spread. An illustration of the three models is provided in Figure 2.1.

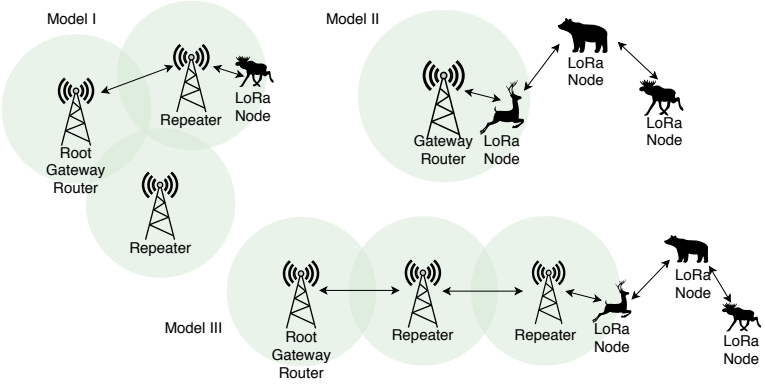

Figure 2.1: Three different models to increase LoRa coverage using a mesh network of LoRa nodes and/or LoRa repeaters. The figure is recreated from [19].

The first model is a mesh network that uses multiple LoRa gateways. Here, only a single 'root' gateway will have an active network connection while other cost effective gateways will be strategically placed in order to have overlapping coverage and act as repeaters. As long as the animal is within the coverage of one gateway, the data will eventually arrive to the root gateway. The second model is based on a mesh network using LoRa nodes. Here, the animals themselves will act as an intermediate gateway and relay data until one such node is within the coverage of a single gateway. To avoid broken links, stationary LoRa 'ghost' nodes could be deployed in strategic areas. The final model is a combination of the two solutions, by using a mesh network consisting of both LoRa nodes and multiple LoRa gateway routers. The models were implemented and tested in a laboratory environment, which yielded positive results. However, the authors conclude that further empirical evaluation is necessary to determine the PDR for each region in several geomorphological situations.

In conclusion, using real-time GPS tracking enabled by the recent development of LPWAN technology has proven to be a valid approach for tracking animals in general. While the current infrastructure of popular LPWAN technologies is still lacking, several countries are currently rolling out the technology as it is developed and improved upon. Despite this, a significant issue still persists: equipping every

single animal with a GPS receiver is rather costly, both economically and in terms of energy consumption [6, 28, 29]. Indeed, alternative solutions may prove this expenditure unnecessary altogether.

2.2.3 Short-range Radio

Typical short-range radio implementations for animal tracking include using very high frequency (VHF) and RFID [8] tags. These implementations are, however, traditionally concerned with tracking animals in smaller areas where installing the required infrastructure might be more feasible. Other solutions are often based on mobile handheld receivers. Some suggestions also include using radios in the 2.4 GHz ISM band. Amongst these, ZigBee has been proposed as a possible alternative.

Bhavsar and Arolkar [30] proposed a ZigBee based network architecture for animal health monitoring. The main focus of the research was to reduce power consumption of each node in a Wireless Sensor Network (WSN). To achieve this, the model was separated into two levels; a local level and a central level. At the local level, a personal area network (PAN) coordinator establish a PAN network for ZigBee enabled sensors in the immediate area. Several PAN coordinators can then be connected to a wireless router at the central level. Several routers are then placed such that an overlapping coverage is assured. In this way, the routers can relay the data to other routers, before eventually reaching a local database that also acts as a gateway to the Internet. The short range of ZigBee would effectively allow for omitting a GPS receiver, because the location of the stationary PAN coordinators is already known. Experiments in rural areas show the feasibility of such a system, where nodes had an estimated battery lifetime of several years. However, the scheme also inadvertently demonstrates the unsuitability of applying such a system in larger, less populated areas with less infrastructure, such as rangelands, given the density of PAN coordinators and routers required due to the inherent short range of ZigBee.

Scheepers *et al.* [31] designed a low-power cost-effective solar panel powered device for wireless livestock tracking called AnTrack. The AnTrack is a self-sustainable collar based design with watertight flexible solar panels mounted on top of the collar. The device can either run directly on power from the solar panels or the rechargeable batteries in the device. AnTrack uses GPS to record its position with an adjustable interval and automatically transmits the logged positional data whenever the device is within range. Two alternative wireless technologies were proposed to accomplish this data transfer. The first was using GSM which would enable using existing infrastructure with better coverage and long-range communication, but would require a SIM card to operate. Moreover, this solution would likely require a reduction in data transfer intervals to avoid increasing the size of either the battery or the solar panel.

The other proposed alternative was to use an ultra-low current 2.4 GHz RF transceiver with a reported range of 1.1 km in a LOS situation. This implementation would allow the device to almost solely operate on the solar panel power directly, except at at night, with the drawback of requiring several base stations to receive the data. Through calculations, the authors proved that this solution would be self-sufficient for both radio technologies, even in scenarios without sunshine for an entire week – if the transmission intervals are adjusted properly (every 15 minutes for the 2.4 GHz RF transceiver and every hour for the GSM radio). The authors concluded that several real-world experiments are necessary to evaluate the performance of the system. However, this seems like a promising solution for prolonging the battery lifetime of such systems. Although not suggested by by the authors, the use of a UAV might help to eliminate the necessity for 2.4 GHz base-stations and thus reducing the overall cost of such an implementation. Despite this, components such as flexible solar panels and the GPS receiver module would likely still be too costly tracking less valuable animals such as sheep.

Recent advancements in wireless communication have resulted in the emergence of small, low-cost, low-power and multifunctional sensor nodes [32]. A wireless sensor network (WSN) is formed by deploying a large amount of sensor nodes to collect data that can relay this information wirelessly as a service for a specific application [33]. WSN are often used in cases where remote monitoring is required [34] and traditionally use stationary sensor nodes. However, in applications such as animal tracking, the nodes could also be mobile. There are several implementations of WSN-based monitoring and tracking applications, however many of these systems rely on GPS for localization and RFID for identification purposes. This results in not only more expensive, but also highly complex systems [6].

Molapo *et al.* [6] designed a real-time livestock tracking system with an integration of sensors and beacon navigation. The WSN-based system consists of tags, beacons and base station nodes, which communicate wirelessly with each other. Tag nodes receive location data from nearby beacon nodes and uses trilateration to determine the location of a specific animal. A round trip time of arrival (glstoa) scheme was implemented after considering several localization techniques such as received signal strength indicator (RSSI) based measurements, angle of arrival (AoA) and time based measurements like time of arrival (ToA) and time differences of arrival (TDoA).

The base station received the estimated positional data in addition to an activity status, determined by motion sensors on the tags, from each animal. This data is in turn uploaded to a web-service in real-time, accessed by an Android interface. The authors chose to use a 2.4 GHz radio, which was able to successfully communicate at distances up to 500 m with a data rate of 2 Mb/s in a LOS situation. A prototype was designed and tested where the maximum error, for tests performed at 1, 3 and 6 meters, was found to be 3.5 m. The implementation of the system seems to indicate that using round trip AoA and trilateration with a 2.4 GHz radio could be a valid approach for tracking livestock. However, the necessity for stationary

beacons to perform the trilateration might prove too costly over larger areas such as unfenced rangelands.

The most common solution for short-range radio animal tracking is using very high frequency (VHF) radio [28]. VHF is simply defined as all radio frequencies ranging from 10 MHz to 300 MHz [35]. Such systems are often implemented by attaching transmitters to wildlife, where large mobile handheld VHF antennas are used in the field to track the animals [13, 6, 28]. Using triangulation techniques with at least two handheld devices, the position of the animal can be found. However, this approach is error prone and impractical for tracking multiple animals simultaneously. While having the advantage of tracking animals that are hidden to the naked eye, the inherent short range of the technology makes such systems very labour intensive and thus costly. Other alternatives include installing permanent infrastructure. Several solutions to mitigate this problem have been recently suggested in the literature.

Rerucha *et al.* [36] designed a miniaturized GPS position logger for tracking very small animals. The main constraint of the design was that the device could not exceed a total weight of 10 g and should additionally have a small form factor such that its presence minimally interfered with animal movements. This was achieved by using a very small and efficient GPS module, VHF transmission capabilities and a small coin cell battery, limiting the battery lifetime to three days. The tracker periodically logs the GPS position at specified time periods. Whenever the tracker receives an impulse from a directional Yagi-type VHF antenna, a data transfer of the recorded positions were initiated, a mechanism denoted as radio triggering. A somewhat successful field test was conducted on bats, where slightly less than 50 % of the deployed trackers yielded usable data of recorded positions. The radio triggering was reportedly observed to work correctly within 25 m with obstacles in the LOS, with an error rate of 0.6 %. Such an implementation show that a combination of a passive and real-time GPS tracking solution with short-range radio could be utilized for tracking very small animals, however the small area covered, short battery life and range indicates that such a solution would not be viable for tracking livestock such as sheep.

Several solutions proposed in the literature aim to automate the animal tracking process, while removing the costly infrastructure requirements. By using an unmanned aerial vehicle (UAV) or drone, the tracking can be performed using short-range radio, where only the UAV itself needs an onboard GPS.

Kaneda and Meada [37] proposed a drone based position measuring system, designed for tracking Tsushima Leopard Cats – a small cat species native to south and East Asia. The scheme involved attaching a small 142.9 MHz oscillator to the animal and equipping a drone with a radio receiver that measures the amplitude (i.e. RSSI) of the radio wave from the oscillator. The drone was then used to scan an area while continuously measuring the amplitude of the received radio signal. Whenever the average amplitude of the received signal becomes large, the authors

conclude that the drone approaches the oscillator and the position of the animal is close to the current position of the drone, measured by using an onboard GPS. The authors did not address the battery lifetime of such an implementation nor situations with the presence of multiple animals in the immediate area. The authors further conclude that the relationship between drone altitude, drone position and magnitude of the received signal must be clarified in future experiments.

Muller*et al.* [38] designed a system for aerial VHF tracking of wildlife using a UAV. By using a multi-channel VHF receiver, the UAV could track multiple animals fitted with VHF transmitters at once. The system was employed and tested to locate the cryptic nests of yellow-eyed penguins, which is traditionally a difficult and time consuming task. The system allowed for faster nest location compared to other methods such as camera fitted UAVs, with a higher cumulative success (number of nests found each day) and a quantified lower search effort required. The authors conclude that aerial VHF tracking can greatly extend the search range and minimize search efforts compared to ground VHF tracking or manual searching.

Nguyen *et al.* [13] designed an autonomous UAV for real-time localization and tracking of multiple radio tagged animals, using VHF radio technology with a custom Yagi antenna and multiple channels. Both a logarithmic distance path loss model (LogPath) and a logarithmic distance path loss model with multi-path fading (MultiPath) model were tested for RSSI based range estimations. The authors additionally modeled the RSSI noise as white Gaussian noise and estimated the likelihood of a measurement value given the true distance of the tag and UAV. Field experiments show that the MultiPath model was more accurate and confirmed the impact of ground reflections, especially close to the signal source. Four autonomous field missions were performed with two mobile and three stationary tags, where an average RMS error of 20 m from the true distance was achieved. The testing was performed over a range of 10 m to 320 m. The focus was seemingly concentrated on improving drone performance in terms of weight and energy budget, rather than ear tag characteristics. Thus, no information of the battery lifetime of the tags was reported.

Karki [39] designed a cost effective Radio Direction Finding (RDF) system, using a Pseudo Doppler (PD) mechanism, in his master thesis. Instead of requiring physical rotation of the receiving antenna, as with traditional doppler implementations, PD employs a grid of electrically isolated VHF monopole antennas, which are sampled sequentially to mimic the physical rotation. The PD mechanism was used to estimate the angle of arrival (AoA) of incoming radio signals by either using FFT or statistical methods, yielding an estimated AoA within 10 degrees of the ground truth. It was observed that the PD RDF yielded more accurate results in addition to higher resolution for small array sizes, when compared to another directional Yagi antenna of the same size. The author also concluded that deploying the PD RDF could be beneficial for UAV-based animal tracking. However, this was not pursued further.

VonEhr *et al.* [40] proposed two approaches for direction finding in wildlife tracking using UAV and VHF. The two approaches are Pseudo Doppler (PD) and Yagi Rotation (YR), where each method corresponds to a common Radio Direction-Finding (RDF) technique. The YR technique was successfully implemented and tested. It was found to have an accuracy of $\pm 20°$, however the maximum range of the system was not found. The PD design was not implemented due to limitations with the software designed radio (SDR) hardware. However, the authors note that such a system would allow researchers to implement dynamic UAV search patterns and advanced tracking functionality.

Bayram *et al.* [28] proposed an aerial radio-based telemetry system for tracking wildlife. Here, the movement of one or several UAVs is used, with a directional Yagi antenna on the UAV and VHF collars on the animals, to obtain a bearing measurement. Several bearing measurements were then merged to form intersecting wedges in order to estimate the position of the animal. The uncertainty of the localization was then quantified by the area of the resulting intersection, where the goal is to reduce the uncertainty below a threshold – minimizing the time it takes to localize an animal. Field experiments showed promising results with the UAV being able to determine the location of the VHF tag in a 5 hectare area in 13 minutes, with an uncertainty threshold of $315\,\mathrm{m}^2$ (approximately equal to a circle with a radius of 10 m). Again, the focus was mainly concentrated on improving the battery lifetime of the UAV and not on the collars themselves.

In conclusion, many exciting UAV enabled tracking systems using short-range wireless communication have recently emerged in the literature. Preliminary results seem to indicate a promising future for such systems. However, it is worth asking whether using the predominant radio technology solutions like RFID and VHF is the best approach going forward, or if an alternative technology could prove more suitable.

2.2.4 Bluetooth Low Energy

Bluetooth Low Energy (Bluetooth LE or BLE) is a wireless personal area network (WPAN) technology which is designed and maintained by the Bluetooth Special Interest Group (Bluetooth SIG). It was introduced in 2010 as part of the Bluetooth 4.0 Core Specification [41], and shares some similar traits with classic Bluetooth. However, classic Bluetooth and similar wireless standards are sometimes criticized for being an overly broad wireless solution that attempt to solve too many problems with opposing interests –leading to certain undesirable compromises. Thus, BLE should not be considered a smaller and highly optimized subset of classic Bluetooth, but rather a similar technology with an entirely different design goal. This design objective was solely focused on creating a wireless standard with the lowest possible power consumption while optimizing for low cost, low bandwidth, low power and low complexity [41]. Furthermore, BLE was designed to act as an

extensible framework for data exchange, rather than specific use-cases as was the case with classic Bluetooth. As a result of this effort, BLE can be considered the first widely adopted true low power wireless technology that can be utilized by applications running on a small coin cell battery for an extended amount of time.

Despite this, there are certainly other low power wireless protocols with similar capabilities, like Zigbee and Z-wave. What makes BLE different is its uncommonly rapid adoption rate compared to other wireless standards in their respective release cycles. Townsend *et al.* [41] attribute this massive growth to the early adoption of BLE by leading smartphone and tablet manufacturers, as the mobile computing market experienced an even larger growth in the same time frame. As a result, the technology became a popular choice for low power embedded devices that could now easily communicate with already owned smartphones.

Indeed, according to the annual Bluetooth Market Update, released by Bluetooth SIG, BLE has become the new market standard for low power wireless communication [42]. The Market Update reports that approximately 3.5 billion dual mode (supporting both Bluetooth classic and BLE) and single mode (BLE only) devices combined, were shipped in 2019 alone. It also suggests a trend in the market where classic Bluetooth devices are replaced with dual mode devices, while the number of annual single mode devices continues to increase. In fact, it is estimated that 7.5 billion single mode devices will be shipped in the period of 2020 to 2024 [42]. This large volume of annual shipped BLE devices has lead to fierce competition between manufacturers, which has rapidly matured the technology and pressed down costs and margins, further increasing its popularity in a positive feedback loop.

Another benefit of using BLE is the availability of cheap System on Chips (SoC) that combine the BLE functionality with microprocessors on a single embedded chip. These SoCs often come with APIs that enable easy development of applications without requiring deep knowledge of the underlying technology. The relatively easy-to-understand data model and lean protocol stack, combined with no licencing cost or fees to access the core specification, results in a low barrier for adoption for developers [41]. This is also the case for users as their smartphone often can act as an interface to BLE devices.

Despite of all these advantages, there are some key limitations to the technology. As BLE aims to be a truly low power wireless protocol, the data throughput is rather limited. However, in many applications (such as UAV assisted animal tracking for instance), only infrequent transmission of small data packets are required. Another limitation is the inherent short transmission range of the protocol. With typical operating ranges of 2 m to 5 m, which can reliably be extended to 30 m in a LOS situation by increasing the transmit power and thus power consumption, the protocol does not seem suited for animal tracking. Indeed, the same range disadvantages outlined for ZigBee in Section 2.2.3 seemingly apply to BLE as well. However, with the emerging Bluetooth long range modes introduced in the Bluetooth 5 core specification, this limitation could be mitigated. A more in depth

introduction to these modes and the BLE protocol in general is presented in Section 3.3. However, in short, it has the potential to match traditional VHF tag implementations in terms of range.

Another limitation of using BLE in general is its use of the unlicensed 2.4 GHz ISM band. Although this is beneficial in terms of requiring no licencing fees, in many areas, the frequency band is highly populated with other BLE, Bluetooth, Wi-Fi and ZigBee devices, leading to interference and congestions in some cases. In contrast, many countries offer several unlicensed bands in the VHF domain, which is generally much less populated. Despite this, when deployed in the context of tracking sheep in mainly unpopulated rangelands, this should not pose as a significant problem. Finally, compared to VHF, BLE and other UHF enabled technologies generally use smaller antennas, allowing for smaller form factor tracking devices.

In conclusion, it might prove beneficial to exploit the inherent low cost and low power of todays BLE SoCs, in addition to the potentially small antenna sizes of BLE, to create an efficient and small form factor ear tag for tracking sheep. By using new Bluetooth long range modes to extend communication distances, a UAV can search for sheep at higher altitudes without distressing the animals and cover a larger search area. This could significantly reduce or eliminate infrastructure costs related to constructing and maintaining radio base stations while requiring no licencing fees.

Moreover, the need for equipping each animal with a GPS receiver can be eliminated by an onboard GPS receiver on the UAV, further decreasing costs and power consumption significantly. The still relatively short range of the communication system can potentially be exploited to implement a very lightweight and simple tracking system, where the UAV simply listens for data packets and logs the unique sheep ID with the current GPS position. This would give a rough estimate of where the sheep are located, which could prove sufficient in areas with few obstacles and little vegetation blocking the line of sight of a farmer. Alternatively, a more advanced system using one or several radio positioning techniques in combination with the movement of the UAV could be implemented for higher localization accuracies, as seen in Section 2.2.3. A combination of the two methods are also possible, where a course search covering a larger area is first performed and higher precision localization is used on location.

In addition, the use of BLE could make the ear tags and UAV compatible with already owned smartphones, tablets or laptops, eliminating the need for expensive hand held devices and allows for easy interface implementation. This could allow for supplementary tracking by smartphones and easy real-time communication with the UAV in the field. Of course, such a system would not provide hourly or daily real-time monitoring and tracking of sheep throughout the season like existing commercial solutions. However, it would significantly reduce operating costs and thus allow every animal to be equipped with the technology while providing sufficient aid for tracking down the sheep when farmers relocate them in the autumn.

2.3 UAV Data Collection

With the recent surge of wireless sensor networks (WSN) research, several solutions involving data collection using UAVs have been proposed in the literature. The use cases of such applications are often envisioned for deploying WSNs over large areas where wireless coverage is sparse. With UAVs increasingly becoming more advanced and cost effective and additionally being capable of autonomous operation, both costs and power consumption of such networks can be decreased. While developing a fully automated drone searching system is beyond the scope of this thesis, it is certainly relevant for implementing a complete sheep tracking system. Thus, a few of the recent advancement in the field is presented in the following sections.

Rashed and Soyturk [43] investigated different UAV mobility or search patterns for sweeping an area with WSN, by considering parameters such as endurance time, altitude, speed and radio type in use. A new metric for formulating the tradeoff between maximizing the number of nodes covered and minimizing the search time with a given search pattern was introduced. A realistic simulation environment was used to compare and evaluate the performance of the systems. While the research is mainly concerned with stationary nodes with known positions, it could potentially be applied to UAV based animal tracking solutions.

Zhan *et al.* [44] proposed an energy efficient UAV enabled data collection scheme for wireless sensor networks. Here the authors are mainly concerned with optimizing the wake-up schedule of the sensor nodes based on an optimized UAV trajectory that ensures minimal energy consumption and reliable data collection. By applying a successive convex optimization technique, an efficient iterative algorithm was proposed to find an optimal solution. Numerical results indicated that the scheme achieved significant network energy savings in comparison with benchmark implementations.

Liu *et al.* [45] proposed an age-optimal trajectory planning scheme for UAV-assisted data collection in WSN. The age of information (AoI) collected from each sensor node is defined as the data uploading time and time elapsed since the UAV left the node. Two age-optimal trajectory planning schemes were proposed and simulated in order to minimize either the age of the oldest sensor node data or the average AoI.

3 Localization Using BLE

This chapter presents the necessary background theory for understanding the proposed solution, the conducted experiments and the results. Fundamental radio communication principles are introduced in Section 3.1 and the four principal radio-based localization techniques are presented in Section 3.2. Moreover, a short introduction to the BLE protocol stack is presented in Section 3.3 while a few considerations related to a UAV-enabled BLE localization scheme is finally presented in Section 3.4.

3.1 Radio Fundamentals

This section introduces necessary theory regarding radio frequency (RF) and wireless communication in general. Most wireless communication today is performed by using RF. In simple terms, an RF system converts an amplified oscillating electric signal, encoded with data, into electromagnetic (EM) radiation using an antenna. The EM-waves travel or propagate with certain properties depending on factors such as antenna geometry, radio frequency power, propagation medium, obstacles and the wavelength of the waves. If a sufficient transmission range is achieved, depending on the aforementioned factors and the sensitivity of the receiving antenna, the receiving antenna converts the EM-waves to an electric signal, which can be further decoded to obtain the transmitted data. There are several possible techniques for encoding data in the transmitted radio signals, however such techniques are generally considered out of scope for this thesis. Finally, most RF communication systems uses a standardized protocol where factors such as the frequency band, channels and data transmission speed is predefined. In addition, the data packet format, data encoding and possibly error correction mechanisms are defined to ensure compatibility between devices, reduce interference and generally create one or more abstraction layers. Examples of such protocols include Bluetooth, Zigbee and LoRaWAN, as discussed in Chapter 2 and Section 3.3.

3.1.1 Basic Principles

Radio Frequency Power

RF power is often expressed and measured using decibel with a milliwatt reference, denoted as dBm, where the output power in decibels reference 1 mW [46]. The

relationship between mW and dBm is given by:

$$P(\text{dBm}) = 10 \cdot \log_{10}(P(\text{mW})), \tag{3.1}$$

and

$$P(\text{mW}) = 10^{\frac{P(\text{dBm})}{10}}. \tag{3.2}$$

Path Loss

Path loss is the attenuation of the power density of an electromagnetic wave that occurs as the wave propagates through space. The main cause of path loss is the natural decrease in power density or signal strength as the wave travels a given distance. The power density of the wavefront is proportional to the inverse square of the distance, d:

$$\text{Power density} \propto \frac{1}{d^2}. \tag{3.3}$$

Free-Space path loss occurs in the event that there are no obstructions between a transmitter and receiver and the signal propagates in a straight line, also known as line-of-sight or LOS, through free space (usually air) [47].

Shadowing

Shadowing is caused by the presence of obstacles in the path between a transmitter and receiver, that attenuate signal power through mechanisms of absorption, reflection, scattering, and diffraction [47]. These variations in received power due to shadowing effects are sometimes referred to as shadow fading and often occur over relatively large distances. These effects are thus known as *large-scale propagation effects* [47].

Multipath Propagation

Multipath propagation is an effect where radio signals are propagated to a receiver via multiple paths due to reflections in the environment. This can cause constructive and destructive interference due to the resulting phase shift from the different propagation lengths. This effect is sometimes referred to as multipath fading [47].

Isotropic Antenna

An isotropic antenna, also known as an omnidirectional antenna, is a theoretical and ideal case in which a radio signal is emitted uniformly in all directions from the antenna [48], as shown in Figure 3.1. At any given distance from the antenna, the transmitted signal power is equal for any direction or angle. This is a useful concept to use as a baseline for characterizing and comparing real antenna designs and geometries.

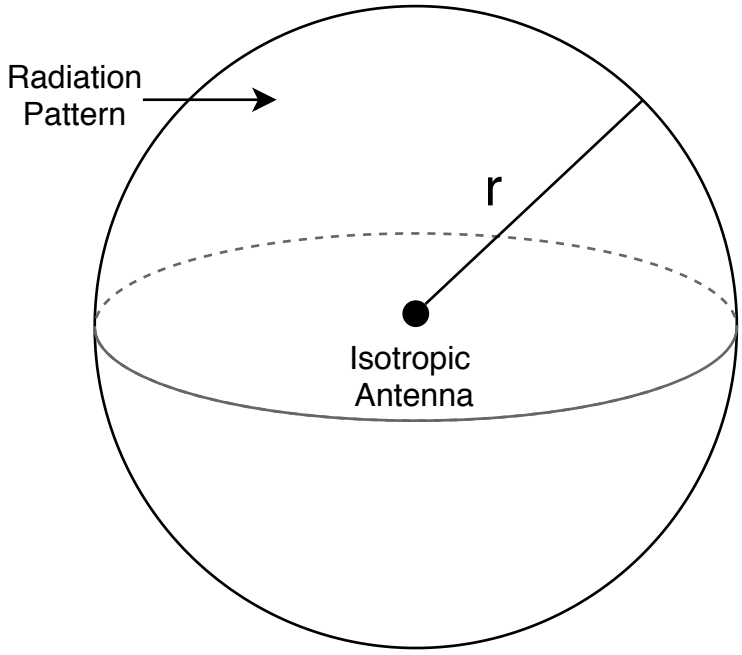

Figure 3.1: Radiation pattern of an isotropic antenna.

Directional Antenna

In a directional antenna, the transmitted signal power at any given distance is greater for some directions or angels compared to others [48]. An example of such an antenna is the monopole antenna, which is formed by replacing the bottom half of a dipole antenna with a ground plane, as shown in Figure 3.2. A monopole antenna has an omnidirectional radiation pattern in the azimuthal plane (all directions perpendicular to the antenna), but varies with the angle in the elevation plane and reaches zero in the zenith of the antenna axis.

While there is a vast number of possible antenna designs available with fundamentally different geometries, a rule of thumb is that the size of an antenna is

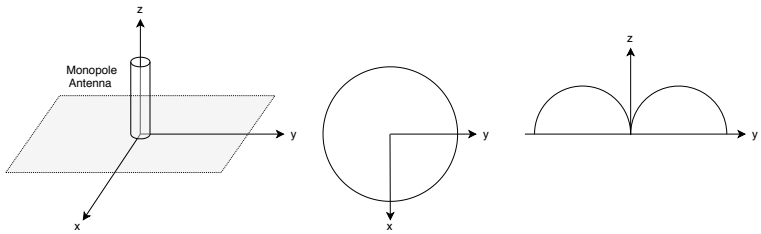

Figure 3.2: Radiation pattern of a quarter wavelength monopole antenna

dependent on the wavelength or frequency of the radio waves in use. Thus, using high frequencies tend to result in smaller antenna designs compared to lower frequencies. An example of this is the quarter wave monopole antenna where the length of the antenna is equal to $\frac{\lambda}{4}$ of the transmitted radio signal and λ is the wavelength of the RF.

Antenna Gain

Antenna gain, G, is the ratio of the signal strength in the direction of the strongest radiation of a given antenna, compared to an ideal isotropic antenna [48]. It is a common measurement for expressing the directivity and electrical efficiency of an antenna and is expressed in units of dBi (decibels-isotropic). For a transmitting antenna, G_t describes the efficiency at which the antenna converts the input power into radio waves in a specific direction. For a receiving antenna, G_r describes the efficiency at which the antenna converts radio waves from the specific direction into output power.

3.1.2 Polarization

The performance of transmitting and receiving antennas are highly dependent of the time-space behavior of the electric ($\vec{E}$) and magnetic ($\vec{H}$) vector components of the EM-wave [49]. The polarization of a radio wave is conventionally defined as equal to the direction of the $\vec{E}$ vector and can be decomposed into a horizontal and vertical component along the x- and y-axis, as shown in Figure 3.3. An antenna is vertically polarized when the E-field of the transmitted EM-wave is perpendicular to the surface of the earth and horizontally polarized when parallel [50], as shown in Figure 3.4. The polarization is evaluated in the far field [51].

If an EM-wave have polarization in a single plane, the wave has a linear polarization (LP). If the EM-wave is polarized in two planes, i.e. it has a vertical and horizontal component, the wave is circularly or elliptically polarized, depending on whether the magnitude of the components are equal or not. In this scenario,

the plane of polarization effectively rotates in a helical pattern as the wave propagates, completing one revolution each wavelength. The direction of the rotation is also significant, where a distinction between a right-hand-circular (RHC) and left-hand-circular (LHC) *sense* is made. Figure 3.5 show an illustration of common polarization states.

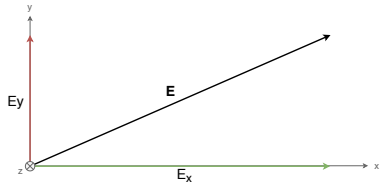

Figure 3.3: The direction of the E-field in an EM-wave, propagating in the z-direction, can be decomposed to a vertical and horizontal polarization component.

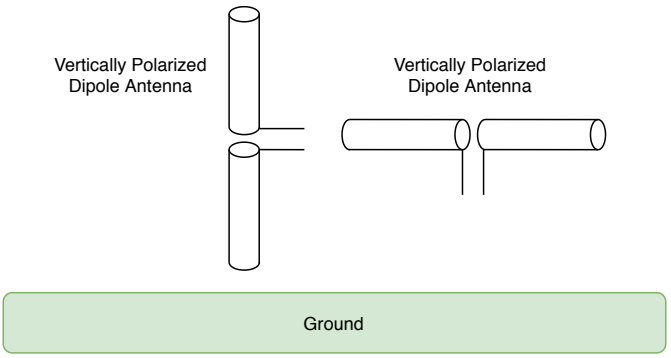

Figure 3.4: An antenna is vertically polarized when the E-field is perpendicular to the surface of the earth and horizontally polarized when parallel.

Many common antenna designs, like the dipole or monopole antenna (e.g. a whip antenna), are LP due to the simplicity and low cost of implementation. In a receiving antenna, the E-field of an incoming EM-wave generates a current in the direction of the $\vec{E}$ vector. As a consequence of the reciprocity theorem, antennas transmit and receive in exactly the same manner [51]. Thus, in order for the receiving antenna to efficiently convert the RF signal to an electric signal, the polarization of the transmitter and receiver must align. In general, for two linearly polarized antennas with a rotational offset of ϕ radians, the power loss due to polarization mismatch is characterized by the polarization loss factor (PLF), given by

$$PLF = \cos^2 \phi \text{ [51]}. \tag{3.4}$$

The PLF is also sometimes referred to as the polarization efficiency, antenna mismatch factor or antenna receiving factor. In a LP antenna system, a misalignment

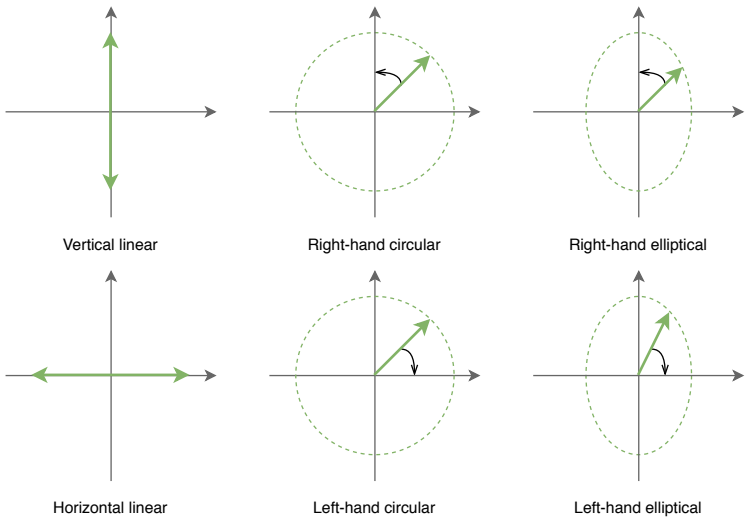

Figure 3.5: Common polarization states of an EM-wave propagating into or out of the plane. EM-waves with polarization in a single plane are linearly polarized. EM-waves with polarization in two planes are either circularly or elliptically polarized depending on the magnitude of the vertical and horizontal components.

of 45° would result in a PLF of 0.5 which, when converted using Eq. 3.1, results in a signal power loss of −3 dBm. A misalignment of 90° would yield a PLF equal to zero, resulting in an infinite polarization mismatch loss. However, in practice, the PLF is more accurately approximated to be 0.01, meaning a polarization mismatch loss of −20 dBm.

The alternative to LP antennas is circularly polarized (CP) antennas. These use more complex geometries to transmit and receive either RHC or LHC polarized radio signals. There are several advantages of using CP antennas [52]. In short, the resulting radio waves are less impacted by factors such as reflection, absorption, weather and multipath propagation. Two CP antennas with the same sense does not suffer any polarization mismatch loss. However, if the antennas use the opposite sense of each other, a mismatch loss of −20 dBm would occur. Moreover, when a CP signal is reflected, the sense is switched to the opposite alternative. That is, RHC will become LHC and vice versa. These properties can be exploited to minimize signal-fading effects such as destructive interference caused by multipath propagation. In fact, these are some of the reasons why GPS uses CP antennas [51].

Finally, it is also possible for a LP antennas to receive radio signals from CP antennas and vice versa. Since CP signals consists of two orthogonal LP waves that are 90 degrees out of phase, the LP antenna would simply receive the in-phase component independent of orientation and the resulting PLF would be 0.5 – leading

to a polarization loss of $-3\,\mathrm{dBm}$ [51].

3.1.3 Radio Propagation Models

While the underlying physics of radio wave propagation is well understood, the sheer complexity of real life radio systems, placed in a multitude of ever changing environments and conditions, makes precise calculations regarding radio wave propagation unfeasible in many cases. As a result, several theoretical and empirical radio propagation models have been developed for different purposes and similar use cases. These are often useful to estimate the possible transmission ranges of an RF system, given certain parameters such as the transmitted RF power, the directivity of the antennas, the receiver sensitivity and the RF wavelength in use. Such models are often formulated in order to predict the received signal power, given a certain distance. While there are numerous models available that focus on solving different problems, they can generally be categorized into models for free space, outdoors and indoors attenuation. Outdoors attenuation models can be further classified into landscape and cityscape focused models. Due to the scope of this thesis, only a few of the free space and outdoors landscape models will be presented moving forward.

Friis Transmission Equation

The relationship between the transmitted power, P_t, and received power, P_r, between two antennas in free space is given by Friis free space equation:

$$\frac{P_r}{P_t} = G_r G_t \left(\frac{\lambda}{4\pi d}\right)^2, \tag{3.5}$$

where G_r and G_t is the gain of the receiving and transmitting antenna respectively, λ is the RF wavelength and d is the distance between the antennas [53]. This model assumes a LOS situation with no multipath propagation, no polarization mismatch and a narrow bandwidth such that it can be approximated with a single wavelength.

By solving Eq. 3.5 for d, the theoretical transmission range between a two antennae with a LOS free-space propagation model is given by

$$20\log_{10}(d) = G_t\ [\mathrm{dBi}] + G_r\ [\mathrm{dBi}] + P_t\ [\mathrm{dBm}] - P_r\ [\mathrm{dBm}] + 20\log_{10}\left(\frac{\lambda}{4\pi}\right), \tag{3.6}$$

where the equation is modified to use decibels (dB) instead of watts (W). The friis transmission equation can also be modified to apply in non-LOS scenarios by

introducing a path loss exponent n. The path loss exponent is usually a value between 2 and 4, and can be obtained empirically [54]. This is often referred to as the free space equation [55] and is shown in Eq. 3.7, where the PLF described in Eq. 3.4 is additionally included.

$$P_r = (PLF)\frac{P_t G_r G_t \lambda^2}{(4\pi)^2 d^n}, \quad 2 \leq n \leq 4. \tag{3.7}$$

Log Distance Path Loss Model

The log distance propagation model is a more simplified free space propagation model, given by

$$\overline{P_0}(d) = P_0 - 10n \log_{10}\left(\frac{d}{d_0}\right), \quad 2 \leq n \leq 4. \tag{3.8}$$

Here, the average received power, $\overline{P_0}$ is estimated as a function of the distance, d, the path loss exponent n and the received power P_0 at a short reference distance d_0. Some variations of the model also add a term describing a random value, using a normal distribution with zero mean, to reflect the attenuation caused by fading effects.

Two-ray Ground Reflection Model

Another LOS based model is the two-ray ground reflection model. The main difference between Friis transmission equation and this model, is that it considers the effect of reflections from the ground, by adding a single reflected path to the modelled system [56], as shown in Figure 3.6. The model is only valid for large scale transmissions where the height of a receiving and transmitting antenna above the ground surface, denoted as h_r and h_t respectively, are smaller than the distance d between them, as shown in the figure.

In this model, the angle of incidence of the reflected ray, θ, is given by

$$\theta = \arctan\left(\frac{h_r + h_t}{d}\right). \tag{3.9}$$

The model further characterizes the ground surface by using a reflection coefficient, Γ, which describes what portion of the signal is being reflected as opposed to absorbed by the ground. The model can be simplified by setting $\Gamma = -1$, meaning that

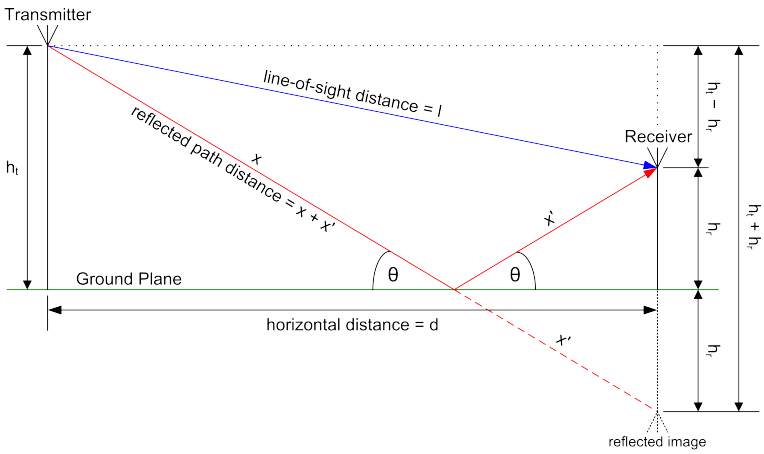

Figure 3.6: TEMP_FIG, Illustration of the Two-ray ground reflection model where a single reflected path and the height of the receiving and transmitting antenna is considered.

the signal is fully reflected. The reflection coefficient is most accurately described by the Fresnel equations [55], which necessitates knowledge of several parameters of the system. In the interest of simplification, a less accurate approximation is provided:

$$\Gamma(\theta) = \frac{\sin\theta - R(\theta)}{\sin\theta + R(\theta)}, \tag{3.10}$$

where $R(\theta) = R_h(\theta)$ or $R(\theta) = R_v(\theta)$ depending on whether the signal is horizontally or vertically polarized [13]. The relationship between $R(\theta)$ and the relative permittivity of the ground, ϵ_r, is shown in Eq. 3.11 and 3.12.

$$R_h(\theta) = \sqrt{\epsilon_r - \cos^2\theta}. \tag{3.11}$$

$$R_v(\theta) = \frac{\sqrt{\epsilon_r - \cos^2\theta}}{\epsilon_r} = \frac{R_h(\theta)}{\epsilon_r}. \tag{3.12}$$

The travelled distance of the two received signals components, namely the LOS signal and the reflected signal, is denoted as d_{los} and d_{ref} and given by

$$\begin{aligned} d_{los} &= \sqrt{d^2 + (h_t - h_r)^2}, \\ d_{ref} &= \sqrt{d^2 + (h_t + h_r)^2}. \end{aligned} \tag{3.13}$$

The phase difference of the two signals, $\Delta\phi$, is shown in Eq. 3.14 and determines whether the received signal undergo constructive or destructive interference which reveal why this model is sometimes referred to as the *two ray interference model* [56].

$$\Delta\phi = \frac{2\pi(d_{ref} - d_{los})}{\lambda}, \tag{3.14}$$

where λ is the wavelength of the transmitted signal. Finally, using the two ray ground reflection model, the received power of the combined LOS and reflected signal is given by

$$P_r = P_t\left(\frac{\lambda}{4\pi}\right)^2 \left| \frac{\sqrt{G_{los}}}{d_{los}} + \Gamma(\theta)\frac{\sqrt{G_{ref}}e^{-j\Delta\phi}}{d_{ref}} \right|^2, \tag{3.15}$$

where G_{los} is the combined antenna gain along the LOS path and G_{ref} is the combined gain along the reflected path [56].

Log Distance Path Loss with Multi-Path Fading

Combining the two-ray ground reflection model and log distance path loss model yields the log distance path loss with multi-path fading model [13], given by

$$\overline{P_0}(d) = P_0 - 10n\log_{10}\left(\frac{d}{d_0}\right) + 10n\log_{10}\left(\left|1 + \Gamma(\theta)e^{-j\Delta\phi}\right|\right). \tag{3.16}$$

Egli Model

The Egli model is an empirical radio propagation model derived for VHF and UHF and is intended for outdoors communication over irregular terrain from a stationary base station to a mobile node [57]. The model does not consider travel through vegetative obstruction [57]. The model is given by

$$P_r = P_t G_r G_t \left(\frac{h_r h_t}{d^2}\right)^2 \left(\frac{40}{f}\right)^2, \quad 30\,\text{MHz} \leq f \leq 3\,\text{GHz}. \tag{3.17}$$

where f is the frequency of the radio signal.

3.2 Radio Localization Techniques

Positioning systems are often characterized as mechanisms that determine the relative coordinates of an object while localization systems considers the environment to place these coordinates on a map [58]. However, these words are often used as synonyms and will be used interchangeably throughout this thesis.

There are several possible approaches for radio-based localization techniques. However, all these techniques generally involve the same method of measuring signal properties from multiple transmitters or having multiple receivers measure signal properties from a single transmitter. There are four fundamental positioning techniques available, namely *triangulation*, *multilateration*, *proximity based systems* and *scene analysis* (also known as *signal pattern matching*) [29, 58], as shown in Figure 3.7. Some systems also use a combination of these techniques to improve accuracy.

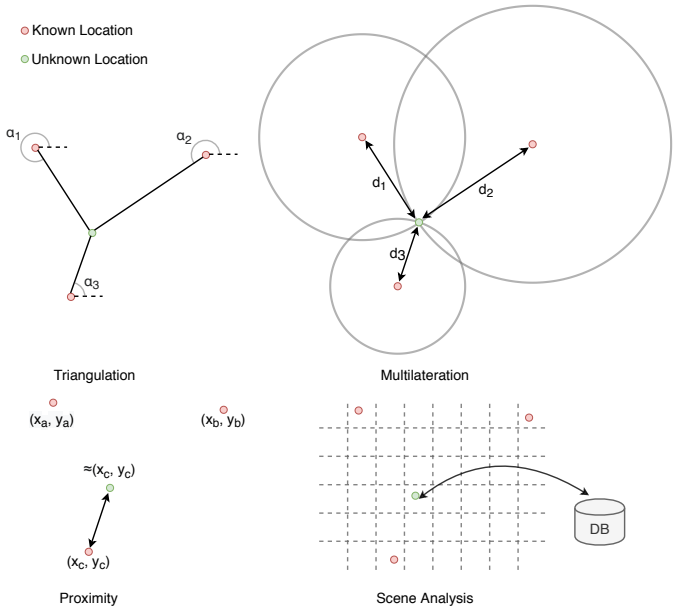

Figure 3.7: The four fundamental radio-based positioning techniques.

3.2.1 Triangulation

Triangulation is the process of determining the position of an object by forming triangles between the object and two or more known positions as shown in Figure 3.7. When the angles of the triangle are known, the unknown position can be

precisely determined using trigonometry. In radio-based triangulation systems, the direction or angle of arrival (DoA or AoA) of a received radio signal is measured to estimate these angles and thus the position. There are several implementations for measuring AoA or performing radio direction finding (RDF) as it is also known by. A common approach is to use either a two- or three-dimensional antenna array with a known geometry to measure incoming signals. From here, the difference in phase, frequency (due to the doppler effect), timing or signal strength detected by the individual antennas can be used to calculate the AoA in two or three dimensions. Such systems can often yield accurate localization estimates, but generally require costly and bulky hardware to perform [6]. Moreover, the estimated angle will often have an uncertainty such that instead of localizing a precise point, the lines of the triangles form 2D wedges or cones as shown in Figure 3.8. The intersection of these wedges or cones can then be used to find an area or volume in which the unknown location resides [28].

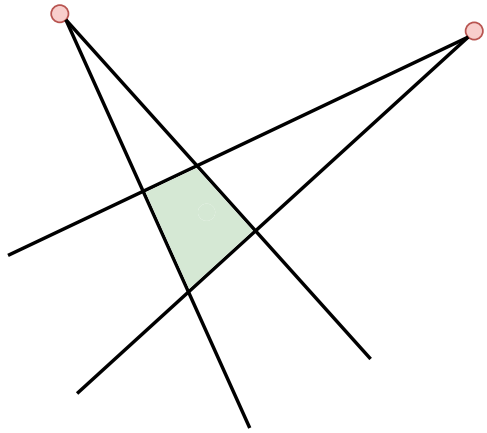

Figure 3.8: Triangulation using the uncertainty of AoA measurements to form wedges where the intersection is approximated as a parallelogram containing the unknown location.

3.2.2 Multilateration

Multilateration is the process of determining the position of an object by estimating the intersection between geometric forms, such as hyperboles, circles or spheres, as shown in Figure 3.7. By performing a distance measurement between the object in question and multiple known positions, the circles or spheres can be formed with a radius equal to this distance with the center placed at the known position. Using distance measurements (also known as pseudo ranges) from three different locations is known as trilateration and is sufficient to estimate a single position in two dimensions, given no uncertainty in the distance measurement [59]. Using four distance measurements and the intersection between the resulting spheres, two

possible three-dimensional positions can be obtained. However, as with the case of GPS, one of these points will be close to the ground while the other is high above the known positions (i.e. satellite or UAV), effectively eliminating one of the possibilities [60]. There are several possible approaches for radio-based distance measurements, such as measuring the time of arrival (ToA), time difference of arrival (TDoA) and received signal strength (RSSI) [58], which will be outlined below.

Intersection Calculation

Figure 3.9 shows a two-dimensional trilateration problem.

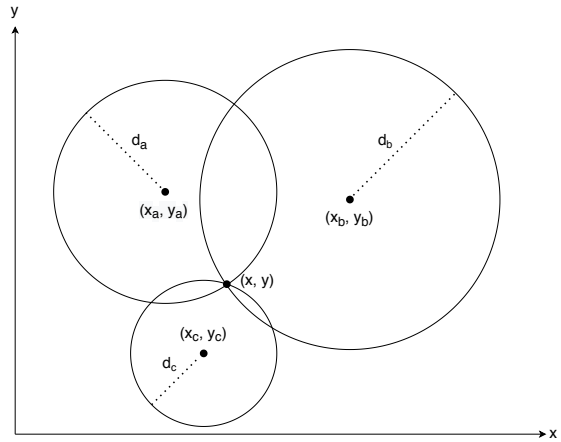

Figure 3.9: Illustration of a trilateration problem in the plane. d_a, d_b and d_c is the measured distance from (x_a, y_a), (x_b, y_b) and (x_c, y_c) to the point located at $(x, y.)$

The intersection of the three circles at point (x, y) is described by

$$\begin{aligned} {d_a}^2 &= (x - x_a)^2 + (y - y_a)^2, \\ {d_b}^2 &= (x - x_b)^2 + (y - y_b)^2, \\ {d_c}^2 &= (x - x_c)^2 + (y - y_c)^2, \end{aligned} \tag{3.18}$$

which, in linear algebraic form, can be simplified to

$$\begin{bmatrix} (x_c - x_a) & (y_c - y_a) \\ (x_c - x_b) & (y_c - y_b) \end{bmatrix} \begin{bmatrix} x \\ y \end{bmatrix} = \begin{bmatrix} \frac{({d_a}^2 - {d_c}^2) + ({x_c}^2 - {x_a}^2) + ({y_c}^2 - {y_a}^2)}{2} \\ \frac{({d_b}^2 - {d_c}^2) + ({x_c}^2 - {x_b}^2) + ({y_c}^2 - {y_b}^2)}{2} \end{bmatrix} \text{ [60].} \tag{3.19}$$

Geometric Dilution of Precision

Geometric dilution of precision (GDoP) is a term most associated with specifying the error propagation in GPS systems due to a given satellite geometry. However, the unitless measurement is also applicable in general multilateration [61]. While a comprehensive mathematical derivation of the concept is considered out of scope for this thesis, a basic introduction to the principle is provided below.

Suppose a trilateration measurement is performed where three pseudo ranges are obtained with a bound error. The pseudo distances are used as the radius to plot circles with an additional larger and smaller circle corresponding to the bound error, forming an annulus or ring, as shown in Figure 3.10. The intersection of the three annuli, shown in green, form an area in which the true location resides. On the left-hand side, the trilateration points is spread out and surround to the point of unknown location. The resulting intersection area is small and such a measurement is considered to have a low GDoP value [62]. The middle case show, somewhat chaotically, an example of a high GDoP value where the trilateration points are clustered on the same side relative to the point of unknown location. The resulting intersection area is thus larger. Finally, the right-hand side shows an example where two possible locations are identified due to poor geometric distribution of trilateration points, here in a straight line.

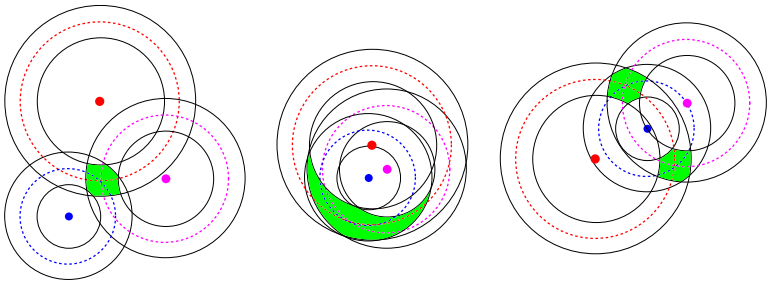

Figure 3.10: Illustration of the importance of a low GDoP when performing multilateration. Three pseudo range measurements with a bound uncertainty is plotted for three cases. The LHS case achieves an acceptable GDoP while the middle has a poor GDoP. The RHS case shows the possibility of an ambiguous result with two possible locations.

In simple terms, the GDoP can be interpreted as the ratio of position error to the range error. In the case of a GPS receiver using four satellites to measure its position, one can form a square between the satellite positions, which further forms a square pyramid with the receiver. When the volume of the pyramid is small, the resulting GDoP value is high or poor. When the volume is increased, the GDoP is lowered and the measurement is more accurate. Increasing the number of satellites or multilateration points in general would lower the GDoP value. In conclusion, the geometric distribution of the multilateration points has a large impact on the

accuracy of the localization scheme.

Received Signal Strength Indicator

RSSI is a measurement of the received signal power. By using a radio propagation model, as described in Section 3.1.3, the measured RSSI can be used to estimate the transmitter-receiver distance. Using RSSI is the most simple approach, as many RF modules have built-in hardware for measuring RSSI [6]. Moreover, such an implementation does neither require further communication between the transmitter and receiver nor any clock synchronization to estimate the distance, making the solution rather power efficient and cost effective. As a result, it is a common implementation for distance measurements in cost effective systems [29]. However, the accuracy of RSSI based distance measurements can vary greatly depending on the propagation model used and factors such as environmental changes, multipath propagation, shadowing effects and interference [6].

Time of Arrival

An alternative to estimating distance using power measurements is to use timing based methods. By exploiting the known radio propagation speed in air (approximately equal to the speed of light), it is possible to measure the time of arrival (ToA) (also known as time of flight (ToF) and time of transmission (ToT)) of the signal and further estimate the propagation distance. There are two basic approaches for measuring ToA, namely using one way or round trip timing [6], as shown in Figure 3.11. In the former, only the duration of transmitting the signal to the receiver is measured. While this does not require any back-and-forth communication, the signal must carry very precise information regarding the time of transmission (ToT). While such systems, like GPS, can produce very accurate results, they require very precise synchronization between the devices and is both costly and difficult to implement [63].

Using round trip timing (RTT) is a much simpler approach where the time it takes to transmit propagate the signal from the known location to the device in question and back is measured. This eliminates the requirement of perfect clock synchronization as only one clock is used. However, such an implementation comes with a few caveats. Firstly, the resolution of the distance measurements is limited by the resolution of the timer. Equation 3.20 shows the maximum resolution possible, or meters per tick (MPT), given a certain clock frequency, f_{clk}, and the speed of light in air c.

$$MPT = \frac{c}{f_{clk}} \tag{3.20}$$

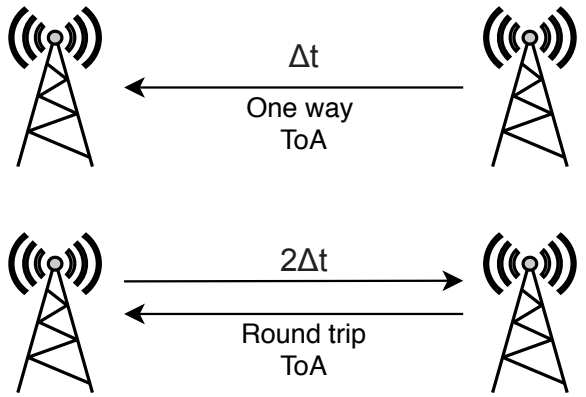

Figure 3.11: Illustration of one way and round trip timing in ToA measuring.

Thus, if the clock frequency of the timer is low, the resolution of the estimated distance could be several meters. As an example, a timer with an f_{clk} of 1 MHz would yield a MPT resolution of approximately 300 m.

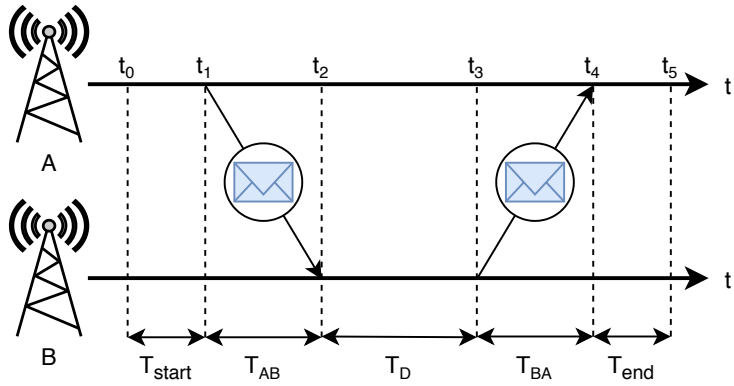

Figure 3.12: Illustration of one way and round trip timing in ToA measuring.

Another caveat is that transmitting, retransmitting and receiving a signal is not instantaneous. Figure 3.12 shows a typical timing diagram of a RTT measurement using two software-defined radios (SDR) A and B. The figure shows the presence of a delay between starting the timer and transmitting the signal from A, called T_{start}, and a similar delay between receiving the reply and stopping the timer called T_{stop}. The ToFs for transmitting an RTT packet from A to B and transmitting a response from B to A, is denoted as T_{AB} and T_{BA} respectively. Additionally, a dwell time T_D is present. T_D represents the delay between B receiving the RTT packet and subsequently responding with a transmission. These delays can be measured and subtracted from the total measured time, T_{tot}, to obtain the RTT as shown in Equation 3.21.

$$RTT = T_{tot} - T_{start} - T_{stop} - T_D = T_{AB} + T_{BA}. \tag{3.21}$$

From here, the distance d, can be calculated as shown in Equation 3.22.

$$d = \frac{RTT \cdot c}{2}. \tag{3.22}$$

However, in practice, the aforementioned delays may not be constant due to the presence of jitter in the hardware. That is, the number of clock ticks between certain events may not be deterministic on some systems while both the main system clock and the timer used for the RTT measurement have inaccuracies often measured in parts per million (PPM). Thus, accounting for both the total jitter uncertainty in number of clock ticks, denoted as T_J, and the RTT clock tick value measured using a timer with a certain f_{clk}, the distance is given by

$$d = \frac{RTT \cdot MPT}{2} \pm T_J \cdot MPT. \tag{3.23}$$

A final caveat is that ToA is only strictly accurate in LOS situations with a homogeneous propagation medium and is susceptible to shadowing effects – resulting in longer transmission times than would otherwise be the case. However, with the ToA solution, multipath effects is less of a concern compared to RSSI based solutions, as the signal traveling the shortest distance will be received first.

Time Difference of Arrival

Time difference of arrival or TDoA, is another timing based technique for measuring distance. To perform a TDoA measurement, two signals with different propagation speeds (usually RF and ultrasound) are transmitted. When the RF signal is received, a timer is started and the ultrasonic receiver is activated. When the ultrasound signal is received, the timer is stopped and the ToA can be calculated. While requiring no clock synchronization, the method is limited by the requirement of additional ultrasound hardware and the inherent short range of ultrasound.

3.2.3 Proximity Based Localization

Proximity based localization is a simple method for performing radio positioning. The most straightforward variant of this is using the cell-ID method [58]. Here, the position of a device is simply determined to be within the area equal to the coverage of whatever base station the device is connected to, as shown in Figure 3.7. This is

the most widely adopted method for conventional GSM networks today [58]. In this implementation, an obvious tradeoff between localization accuracy and the amount of base stations required to cover an area, given the wireless transmission range, is present. Moreover, to ensure full coverage over an entire area, the base stations would require overlapping coverage, possibly resulting in ambiguity towards which base station is closer. However, since the device in question often has a built-in RSSI sensor, it can subsequently connect to the base station with the highest measured signal power.

More advanced proximity based localization techniques involve WSNs and recursive multilateration techniques [59]. In such a system, the WSN is formed as a hierarchy where the higher mobile or stationary nodes already know their position through some of the previously mentioned localization techniques. These nodes can then act as beacons that periodically broadcast their current position, allowing nearby lower nodes to estimate their own location. A simple approach would be to calculate the centroid of all the obtained locations within a certain time frame. A more accurate system would be to implement multilateration. However, given a high probability of nodes without the proximity of a beacon, the nodes with an already obtained estimate can in turn broadcast their estimated position, allowing for an iterative multilateration scheme. Such a solution would obviously lead to an accumulation of localization error, but could effectively cover large areas.

3.2.4 Scene Analysis

Scene analysis, signal pattern matching or fingerprinting is the process of dividing an area into cells and associating each cell with a unique fingerprint or signature [58, 29]. This method utilize the dreaded multipath effect to its advantage, by measuring the signal structure characteristics and channel delay spread in addition to the time delay and RSSI values for each cell. These measurements form the fingerprint related to each cell and is further stored in a database. When the scene analysis system later receives a signal from a mobile device, the database is used to find the closest match – pinning the location to a single cell. While this system is rather robust and dependable, the obvious drawback is the substantial effort required for generating the database [29].

3.3 BLE Protocol Stack

The Bluetooth Low Energy (BLE) protocol is specified in the latest release of the Bluetooth Core Specification [64] and is several thousand pages long. While a complete description of the BLE protocol is certainly out of scope for this thesis, a brief introduction of necessary BLE protocol stack concepts is provided below. For further elaboration on these concepts, the reader is referred to the excellent *Getting*

Started With Bluetooth Low Energy book from Townsend *et al.* [41], which served as the main source for this section. However, as this book was published before the release of the Bluetooth 5 Core specification, the information is supplemented with other sources including the current core specification itself [64].

The BLE protocol stack can generally be divided into three parts, namely *application*, *host* and *controller* [41], as shown in Figure 3.3. The application is the highest layer of the stack and varies widely in implementation depending on the use case of the system. The host consists of several layers that form the more advanced features of the BLE protocol and is often implemented in software. The controller is interfaced with the host through a host controller interface (HCI) and contains the lower layers of the protocol that implements the fundamental features of the BLE protocol stack.

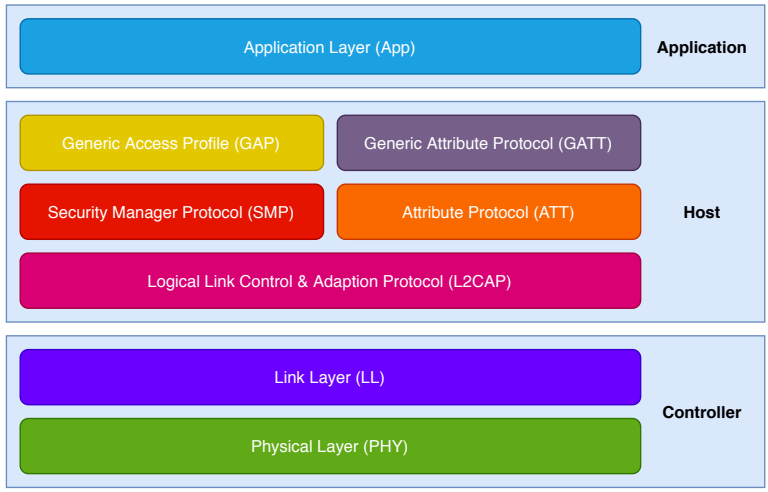

Figure 3.13: Overview of the BLE protocol stack consisting of the application, host and controller with their constituent layers.

3.3.1 Controller Layers

The controller layers consists of the physical layer and the link layer. Understanding some of the properties of these low level layers are necessary for further explanations in Chapter 4 and 5. Thus, a somewhat detailed introduction of these concepts is provided in this section.

Physical Layer

The physical (PHY) layer is responsible for the actual radio communication and is capable of modulating and demodulating analog signals and converting the data to and from a digital representation. To encode and decide the data, a Gaussian Frequency Shift Keying (GFSK) modulation scheme is used. The radio uses the 2.4 GHz ISM band to communicate over 40 separate channels, where three of the channels are used exclusively for advertising while the remaining channels are used for data transfers. To reduce the effect of radio interference, the standard use a *frequency hopping spread spectrum* technique where the radio *hops* between channels on each connection event, dictated by a *hop* value communicated when a connection is established [41].

Link Layer

The link layer (LL) is commonly implemented as a combination of hardware and software and directly interface with the PHY layer. It is responsible for managing fundamental properties of the stack such as device roles, addresses, packet format, connections, encryption and error correction in addition to the strict timing requirements required to maintain links with other devices.

Packet format

BLE uses a single packet format for both advertising channel packets and data channel packets [64]. A packet consists of four components as shown in Figure 3.14.

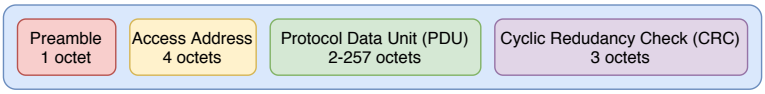

Figure 3.14: Format of a BLE packet.

where the two first octets of the PDU are called the *header* and defines the packet type. The remaining octets of the PDU is called the *payload*, which contains configurable user data.

Device roles

In BLE terminology, a BLE device may have different names depending on the situation and its role. A *peripheral* device can transmit advertising packets while a *central* device can scan for advertising packets and establish a link by sending a connection request. When a central establish a connection, it is called a master,

and the connected peripheral is called a slave. A device may have multiple roles simultaneously where a master can connect to multiple slaves and a slave can connect to multiple masters. The BLE protocol has an inherent asymmetry in the link layer as the role of master requires a higher degree of computational resources, allowing for simpler and thus low cost peripherals.

Advertising

Peripheral devices can transmit advertising packets for two main reasons; either to establish a connection to a central or to broadcast information without a connection. Advertising packets can be classified with three different properties, namely whether the advertisement is *connectable*, *scannable* and *directed* or not. An advertising packet is either connectable or non-connectable depending on whether the peripheral device allow a connection to be established or if the packet is only used to broadcast a message. An advertising packet is either scannable or non-scannable depending on whether the peripheral will respond to scan request from the central. Finally, an advertisement packet can be directed or undirected depending on whether the header of the packet contains the address of a specific central device or not. In directed packets, no other payload is allowed while undirected packets are intended for any scanning device and can contain user data in the payload. In practice, four advertising packet types are allowed in the Generic Attribute Profile (GAP), as shown in Table 3.1, and is defined by the header of the PDU.

Table 3.1: BLE advertising packet types.

GAP Name	Connectable	Scannable	Directed
Connectable Undirected	✓	✓	✗
Connectable Directed	✓	✗	✓
Non-connectable Undirected	✗	✗	✗
Scannable Undirected	✗	✓	✗

A peripheral device can advertise at a fixed *advertising interval* ranging from 20 ms to 10.24 s. A higher advertising interval increases the likelihood of the packets being received by a scanning central at the cost of higher power consumption.

Scanning

Central devices can perform scanning either actively or passively. Passive scanning only entail listening for and receiving advertising packets. An active scanner can transmit scan requests via a BLE packet to request additional information from an advertising peripheral through a scan response. Whether a packet is a scan request or a scan response is defined in the header of the PDU. Since the advertising

packets are transmitted on three separate channels, the scanner must alternately switch between the channels. Moreover, the act of scanning is substantially more energy demanding than advertising in general [65]. Many applications therefore use a *scan window* that describes the duration of scanning within a periodic *scan interval* in order to decrease power consumption on the central devices. With such implementations, the central device does not scan continuously and additionally hop between the advertising channels when it does. Thus, an advertising packet will only be received successfully when the scan interval randomly overlap with the advertising interval on the correct channel [41].

Manufacturer Specific Data

Members of the Bluetooth Bluetooth SIG are assigned a unique company specific identifier number. This ID can be included along with manufacturer specific data in the payload of an advertising packet. This can be used to easily convey information about the peripheral device, such as the device model or id, to a central device from a specific manufacturer.

Extended Advertising

In the Bluetooth 4.0 specification, advertising packets can be transmitted on three different channels, where an advertising packet can hold up to 37 bytes of data. In the Bluetooth 5 specification, the advertising mechanism is improved by introducing the concept of extended advertising [64]. This feature allows for sending a small header packet on the three primary advertising channels that point to a larger payload, which will be transmitted at a later time on one of the 37 data channels [66]. This method enables larger payloads while limiting problems with congestion as the payload does not need to be transmitted on all three main channels. Furthermore, each advertising packet can hold up to 255 bytes of data which can be further chained together to perform an advertisement with a total payload of 1650 bytes [64].

This more efficient use of the 2.4 GHz ISM band also allows for new Low Energy Physical layer (LE PHY) modes to be introduced. Using extended advertising, the new Bluetooth 5 supports advertising with the following LE PHY modes [66]:

- LE 1M PHY: 1 Mb/s bit rate, 1 Msym/s symbol rate. This is the same PHY mode used in Bluetooth 4.0.
- Coded PHY: 1 Mb/s bit rate, 500 ksym/s or 125 ksym/s symbol rate, where each bit is encoded into 2 or 8 bits, respectively, in order to use a forward error correction algorithm that enables a higher bit error tolerance which should improve transmission range.

- LE 2M PHY: 2 Mb/s bit rate, 2 Msym/s symbol rate. The symbol rate is doubled to increase the payload transfer speed at a small cost of range.

Connections

A connection can be initiated when a central device receive a connectable advertising packet and a connection request is sent. A connection is simply a sequence of periodic data exchanges called *connection events* between the a slave and a master [41]. There are three basic connection parameters that characterize a connection. The *connection interval* determines the interval between connection events, and thus the data throughput, and can range from 7.5 ms to 4 s. The *slave latency* determines the number of connection events a slave can omit before a disconnection occurs. The *connection supervision timeout* sets the maximum time between receiving valid data packets before the connection is considered lost. These parameters can be determined and changed by the master at any time. However, both the master and the slave can also request a change of connection parameters during a connection if it is deemed advantageous. An important point to consider is that each time a peripheral transmits a connectable or scannable advertising packet, it also has to scan for an incoming connection or scan request for a short time, further increasing power consumption. Moreover, whenever a central device receives an advertising packet from a peripheral that it intends to establish a connection with, it must wait until the *next* advertising packet is received before transmitting the connection request to ensure that the peripheral device is scanning for it.

3.3.2 Host Layers

The host layers is made up of a Logical Link Control and Adaption Protocol (L2CAP), Security Manager Protocol (SMP), Attribute Protocol (ATT), Generic Access Profile (GAP) and Generic Attribute Profile (GATT) layer [41]. While detailed knowledge of most of these layers is deemed unnecessary for subsequent chapters, a brief overview is provided below for the sake of completeness.

Logical Link Control and Adaption Protocol

The L2CAP layer perform protocol multiplexing, where the data from the different protocols in the upper layers is converted to smaller chunks that conform to the standard BLE packet format and vice versa.

Security Manager Protocol

The Security Manager Protocol (SMP) layer, as the name indicates, provides security to the BLE stack by defining how security keys are generated and exchanged. This is achieved through three procedures, namely *pairing*, *bonding* and *encryption re-establishment*. In the pairing procedure, a temporary common key is generated to initiate an encrypted link. The bonding procedure follows a sequence of pairing, where permanent security keys are exchanged to facilitate quick and secure connections in the future. Finally, the encryption re-establishment procedure defines how to use the stored keys from bonded devices in subsequent connections.

Generic Access Profile

The Generic Access Profile (GAP) defines how devices perform control procedures such as device discovery, connections and security establishment to ensure interoperability between devices from different manufacturers and vendors [41]. For instance, GAP formally defines the BLE advertising packet types as shown in Table 3.1. Generally, GAP is used to define device role pairs, either broadcaster/observer or peripheral/central and device modes such as broadcasting, discoverability, connectability, bonding and periodic advertising [67]. It additionally manages security and both advertising and connection parameters. In other words, it defines the actual procedure of device discovery and connection establishment using the available mechanisms of the link layer. It can thus be characterized as the uppermost control layer of the stack [41].

Attribute Protocol

The Attribute Protocol is a stateless client/server protocol based on *attributes* presented by a device [41]. It defines how data is transferred between devices, where a client can request data from a server and the server replies with the requested data. A BLE device can be either a client, server or both, independent of whether it is a master or slave. If a request is pending, no other requests may be sent. The attributes is in practice a predefined set of commands that are grouped in request/response pairs.

Generic Attribute Profile

The Generic Attribute Profile GATT layer is enabled by the lower ATT layer and is the backbone of BLE data transfer [41]. It defines how data is organized and exchanged between applications by managing a generic data objects, known as GATT-based profiles, that can be used by a range of different applications. Using

the same server/client model as ATT as the fundament, the data can be encapsulated into a hierarchy called *services*. Each service is made up of one or several *characteristics* which consists of conceptually related user data and metadata. In summary, the GATT layer allows BLE enabled applications to offer standardized or vendor-defined services to other BLE enabled applications. An example of this is the Bluetooth SIG-defined GATT-based profile called the *Glucose Profile*, which facilitates a secure transfer of measured glucose levels and ensures interoperability between different implementations of such glucose measuring systems.

3.4 UAV-Enabled BLE Localization

There are several considerations related to a UAV-enabled BLE localization based system. This section presents some of these considerations, including the determination of the effective transmission range and area coverage given a specific search pattern of the UAV. This can then be used to determine the advertising interval of the peripherals being located.

3.4.1 Transmission Range

This subsection describes transmission ranges related to a UAV-enabled searching and localization system using BLE. However, it is necessary to first define the term. It is possible to define transmission range as the maximum distance at which the electromagnetic energy from a radio source can be detected. However, a more useful definition is describing transmission range as the maximum range at which data can be correctly extracted from a received signal [68]. This definition can be further narrowed to incorporate how reliable such transmissions are, by setting a minimum threshold of the acceptable average *packet delivery ratio* (PDR) at a given distance. PDR is a simple, but useful metric that shows the relationship between the number of received data packets, N_r, to the number of transmitted packets, N_t, given by

$$PDR = \frac{N_r}{N_t}. \tag{3.24}$$

Thus, the transmission range, r_t, is henceforth defined at the maximum distance a receiver can reliably extract data from the transmitted signal with a given PDR threshold.

Using Bluetooth 4.0, the only alternative for increasing the transmission range is to increase radio transmission power. Increasing the transmission range would thus come with a severe cost in the average energy consumption of a given applica-

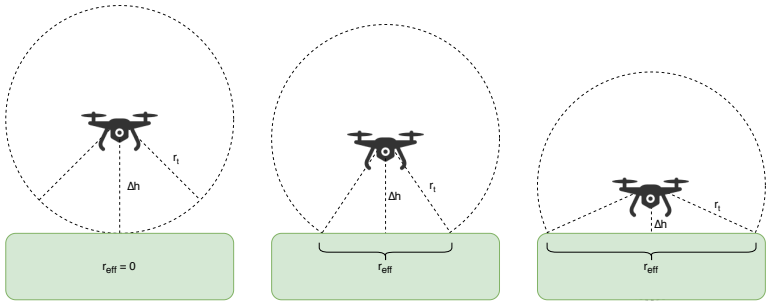

Figure 3.15: Illustration of the effective transmission range, r_{eff}, with different UAV heights relative to a advertising peripheral, Δh, and a transmission range r_t. Figure is reproduced from [43].

tion [68]. With the introduction of the Coded PHY mode in Bluetooth 5, another alternative is made available with much lower penalties in average energy consumption [64]. However, increasing the number of transmitted symbols by 2 or 8 for any given payload will also increase the amount of time the radio must remain active for a single transmission. Hence, increasing the transmission range with Coded PHY also comes with an increase in average energy consumption, albeit much less than increasing transmission power.

Assuming a known transmission range, r_t, in a LOS situation, the effective coverage of an area for a UAV equipped with a radio receiver estimated by finding the *effective transmission range*, denoted as r_{eff}. By considering the height difference between the receiving antenna and the transmitting antenna, Δh, and using the Pythagorean theorem, r_{eff} can be determined by projecting r_t from 3D-space to a 2D-plane:

$$r_{eff} = \sqrt{{r_t}^2 - \Delta h^2}. \tag{3.25}$$

Thus, the effective coverage of an area is both dependent on the transmission range and altitude of the UAV as shown in figure 3.15.

3.4.2 UAV Search Pattern

There are several possible search patterns available for a UAV-assisted data collection scheme, as briefly discussed in Section 2.3. Ideally, in a UAV-assisted BLE localization system, the UAV should use an autonomous and dynamic search pattern which is updated in real-time as localization information is obtained. However, such a system is considered out of scope for this thesis. An alternative is to use some of the basic solutions discussed in a paper by Rashed and Soyturk [43], which

include a parallel search pattern.

Suppose a UAV is searching for advertising packets in a parallel search pattern, with a distance d_s between the parallel lines as shown in Figure 3.16. If $d_s > 2r_{eff}$, the search area will not be fully covered. Using $d_s = 2r_{eff}$, the area is technically fully covered, however if the peripheral is placed in the middle of two parallel lines, as shown in the figure, the UAV is only within coverage for an infinitesimal length on both sides. Thus, in order to fully cover an area, $d_s < 2r_{eff}$, to ensure the reception of a peripheral advertising packet when placed in the worst case position.

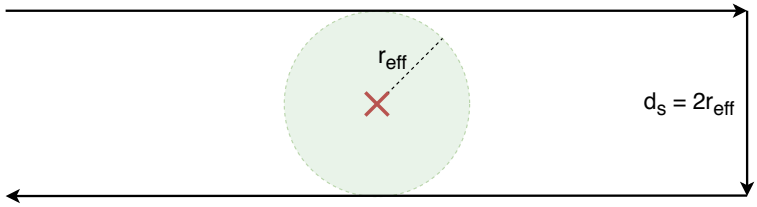

Figure 3.16: Worst case placement of a peripheral advertising device, marked with X, when considering coverage with an effective transmission range r_{eff}, given a parallel UAV search pattern with distance d_s.

However, such a scheme would not be applicable for a multilateration-based localization system. Suppose a peripheral is placed directly under one of the parallel lines as shown in Figure 3.17. Recall from Section 3.2.2 that several distance measurement conducted on a straight line would yield an ambiguous result. Thus, in order to conduct a multilateration localization measurement with an acceptable GDoP in a parallel search pattern, distance measurements must be performed on at least two parallel lines. This is only achievable when $d_s < r_{eff}$.

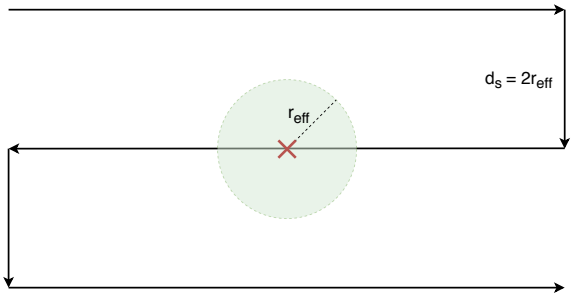

Figure 3.17: Worst case placement of a peripheral advertising device, marked with X, when considering multilateration with an effective transmission range r_{eff}, given a parallel UAV search pattern with distance d_s. Notice that using this value for d_s will result in distance measurements being performed only in a straight line.

Figure 3.18 shows a worst case scenario placement of a peripheral device, where $d_s < r_{eff}$.

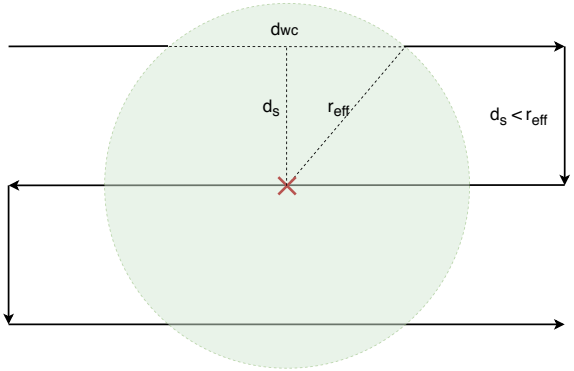

Figure 3.18: Worst case placement of a peripheral advertising device, marked with X, when considering multilateration with an effective transmission range r_{eff}, given a parallel UAV search pattern with distance d_s. The worst case distance the UAV can travel and still be within transmission range is denoted as d_{wc}.

The worst case distance where the UAV is within coverage, d_{wc}, is then given by

$$d_{wc} = 2\sqrt{{r_{eff}}^2 - {d_s}^2}, \tag{3.26}$$

which can be used to further estimate the advertising interval.

3.4.3 Advertising Interval

Given a UAV speed, s_{uav}, the minimum advertising period, i.e. the interval between advertisement packets, T_{Amin}, that ensures at least one advertising signal is being transmitted while the UAV is in range is given by

$$T_{Amin} = \frac{d_{wc}}{s_{uav}}. \tag{3.27}$$

The actual minimum advertising interval in the worst case scenario, T_{wc}, can then be estimated by considering the expected PDR and the fact that receiving an advertisement packet just before leaving the transmission range might not be beneficial if distance measurements are to be performed. Thus, at least one advertising packet should be received while the UAV travels in the first half of the total d_{wc} length. This is achieved by dividing T_{Amin} by two and multiplying with the expected PDR. Moreover, if a connection is to be established, recall that the central must wait until the next advertising packet is received to transmit a connection request as outlined in Section 3.3. Thus, the term should further be divided by two and is given by

$$T_{wc} = (PDR)\frac{T_{Amin}}{4}. \tag{3.28}$$

Furthermore, multiple peripheral devices could roughly occupy the same location, meaning that multiple peripheral devices would be within coverage at the same time. This could lead to a scenario where the radio on the UAV is occupied with performing distance measurements and thus not able to send a connection request at the next advertising event. This could be accounted for by further dividing by a number equal to the estimated number of peripherals in one location. However, this would probably result in an unnecessarily excessive power consumption as knowing the location of a single peripheral would likely be sufficient to locate the nearby devices. Finally, the worst case estimation is likely too strict, as most scenarios would not be the worst case, and would also lead to an excessive power consumption.

4 System Architecture

This chapter outlines the proposed solution for a novel and cost-effective sheep localization system. The system rely on using using BLE long range to enable wireless communication between cost-effective and power efficient ear tags on the sheep that act as peripherals and a BLE-enabled UAV that act as the central. One or more UAVs can search an area with a certain search pattern while scanning for advertising packets that are periodically transmitted from the ear tags. From here, the UAV can exploit the relatively short transmission range of BLE and its onboard GPS to perform proximity based localization. Alternatively, the UAV can use multilateration to drastically decrease the localization uncertainty at the cost of higher power consumption. Additional details and the reasoning behind this system architecture is provided in the following sections.

4.1 Wireless Communication Technology

As discussed in Section 2.1, the vision based animal tracking systems have potential to become a reliable, cost effective and non-intrusive solution. However, the underlying technology is as of yet either too expensive or too inaccurate to track multiple animals spanning vast areas while having significant challenges related to identifying individual animals. For this reason, a radio-based localization system is proposed. Nevertheless, the vision based technologies may prove to serve as a useful supplement in a radio-based localization scheme in future implementations.

The use of long-range radio often necessitates the use of GPS as outlined in Section 2.2.1 and 2.2.2. While GPS-based solutions can yield precise localization and real-time tracking, the inherent economic and power consumption costs, in addition to the resultant larger form factor of such systems, may render them unfeasible or suboptimal for tracking less economically valuable and smaller animals such as sheep. For this reason, a system that does not require a multitude of GPS receivers is desireable. A possible alternative is to use other radio localization techniques with an LPWAN-based system. For instance, a recent paper by Gu *et al.* [69] investigated opportunities and challenges related to LoRa-based localization. However, they ultimately concluded that the existing TDoA and RSSI based approaches for multilateration can currently only achieve sub-kilometer accuracies because of the uneven terrain and obstacles in such areas, causing strong signal attenuation and multipath propagation. Moreover, a LoRa-based TDoA would require highly customized hardware, leading to overhead and high cost of deployment. Another alternative is to use an LPWAN technology with a scene analysis localization ap-

proach as described in Section 3.2.4. However, such an implementation would require an exhaustive effort to create the required fingerprinting database and does not address the final drawback with LPWAN: the lack of infrastructure in these uncultivated highland areas.

As a result of this, a short-range radio-based localization scheme is proposed. The inherent short range of such a system can be exploited to perform relatively accurate proximity based localization such as the cell-ID method discussed in Section 3.2.3. However, an obvious disadvantage is that short-range radio technology traditionally requires an unfeasible amount of evenly spread base stations, drastically increasing infrastructure demands. To mitigate this issue, one or several mobile base stations can be deployed in the form of UAVs. Disregarding the operation of the UAV themselves, the infrastructure requirements would effectively be removed all together. By equipping the UAV with a GPS receiver, the precision of GPS localization can be utilized without equipping each sheep with the technology, significantly reducing costs. When it comes to which short-range radio technology should be deployed, the use of BLE is proposed due to the multitude of reasons provided in Section 2.2.4. In short, the wide availability of BLE SoCs would allow for the implementation of low-cost, power efficient and small form factor ear tags while ensuring interoperability with devices such as smartphones. The use of the Coded PHY modes would also give BLE an advantage in terms of transmission range over other 2.4 GHz-based protocols at the cost of lower data transmission speeds. This cost is likely negligible Since only a small payload would be

4.2 Localization Method

The four principal radio-based localization techniques outlined in Section 3.2 are traditionally implemented with several stationary base stations with known locations. However, they can also be implemented using one or multiple mobile base stations equipped with a GPS receiver. Some techniques may be better suited for such an approach compared to others though. With a scene analysis approach, the complexity of generating a unique fingerprint for each cell is increased by several magnitudes due to the variables introduced by the UAV, such as height, antenna orientation and speed. Such systems also require relatively advanced hardware that might exceed the maximum payload of the UAV or at least substantially decrease flight time. Finally, using short-range radio, the area of the cells would have to be relatively small to increase precision beyond a simple proximity based approach, which would further increase complexity and the effort required for generating the fingerprint database.

Using a proximity based localization technique is by far the simplest approach. This requires no back and forth communication between the UAV and the ear tags. The ear tag peripherals can simply periodically transmit non-connectable undirected

advertising packets containing a manufacturer specific ID with a unique tag ID in the payload. Between transmissions, the tag can simply enter a low power mode with miniscule power consumption. This would be the most efficient approach in terms of power consumption as the peripheral radio would not need to scan for connection requests from the central UAV. At first glance, it might seem beneficial for the tags to act as central devices scanning for advertising packets from the UAV. However, recall from Section 3.3 that scanning is generally more power consuming than advertising. Moreover, the tags would have to transmit a reply after receiving an advertisement, further increasing energy consumption.

In the simplest proximity based implementation, the central UAV can merely log the received tag ID with its current GPS location. This would further yield an estimated area, in which the tag likely resides, equal to a circle with the effective transmission range of the communication system as the radius and centered on the logged GPS position. While the resulting uncertainty of the ear tag location would be rather large, it could be further reduced by finding the intersection area between received advertisements from multiple UAV locations. This would be a simple multilateration and proximity-based hybrid where no distance measurement is performed in real-time.

To further increase the accuracy of the proximity based system, the ear tags could be deployed as nodes in a WSN. As described in Section 3.2.3, the nodes could perform recursive multilateration to estimate their current location and broadcast this information to other nodes. However, obtaining this information would require the deployment of a UAV which could perform the multilateration instead. There is no need for the nodes to know their location at all times without the means to convey this information to a central system. Such a solution would thus lead to unnecessary energy consumption. As a side note, it could, however, prove worthwhile in a LPWAN-based scheme where only a select amount of tags are equipped with a GPS receiver.

To provide more accurate localization of the sheep while using BLE, the mobile UAV base station could perform either triangulation or multilateration. Performing AoA measurements for triangulation on a UAV would require the use of more complex hardware, such as an antenna array, compared to a multilateration scheme. This could limit the flight time of the UAV due to an increase in payload and would ultimately increase the cost of the system. Moreover, such a system would need to record the bearing or orientation of the antenna and thus the UAV to use a received signal for triangulation. As an alternative, the UAV could use a highly directive antenna where the bearing of the UAV is used as the measured AoAwhen receiving a signal. This would require a localization system that is highly integrated with the UAV itself to autonomously control the UAV orientation in real-time in order to decrease localization uncertainty. Such a system could limit the rate of adoption due to the requirement of using a compatible UAV as opposed to having a separate low cost and light weight module attached to any UAV.

AoA accuracy can also suffer from multipath propagation effects that ultimately cause incorrect measurements. While an aerial triangulation-based system was designed and tested with VHF-based radio communication and positive results in [28], it could prove more beneficial in terms of accuracy and cost to use multilateration. Indeed, in a comprehensive literature survey regarding cellular mobile localization methods, del Peral-Rosado*et al.* [58] concluded that multilateration and hybrid localization methods have shown the best performance in the literature. Thus, the proposed solution will use a combination of a simple proximity based scheme for coarse localization and a multilateration scheme for more precise localization when deemed necessary.

There are three main approaches for measuring distances using radio in a multilateration scheme, as outlined in Section 3.2.2. Using TDoA is generally unfeasible for these types of applications as each ear tag would require an additional ultrasonic transmitter. This leaves the RSSI- and ToA-based approaches, which both have significant advantages and disadvantages. The main advantage of using RSSI is that most radio receivers have an embedded RSSI sensor. This would mean that a distance measurement could be performed by receiving a single advertisement packet and using one of the radio propagation models described in Section 3.1.3, without further alterations of the proximity based solutions described above. This would likely improve the accuracy of the localization. However, the accuracy of RSSI is very susceptible to both multipath and shadow fading.

Using one-way ToA is likely unfeasible as the ear tag would either have to perform strict time-keeping or at least use a very precise clock that is synchronized with the UAV to transmit the ToT in advertising packets. The alternative implementation of one-way ToA is that the UAV transmits ToT information and the tag performs the localization. This would, however, be a less accurate implementation of a GPS receiver and would likely result in high power consumption as the tag would need to scan for signals and further transmit its location when calculated.

Using a round trip ToA technique, by performing round trip timing (RTT), has the potential to yield very accurate and cost-effective distance measurements. This method is less susceptible to multipath propagation and the movement of the UAV could reduce shadowing effects that cause packet delivery failure. However, the main disadvantage is that it requires back-and-forth communication between the tag and the UAV. Ideally, round trip ToA would be performed with the tag continuously listening for RTT packets and subsequently responding upon reception after a deterministic delay. Using the timing strict BLE protocol stack would not easily allow for such an implementation, however. This lack of flexibility would not yield the reliable timing measurement precision required to measure the ToA. Moreover, scanning continuously for RTT packets would result in a large power consumption for the tags.

To mitigate these issues, the proposed solution involve a compromise. As with the proximity based solution, the ear tags will periodically alternate between ad-

vertising and sleeping to conserve power. However, the tag will use connectable undirected advertising packets to allow the UAV to establish a connection whenever in range. This implementation would result in a power consumption penalty as the peripheral tag would need to scan for a connection request after each advertisement as described in Section 3.3. However, this penalty would be comparatively lower than the alternative which involve continuous scanning. From here, a RTT-based distance measurement service can be offered as a user defined service through the GATT protocol.

Recall from Section 3.2.2 that both the timer resolution and jitter in hardware would introduce an uncertainty in RTT-based distance measurements for SDR implementations, as shown in Eq. 3.23. To reduce this uncertainty, it is possible rapidly perform several RTT measurements and find the average distance. Thus, after a connection has been established, the RTT service is initiated, where the number of RTT packets, N, are agreed upon before both master and slave terminate the BLE connection. From here, the UAV starts a timer, transmits an RTT packet using the SDR and wait for a reply from the tag in order to stop the timer. The tag continuously scan for an RTT packet using the SDR and reply as fast as possible. This is repeated N times until the RTT distance measurement is completed. Both the tag and the UAV use a timeout mechanism to ensure that the devices do not enter an inescapable state where they wait for an RTT packet indefinitely due to being out of range or having poor transmission conditions leading to packets being dropped. After N packets have been transmitted and received or a timeout occurs, the tag proceeds to advertise as normal while the UAV computes the average distance and stores it with the tag ID and current GPS position, before resuming BLE scanning.

To be clear, the actual RTT measurement is performed by using the onboard 2.4 GHz software defined radio without using the BLE protocol. However, the procedure is initiated using BLE. Moreover, it is still possible to utilize most of the PHY and link layer mechanisms defined in the BLE protocol, such as ensuring correct transmission of the payload using CRC. The payload can then contain the information such as the RTT packet number, the tag ID or a key that is exchanged through the RTT service to dissuade interference and ensure correct operation. More importantly, the coded PHY mode can still be used to maintain the effective range. While such an RTT measurement could be rather costly in terms of power consumption, a single tag would likely only have to perform this zero to a few dozen times during the free ranging season of the sheep, making the expense negligible. Moreover, the RTT measurement should be completed as fast as possible to implement a race to idle scheme. Finally, during an RTT measurement, the transmission power could be increased to the maximum allowed value to minimize the impact of shadowing effects caused by vegetation for instance.

4.3 System on Sheep

All tough a complete implementation is out of scope for this thesis, the main idea behind a complete system for sheep localization, nicknamed System on Sheep (SoS), is presented here.

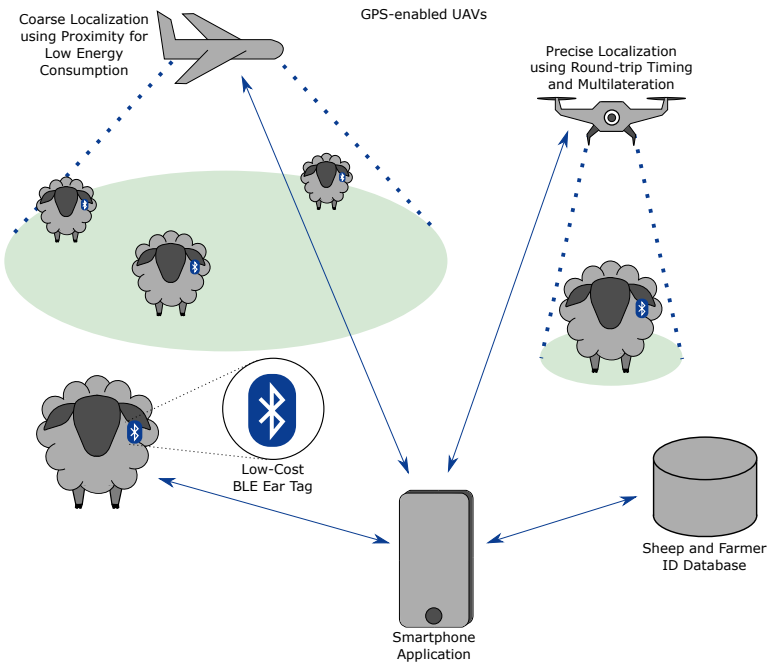

Figure 4.1: System on Sheep use-case.

In this system, sheep are equipped with small form factor and low-cost ear tags consisting of a BLE SoC, a PCB antenna and a simple coin cell battery. The tags have a unique ID related to both the farmer an the individual sheep, stored in a database, and is periodically transmitted in the payload of connectable advertising packets. This ID value can be configured before deployment through a secure BLE connection from a smartphone application by the farmer. The tags could also be implemented with an additional RFID transmitter to facilitate simple identification in the off-season.

The tags can additionally be configured through the app to use a low energy (and thus relatively imprecise) timekeeping scheme, by using a low frequency real time counter peripheral in the SoC. From here, a start-up date can be defined where the tag remains in a low power mode, only waking up to perform the time-keeping. When reaching the start-up date, the tag starts advertising to facilitate localization. All though the time keeping scheme is imprecise and could deviate with several minutes after a few years, it should not cause the device to start up at the wrong

date. The start-up date can then be configured to be at the end of the free range season to significantly prolong the battery life of the tags with multiple years. To create an even more energy conserving system, the timekeeping scheme can be used to only advertise during the day while entering a deep sleep mode at night.

To locate the sheep, a module that is more expensive than the tags, but still relatively cost effective and lightweight, can be installed as the payload of any UAV. Allowing the module to operate as an independent entity could allow for a wider adoption of SoS as the technology is not dependent on a specific UAV. The module can either be powered directly from the battery of the UAV or have a separate battery pack. The module would further consist of an antenna, a BLE SoC, a GPS receiver, a precise high frequency crystal oscillator and a storage device such as an SD Card card module to keep a record of the localized sheep. The module should also be capable of establishing a connection with the smartphone application, where either the coarse or precise localization scheme can be selected. The smartphone application can then receive the localization data and show the location of sheep on a map. Moreover, if the system locates a sheep with an ID from a different farmer, the application could update the map of the respective owner using the aforementioned database and thus allow for cooperation between farmers.

A typical use-case for System on Sheep is envisioned in Figure 4.1. At the end of the free range season, the tags starts advertising during the day with an interval configured by the smartphone application. The interval and even packet type is configured depending on how the farmer wish to locate the sheep. Hikers can voluntarily install the smartphone app, which could perform coarse localization and report the localization data to farmers. Hikers can additionally inform farmers of deceased or injured sheep by using the onboard GPS of the smartphone through the app. When its time to relocate the sheep, the farmer can use a fixed wing drone, that can cover a large area using a parallel search pattern, equipped with the module to perform coarse localization of the sheep and give a rough estimate of where they reside. To save operating costs, the drone could even be shared between multiple farms. The coarse localization is performed using the proximity and multilateration based hybrid where the RSSI value is used to increase precision.

The sheep location information can either be transmitted in real time using a long distance radio or even satellite communication. Alternatively, the data can be obtained after the searching route is complete through a BLE connection or the storage medium. When searching such a large area, the precise location of the sheep is not important due to the fact that sheep are mobile and will likely have moved before the farmer get to the location.

When a plan for sheep relocation is formed, the farmer can bring a multi-rotor drone in the field. Most sheep will be easily visible with eyesight alone and the farmer can be further assisted by using the smartphone application for coarse localization. However, some sheep might still be difficult to detect. When this is the case, the farmer can use the multi rotor drone equipped with the SoS module to perform

RTT-based multilateration and transmit the relatively precise location of the sheep over BLE to the smartphone app in real-time. The drone can even be equipped with a visual sensor such as a thermal camera to further assist the localization. Finally, when all the sheep are relocated, the tags can be configured to go back to a deep sleep state or alternatively turned completely off until the next free range season, to allow a battery lifetime of several years. An estimation of the remaining battery lifetime can also be obtained through the BLE connection.

5 Implementation

Several field experiments were conducted in order to investigate the feasibility of implementing the proposed system outlined in Chapter 4. Four main experiments were conducted, where a preliminary investigation on the ground is presented in Section 5.1. Experiments with using a UAV and the impact of antenna directivity in addition to polarization mismatch is presented in Section 5.2. Both sections also include an investigation regarding the utility of using RSSI for distance measurements. Section 5.3 investigate the performance and accuracy of using round trip timing AoA to estimate distance. Finally, a small field trial for a multilateration-based localization scheme is presented in Section 5.4.

Since the results of each experiment directly impact the implementation of the subsequent experiments, a less traditional approach for presenting the results is used in this thesis. Thus, each of the following sections will contain both the methodology and the results of each experiment. Moreover, the results are discussed as they are presented to better convey the reasoning behind the methodology of the following experiments. The results and performance of the overall system will be discussed in a more general sense in Chapter 6.

5.1 Preliminary Investigation

A preliminary investigation was conducted to get an overview of critical factors and variables that determine the overall performance of the system. The goal of the investigation was to establish an expectation of the average PDR, given a certain distance between an advertising peripheral and scanning central, in addition to determining the impact on the PDR when using different radio frequency transmitting powers and relative antenna angels between the devices. Another goal was to determine the relative performance of using the new BLE long range or coded PHY mode, compared to the traditional LE PHY. Finally, an investigation into the utility of using the log distance path loss and free space propagation models to determine the distance between the devices using RSSI was conducted.

5.1.1 Methodology

Device Selection

The nRF52840 SoC from Nordic Semiconductor was chosen as both the central and peripheral device in the experiment. This device was mainly chosen because it supports the new Bluetooth 5 transfer modes and has a highly sensitive 2.4 GHz transceiver with a −95 dBm and −103 dBm sensitivity for LE PHY and Coded PHY, respectively [65]. The device can be configured to use a wide range of radio frequency transmission powers from −20 dBm to 8 dBm with steps of 4 dBm. The device also features a relatively large flash memory and RAM of 1 MiB and 256 KiB respectively, which is useful when storing the measurements, in addition to a powerful but low-power ARM Cortex-M4 32-bit processor that can quickly process an advertising packet. The device is supported with an official PCB development kit, nRF52840 DK, which comes with beneficial features for easy programming and debugging of the device, in addition to an onboard monopole quarter wavelength PCB antenna [70], as illustrated in Figure 5.1. Lastly, the device is supported by a wide variety of useful software libraries as well as precompiled binary files for the BLE protocol stack, referred to by Nordic Semiconductor as a SoftDevice, which handles the BLE communication through an API and acts as a small OS. These software features are freely available as a downloadable Software Development Kit (SDK).

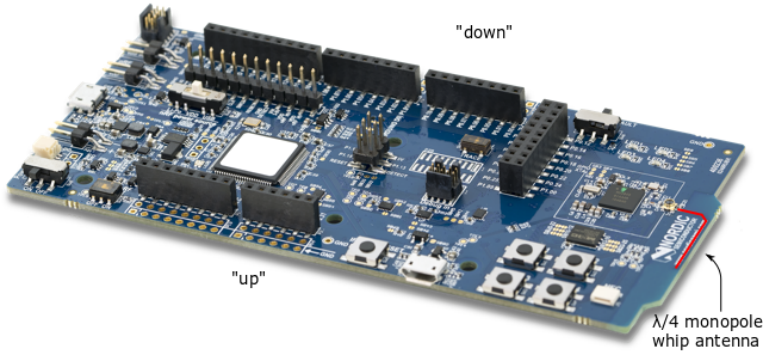

Figure 5.1: Picture of the *front side* of an nRF52840 Development Kit, courtesy of Nordic Semiconductor, with a highlighted PCB antenna and orientation labels.

The use of a similar, but lower-end nRF52811 SoC is ideal for implementing the peripheral advertising devices or ear tags since it has many of the same capabilities as the nRF52840, but at a significantly lower price range. The main difference is that nRF52811 has a smaller 192 KiB flash storage and 24 KiB RAM [71]. However, the peripheral device should do as little processing as possible to reduce power consumption and deploying the SoftDevice version called S140 only require require 133 KiB and 5.10 KiB respectively. Thus, the memory limitations should not con-

stitute a significant problem. Another advantage is that the nRF52811 offer the best transceiver sensitivity in the nRF52-family with 97 dBm and 104 dBm for LE PHY and Coded PHY respectively [71]. Finally, the nRF52811 offers the same range of radio frequency transmission powers as nRF52840, except for the maximum value being limited to 4 dBm. However, there is unfortunately no standard development kit available for this SoC. To mitigate this issue without having do develop a custom PCB, the nRF52840 DK was chosen to emulate the behavior of nRF52811 by ensuring that the device was configured to only utilize the capabilities of nRF52811 when acting as the peripheral device.

Device Configuration and Set-up

The experiment was conducted by transmitting 100 advertising packets with eight different radio frequency transmission powers, at two different heights from the ground and three different transmission antenna angels relative to the receiving antenna angle. This sequence was then repeated every 100 m from 100 m to 900 m for both the LE PHY and Coded PHY modes. The central device with its PCB antenna was placed on a tripod 200 cm above the ground as shown in Figure 5.2. The peripheral device was then manually carried to $N \cdot 100$ m distances on an open field and held in the correct height and rotation for the duration of sending the 100 packets for each radio transmission frequency power. The distances between the devices was measured in the field using the onboard GPS of a smartphone and could therefore be accompanied by a potential inaccuracy of a few meters.

All the parameters combinations used are listed in Table 5.1. The different radio frequency transmission powers were chosen due to the availability on the SoC, whereby the 8 dBm option was excluded as the nRF52811 does not have this capability. The 200 cm central device height was chosen due to the maximum height of the available tripod, as shown in Figure A.1 in Appendix A, where the advertising peripheral height of 200 cm was chosen to facilitate a direct LOS whenever possible. The other peripheral device height of 70 cm was chosen to simulate the height of a typical Norwegian sheep [2], to see whether being closer to the ground had a measurable impact on the PDR or RSSI values. The different antenna angels were chosen to simulate a small selection of scenarios regarding the relative antenna position on both the ear-tag and UAV to investigate its impact on PDR and RSSI values.

To be clear, the PCB was held such that the *front side* was pointing towards the central where the up orientation, illustrated in Figure 5.1, was facing the sky and the down orientation was facing the ground in the 90° position as illustrated in Figure 5.2.

For clarity, an upwards and a downwards orientation of the PCB was defined as illustrated in Figure 5.1. In experiments investigating the impact of relative antenna angles on PDR, a so-called 90° orientation was defined as the *front side* of

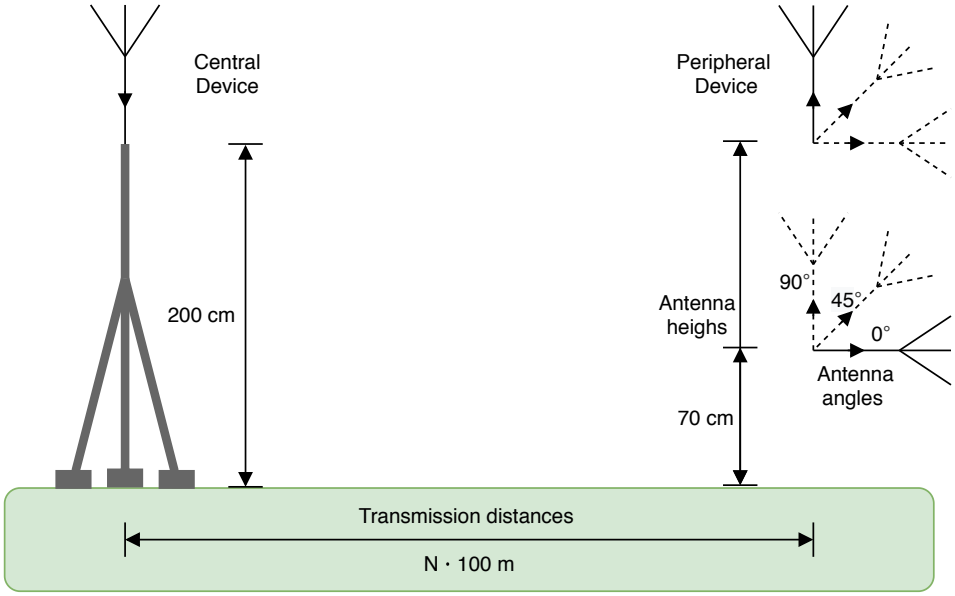

Figure 5.2: Test set-up for the preliminary investigation.

the PCB facing the central device with its assigned *up* direction towards the sky and its *down* direction towards the ground. In this position, both the transmitting and receiving antenna were vertically polarized as described in Section 3.1.2. Accordingly, the 0° orientation refers to the situation where the front side of the kit is facing the sky and the *down* direction is oriented towards the central device. In this position, the transmitter antenna is horizontally polarized and the zenith of the transmitter is pointing towards the vertically polarized receiving antenna. Under the assumption of the radiation pattern being zero along the zenith, in accordance with theory presented in Section 3.1, the 0° position corresponds to the theoretically worst case orientation whilst still maintaining LOS. Conversely, the 90° position with its vertically polarized antenna corresponds to the theoretically best case orientation of the PCB kit in terms of polarization and radiation pattern. The 45° orientation then form a middle case scenario where there is no polarization loss factor, but the directivity is reduced because the radiation pattern varies with the angle in the elevation plane.

Both the peripheral and central device was configured to use SoftDevice S140, from version 16 of the nRF5 SDK, as it is a feature-rich central and peripheral BLE protocol stack for both the nRF52811 and nRF52840 SoC that support Bluetooth Long Range [72], [73]. However, only the coded PHY mode using 8 bits to encode the data is supported. The peripheral device was configured to transmit non-connectable undirected advertising packets with the shortest possible advertising interval of 20 ms, to minimize the duration of transmitting the total of 86,400 advertising packets required for all the parameter combinations. The number of

Table 5.1: All combinations of parameter values in the preliminary investigation.

Parameters	Values
P_t [dBm]	4, 3, 0, -4, -8, -12, -16, -20
Antenna Angle [°]	90, 45, 0
Height [cm]	200, 70
PHY Mode	Coded, LE
Transmission Distance [100 m]	1, 2, 3, 4, 5, 6, 7, 8, 9
Advertising Interval [ms]	20
Advertising Packets	100

transmitted advertising packets for each parameter combination was chosen as a compromise between increasing the probability of an accurate average PDR measurement, while reducing the duration of completing such a measurement.

The peripheral device was programmed as a finite state machine or FSM where each state correspond to one configuration of the test set-up as shown in Figure 5.2. Upon receiving an onboard button press event, a state transition to the next parameter combination is triggered and the device subsequently transmits all the 100 advertising packets for each radio frequency transmission power. The current height, rotation and radio frequency transmission power was then encoded into the payload of each advertising packet by using the manufacturer specific data section. The on-chip UART peripheral was further used to implement serial communication through the onboard micro-USB socket, where messages indicating the current FSM state were transmitted to an external terminal. The terminal messages were used as instructions to ensure the correct manual positioning of the advertising device, in terms of height and rotation, in addition to ensuring that the central device was scanning for advertising packets in the correct PHY mode.

The central device was also programmed as an FSM consisting of two states: scanning mode and input mode. In input mode, no scanning for advertising packets was performed, while the current transmission distance between the devices and the current PHY mode could be selected. This was achieved by using an interface consisting of the onboard buttons of the DK and an external terminal displaying serial communication via the micro-USB socket. If the SoftDevice was configured to scan in both LE PHY and Coded PHY modes simultaneously, the central device would experience significant packet losses due to the radio having to constantly switch between the two modes. Therefore, the central device was configured to continuously scan in only one mode at a time.

A button press event from one of the buttons would then trigger a state transition to scanning mode. Herein, the device was configured to continuously scan for advertising packets. In the event of receiving an advertising packet, the software would verify a match of the company specific ID in the manufacturer specific data. Whenever a match was identified, the received parameter values in the packet were

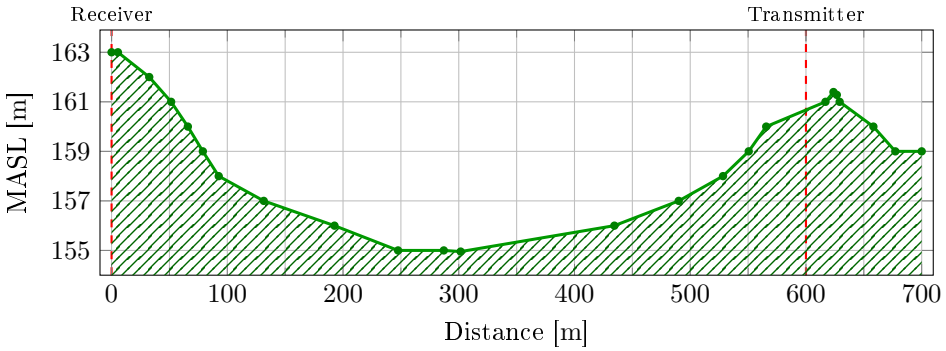

Figure 5.3: Topographic cross-section profile of the field where the first measurements with receiver-transmitter distances of 100 m to 600 m were conducted. Map and geographic data provided by [75].

stored in RAM along with the measured RSSI, current transmission distance and the PHY mode. Another button press event would then trigger a state transition to input mode, where the current stored data would immediately be saved on an external micro SD Card through an SPI connection with a R/W adapter. This ensured that writing to the micro SD Card would not interfere with the scanning tasks of the device, while minimizing data loss due to certain events such as power loss.

The source code for both the central and peripheral device along with the obtained raw and processed results are located in [74].

Testing environment

The experiment was conducted in the outdoors on a field as shown in Figure A.4 in Appendix A. The field was chosen for its relatively open and flat area with a low presence of obstacles that can cause shadowing effects as described in Section 3.1. Figure 5.3 shows the topographic cross section profile with meters above sea level or MASL of the field where the first 100 m to 600 m of the experiments were conducted. An aerial photograph of the field, with the cross section marked, is shown in Figure A.2 in Appendix A. Here, the receiver or central device was stationary, while the transmitter or peripheral device was moved further away. The plot shows that LOS was maintained for all the measurement distances, except at the 700 m mark where the landscape dips in altitude.

To facilitate measurements above 700 m whilst maintaining LOS, the transmitter was placed in a stationary position at the 600 m mark emphasized by the red line in FigureFigure 5.3, while the previously stationary receiver was moved back incrementally. Figure 5.4 illustrates the topographic cross sectional profile of this

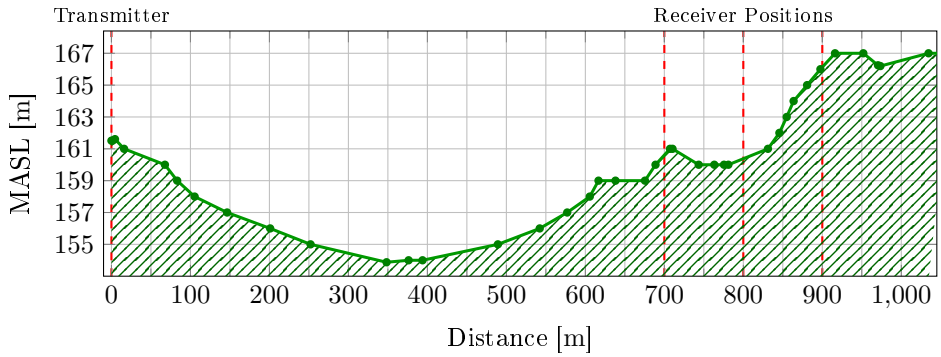

Figure 5.4: Topographic cross-section profile of the field where the measurements with receiver-transmitter distances of 700 m to 900 m were conducted. Map and geographic data provided by [75].

path with the receiver positions marked in red. An aerial photograph of the field, with the cross section marked, is shown in Figure A.3 in Appendix A. Here the LOS was maintained on the 700 m and 900 m mark, whereas small dips in the landscape at the 800 and 1000 m mark could possibly have compromised the LOS to some extent.

5.1.2 Results

Comparing PHY Modes

Using Friis transmission equation solved for the transmission distance as shown in Eq. 3.6, the theoretical transmission range in a LOS situation can be obtained for both the LE and Coded PHY modes. The gain of the receiving and transmitting antenna on the development kit is listed as 0 dBi by the manufacturers and thus $G_t = G_r = 0$ is used. While BLE operates in a range of different frequencies in the 2.4 GHz band, the wavelength can within reason be approximated to $\lambda = 0.125$ m. Finally, the received power can be set equal to the receiver sensitivity on the development kit, resulting in $P_r = -95$ dBm and $P_r = -103$ dBm for the LE and coded PHY mode respectively. The resulting theoretical ranges for different transmission powers, P_t, are tabulated in Table 5.2. As can be seen, the theoretical transmission range is almost three times longer using coded PHY.

Figure 5.5 and 5.6 show the received PDR at each distance for each P_t value in the best case position of the peripheral, i.e. in 90° orientation with a height of 200 cm. None of the tests yielded a PDR of 1, and the maximum PDR obtained was 0.85. This is likely due to the fact that the scanning central must switch between the three advertising channels in order to detect the packet and will miss some of the

Table 5.2: Maximum theoretical transmission range using the nRF52840 DK.

P_t [dBm]	LE PHY [m]	Coded PHY [m]
-20	56	141
-16	89	223
-12	141	353
-8	223	559
-4	353	887
0	559	1405
3	790	1985
4	887	2227

packets as a result. At 1000 m, no packets were detected by the receiver at all, which is likely the result of loosing LOS due to a dip in the landscape as shown in Figure 5.4 and obstructions such as a small line of trees. A very small amount of packets were detected at the 800 m mark in the coded PHY case, which is likely the result of another dip in the landscape, as shown in the topographical cross-section.

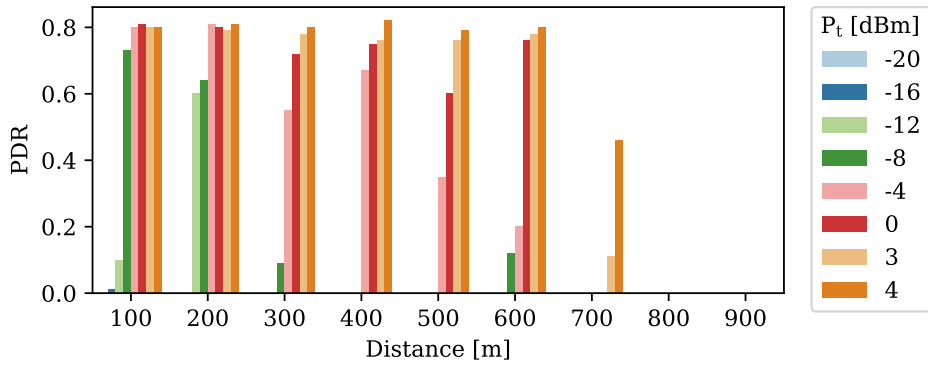

Figure 5.5: PDR for each distance and P_t using LE PHY, a 200 cm height and the 90° orientation for the peripheral device.

The results seem to resemble the predicted theoretical distances to some extent. For instance, in the case of LE PHY with $P_t = 0$ dBm, the packets are received with a high PDR value at 600 m, but no packets are received at 700 m while the propagation model predicted a maximum transmission range of 559 m. On the other hand, for $P_t = -4$ dBm, packets are received at 600 m despite the propagation model predicting a maximum range of 353 m. However, the PDR value did decrease rapidly beyond 400 m. Moreover, in the case of coded PHY using $P_t = -8$ dBm, no packets were received beyond 600 m, which is not too far off the predicted maximum transmission range of 559 m. Lastly, the results confirm that a higher P_t value generally yields higher PDR values, especially at longer distances.

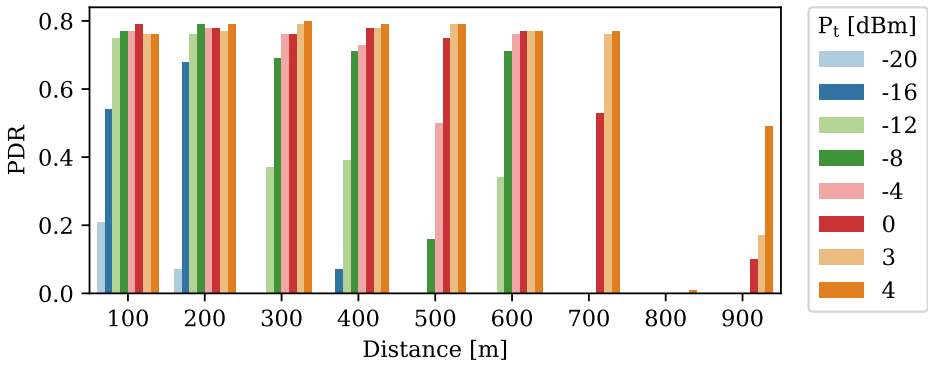

Figure 5.6: PDR for each distance and P_t using coded PHY, a 200 cm height and the 90° orientation for the peripheral device.

A direct comparison of the LE and coded PHY implementation is provided in Figure 5.7. Here, the average PDR based on all angles, heights and P_t values are shown for each distance. The results show that coded PHY generally outperforms LE PHY in terms of average PDR value and transmission range, regardless of orientation, height and P_t value.

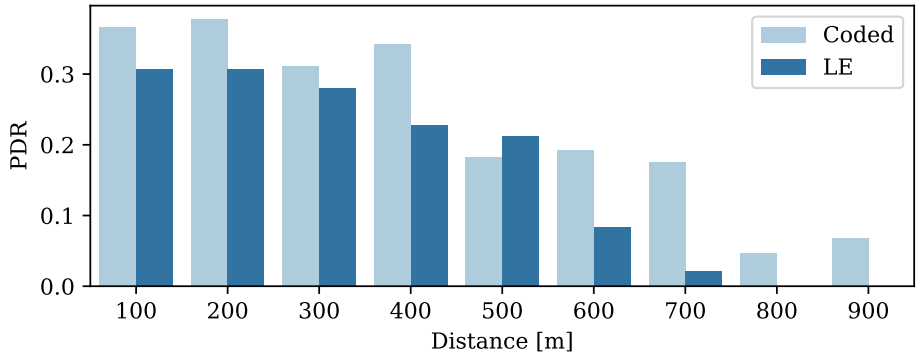

Figure 5.7: Average PDR performance of LE versus coded PHY using all angels, heights and transmit powers.

A Power Profiling Kit or PPK from Nordic Semiconductor was used to measure the current consumption of the SoC during a transmission of an advertising packet. This was achieved by connecting the PPK to the nRF52840 DK and using an external power supply to ensure correct measurements where the device operate at 3.3 V. From here, an application called nRF Connect with built-in power profiler software from Nordic Semiconductor, was used to read out the measured current with a sampling interval of 0.13 ms. Figure 5.8 show the current consumption

of the device when transmitting a single non-connectable undirected advertising packet using LE PHY, $P_t = 4\,\text{dBm}$ and a payload containing the the manufacturer specific data consisting of a company identifier and three additional bytes. These bytes described the tag ID, the current P_t value being used and a measurement sequence number. Figure 5.9 show the current consumption of transmitting an advertising packet using the same parameters as in Figure 5.8, except using coded PHY.

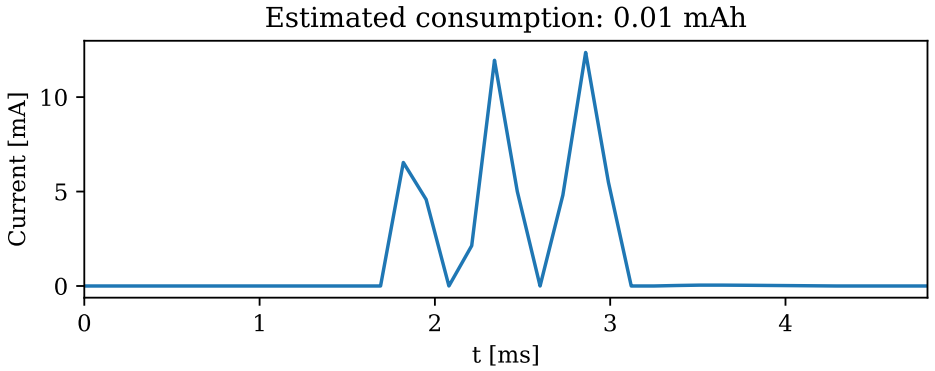

Figure 5.8: Current consumption of a LE PHY advertisement using $P_t = 4\,\text{dBm}$.

By summarizing the sampling values and multiplying with the sampling rate, an estimation of the power consumption in mAh can be found. The calculated power consumption for LE PHY and coded PHY with $P_t = 4\,\text{dBm}$ are presented as the titles in Figure 5.8 and 5.9 respectively. The plots show that advertising using coded PHY leads to a severe penalty in power consumption, with an eight times increase compared to LE PHY. However, using coded PHY can achieve a similar performance, in terms of range and PDR, compared to LE PHY with a much lower P_t value, somewhat mitigating this penalty.

In conclusion, the use of coded PHY seems to be advantageous in terms of transmission range and PDR despite the increased power consumption and will be used by default in subsequent experiments and when presenting the results in the following sections.

Angle and Height

Figure 5.10 shows the average PDR for each angle and distance with both heights and all P_t values. The results confirm that the average PDR is affected by the angle of the transmitting antenna and illustrates that careful consideration of how the ear tag antenna is implemented is necessary to ensure an acceptable performance of the system.

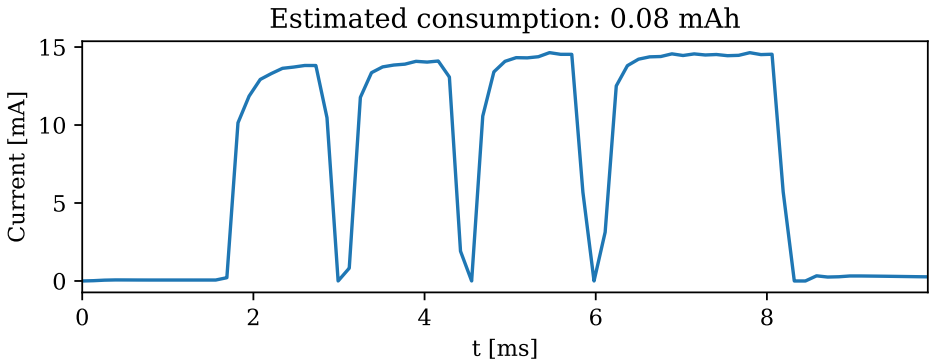

Figure 5.9: Current consumption of a coded PHY advertisement transmission using $P_t = 4\,\text{dBm}$.

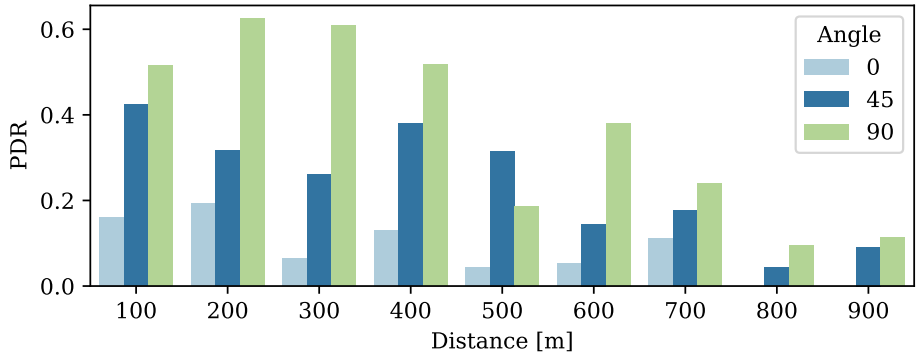

Figure 5.10: Effect on average PDR when using three different angles with both heights and all P_t values.

Figure 5.11 shows the average PDR for both of the heights used in the investigation with all angles and P_t values. The results show that the height difference yields largely inconclusive results as 200 cm seems to outperform 70 cm at some distances and vice versa. Moreover, in retrospect, the particular experiment does not translate well into an ear-tag peripheral to UAV-enabled central scenario as the LOS environment will significantly differ.

RSSI Measurements

Figure 5.12 show a boxplot for the measured RSSI values at each distance of the three angles investigated given a specific height of 200 cm and $P_t = 4\,\text{dBm}$. The

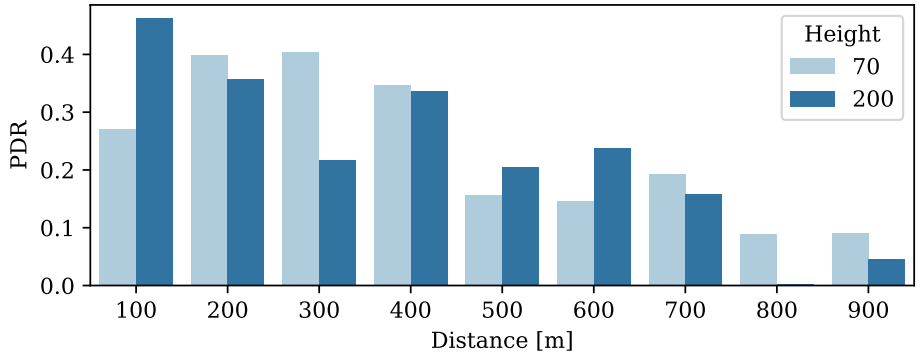

Figure 5.11: Effect on average PDR when using the two different heights with all angles and P_t values.

median value is shown as a line on the boxes while outliers are marked with diamonds.

Based on the widespread boxes of the plot, it is evident that RSSI values obtained for a given antenna orientation and distance tend to vary greatly. Moreover, the measured RSSI values differ significantly depending on the antenna angles used even at the same distance. This same trend was observed regardless of Pt and peripheral height. In other words, an RSSI measurement can yield a wide range of values, even under the same testing conditions, and is highly dependent on the orientation of the transmitting antenna, both in terms of antenna directivity and polarization mismatch. Figure 5.13 shows the distribution of measured RSSI values in a histogram at distances from 100 to 600 m. This further show that a single RSSI measurement is generally unreliable for distance estimation.

Since a single RSSI measurement can not be considered reliable in terms of distance estimation, several statistical approaches applied to multiple RSSI values can be used. Figure 5.14 show the maximum, minimum, arithmetic mean, median and mode of the measured RSSI value at each distance given the 200 cm height, 90° angle and $P_t = 4\,\text{dBm}$. The figure also contains a graph showing the free space propagation model as described by Eq. 3.7 using $PLF = 1$ and $G_t = G_r = 0\,\text{dBm}$ for $n = 2$. Finally, the log distance path loss model, described by Eq. 3.8 is plotted with a measured $P_0 = -40\,\text{dBm}$ at $d_0 = 1\,\text{m}$ for $n = 2$. The distance is plotted using a logarithmic scale. Corresponding plots showing a similar trend with different P_t values are shown in Figure A.5, A.6 and A.7 in Appendix A.

The figures show that the log distance path loss propagation model is yield practically identical results to the free space model with a PLF value of 1. Higher values for n would shift the graphs towards lower RSSI values and yield even less accurate distance estimates. Moreover, the models routinely underestimated the measured

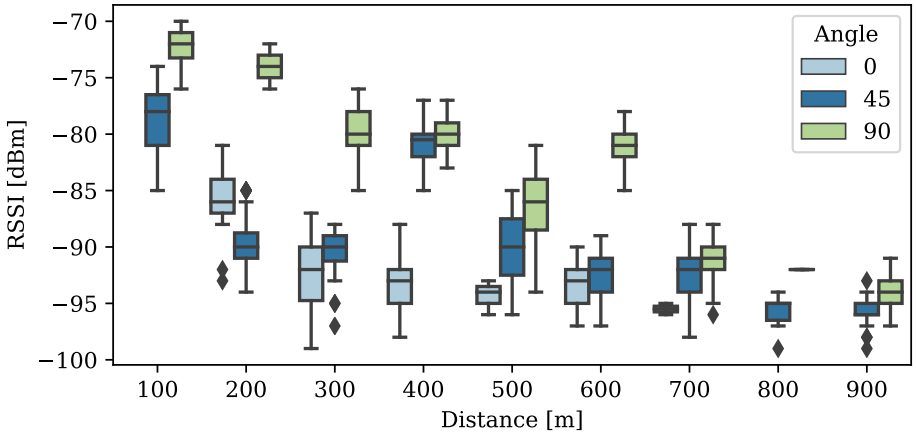

Figure 5.12: Boxplot of measured RSSI values at each distance for each angle with a height of 200 cm and $P_t = 4$ dBm

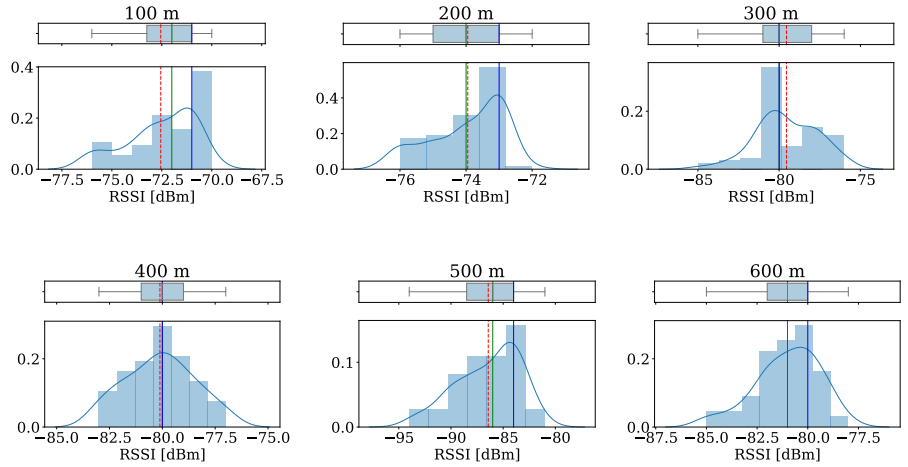

Figure 5.13: Histograms showing the distribution of the measured RSSI values with a height of 200 cm, a 90° angle and $P_t = 4$ dBm for 100 to 600 m. The red line shows the mean value, the green shows the median and the blue is the mode (most common value).

RSSI values of the system by approximately 5 to 10 dBm, with the exception of some minimum values at longer distances. The models could thus be calibrated by adding a correctional factor or offset of 5 dBm to yield more accurate distance estimates for the given stationary system. Furthermore, the results exhibit a trend of

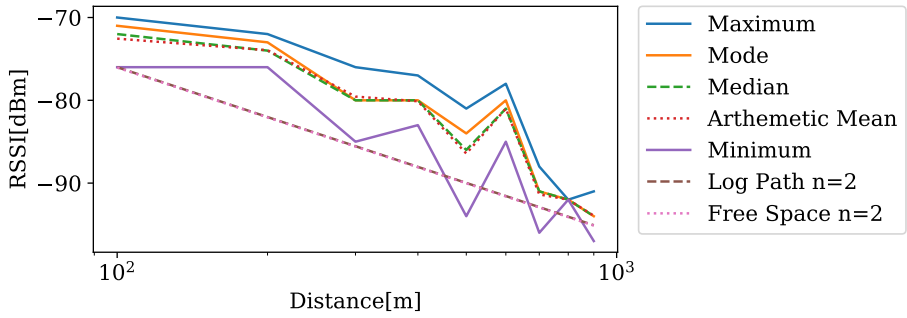

Figure 5.14: Measured RSSI values at each distance with a height of 200 cm, 90° orientation and $P_t = 4$ dBm versus the free space and log distance propagation models using an attenuation constant value of $n = 2$.

decreasing RSSI values with increasing distance, as expected. However, the trend is not linear like the models predict. For instance, the most prevalent RSSI value at 600 m is approximately equal to that of 300 m. This is likely due to constructive interference from reflections, resulting in large uncertainties related to distance estimation.

Finally, plotting for the 0° position yields similar results as shown in Figure 5.15. Herein, the same values are used for the log distance propagation model. The free space propagation model is plotted using a PLF value equal to zero due to the polarization mismatch, which is approximated to −20 dBm in practice. Moreover, in the 0° position, the antenna should theoretically have an infinitely negative gain in the direction of the receiving antenna which should result in no packets being received. However, this is not the case as can be seen on the figure. This is likely due to the fact that the implemented PCB antenna is not strictly equal to a theoretical quarter wavelength monopole antenna, as illustrated in Figure 3.2, and is rather L-shaped and flat as shown in Figure 5.1. Thus, the radiation pattern will also differ to that of a theoretical monopole antenna. This could result in signals being transmitted from the short side of the L-shape, which is in the elevation plane. Another possibility is that the signal is reflected off the ground and transmitted towards the receiver. This will be discussed further in the next section. The plots show that the measured RSSI values are more linear in the 0° case and that the log path models seems to yield more accurate distance estimations. Moreover, using the low PLF value in the free space propagation model seems to overestimate the impact of polarization mismatch.

In conclusion, the preliminary results show that several RSSI measurements would have to be performed in order to obtain a more reliable distance estimate due to the unreliability of single measurements. However, which type of statistical approach should be used is largely inconclusive. It is possible to argue that the measurement

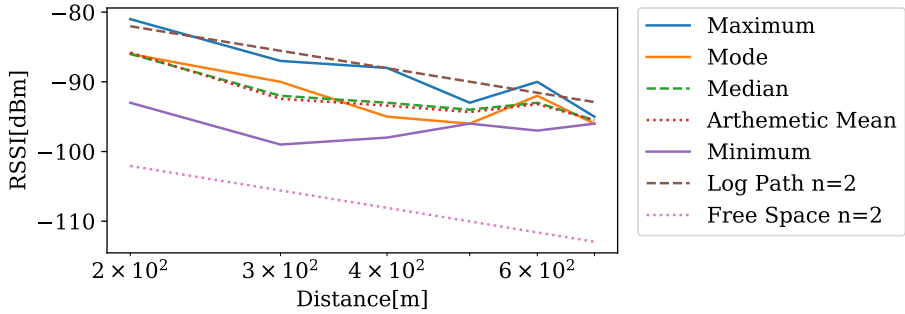

Figure 5.15: Measured RSSI values at each distance with a height of 200 cm, 0° orientation and $P_t = 4$ dBm versus the free space and log distance propagation models using an attenuation constant value of $n = 2$.

with the largest RSSI value is the signal which has experienced the least fading and other signal attenuation effects and should therefore most accurately represent the free space propagation model. However, this reasoning does not take the possibility of constructive or destructive interference caused by multipath propagation into consideration. Thus, based on these preliminary results, the free space and log distance propagation models does not seem to accurately predict the transmission distance in a LOS situation on the ground. Finally, the measured RSSI value is largely susceptible to the orientation of the transmitting antenna. This could be detrimental for a RSSI-based multilateration scheme, where the antenna orientation on the ear-tag is directly determined by the orientation of the head of the sheep and the orientation of the receiving antenna on the UAV is determined by the UAV orientation.

5.2 Aerial Investigation

This section presents experiments conducted to establish the effective transmission range of the system when using coded PHY and a quadcopter drone. Moreover, the impact of antenna orientation and polarization on the transmission range and PDR was further explored with an additional experiment testing the utility of a circularly polarized receiving antenna on the UAV. Finally, the effects of multipath propagation were investigated by comparing the experimentally obtained results to those predicted by the two ray ground reflection propagation model, the log distance path loss with multi-path fading model and the Egli model.

5.2.1 Methodology

Device Selection

The UAV was implemented as a relatively cheap quadcopter drone built from a kit. The drone could be controlled manually through a smartphone interface connected to a controller or set to follow a predetermined path for autonomous operation. The drone is depicted in Figure B.1 in Appendix B. While the drone has an onboard GPS receiver and is capable of interfacing with the nRF52840 DK through either UART, SPI or I2C, it was decided that designing an independent module was desireable for reasons outlined in Chapter 4.

Thus, a GPS receiver PCB shield was used to obtain and log the location of the UAV through an UART interface to the nRF52840 DK. The shield contains a FGPMMOPA6H GPS receiver module which uses the MTK3339 chipset from MediaTek Labs. It is listed as having an accuracy of 3 m with a 50 % circular error probability (CEP) in the datasheet [76].

In order to test the performance of a circularly polarized receiver antenna on the UAV, a simple four blade 2.4 GHz cloverleaf antenna, which is depicted in Figure B.2 in Appendix B, was used. The antenna has an RP-SMA plug interface which was connected to a MXHS83QE3000 antenna measurement probe from Murata Electronics through a RP-SMA to SMA adapter. The probe was further connected to the kit through a SWF connector, in which an internal switch disconnects the onboard antenna of the nRF52840 DK [72] and ensures an impedance match of 50 Ω.

Device Configuration and Set-Up

The experiments were conducted in the same field as described in Section 5.1. Similar to the preliminary investigation, the peripheral devices were configured to transmit 100 advertising packets with five different RF powers using coded PHY and four different antenna orientations at a single height above ground. The central device was mounted on the UAV such that the PCB antenna was horizontally polarized as shown in Figure B.1 and later equipped with the cloverleaf antenna as shown in Figure B.3. Two peripheral devices were placed in the same location as where the transmitter was located in Figure 5.4 at the height of an average Norwegian sheep and their GPS position was recorded using the GPS receiver.

One of the devices was mounted with a horizontal antenna polarization whereas the other peripheral was mounted with a vertical polarization. At first, both devices were oriented in a so called *best case* orientation before the experiment was repeated using the *worst case* orientation. The peripheral orientations were chosen to investigate the impact of antenna polarization mismatch on PDR, and to

establish a baseline to which the performance of a circularly polarized antenna on the UAV can be compared. These configurations will be explained in greater detail below. The UAV was configured to follow a predetermined path, roughly equal to the path depicted in Figure A.3, where it would remain stationary at a 100 m altitude for the duration of receiving the sequence of advertising packets from each peripheral device. The UAV would then proceed to incrementally move 50 m away from the peripheral devices along an overhead line where another measurement was conducted. This was repeated until the drone reached an overhead distance of 1000 m.

Table 5.3: All combinations of parameter values in the aerial investigation.

Parameters	Values
P_t [dBm]	4, 3, 0, -4, -8
PHY Mode	Coded
Advertising Interval [ms]	20
Advertising Packets	100
Peripheral Orientation	V_{BC}, H_{BC}, V_{WC}, H_{WC}
Peripheral Height [cm]	70
Transmission Distance [m]	50, 100,..., 1000
UAV Altitude [m]	100
Central Antenna Polarization	LPH, RHC

All parameter combinations used in the experiments are listed in Table 5.3. It was decided to use several P_t values to investigate the tradeoff between the effective transmission range with a certain PDR and the power consumption when using a UAV. Based on the results of the previous experiment, the -12, -16 and -20 dBm values were omitted due the their low performance. The advertising interval and number of packets remained the same as the previous field experiment.

The peripheral devices were configured to transmit non-connectable undirected advertising packets using the S140 SoftDevice and coded PHY for additional range. The payload of the packets contained manufacturer specific data describing the tag ID, the transmission power used and the measurement number. The measurement number would be incremented after the transmission of all the packets were completed while the tag ID could be selected using buttons and a LED interface on the development kit. Moreover, to ensure that the measurements were performed reliably in terms of a fixed transmission distance, the peripheral devices were configured to only start transmission upon a button press from an external panel when the UAV had reached the next transmission distance. This also ensured that the peripheral devices did not interfere with each other by transmitting simultaneously. Moreover, the external panel was used to minimize shadow effects caused by the hand obstructing the LOS.

The UAV altitude was somewhat arbitrarily chosen such that a minimal distur-

bance of the sheep is ensured while also complying with Norwegian drone regulation regarding maximum altitudes without a licence and ensuring that the effective coverage is not overly reduced due to a high altitude. The transmission distances were chosen to increase the resolution of the measurements compared to the preliminary investigation while still ensuring that the UAV could reach the farthest distance on a single battery charge.

Figure 5.16 show a simplified illustration of the advantages and disadvantages of using vertical versus horizontal polarization on the receiving antenna. If the UAV uses a vertically polarized antenna, the radiation pattern causes a lower gain below the UAV which theoretically reaches zero directly below the UAV. This could be detrimental for the performance of the system when detecting ear tags that are located below the UAV. This is not the case when using a horizontally polarized antenna as can be seen in the figure. In this case, the drawback is that the gain of the antenna theoretically zero in one direction in the plane located at the same height of the antenna due to the torus shape of the radiation pattern. However, this can be considered less problematic as the UAV does not have the same altitude as the ear tags. Considering the low probability of ear tags being located directly on the search path however, the horizontally polarized antenna should be placed parallel to the UAV direction of movement. Regardless, in this particular experiment, the peripheral devices were actually placed directly in the drone path. Thus, the horizontally polarized antenna was mounted perpendicular to the direction of movement, as shown in Figure B.1.

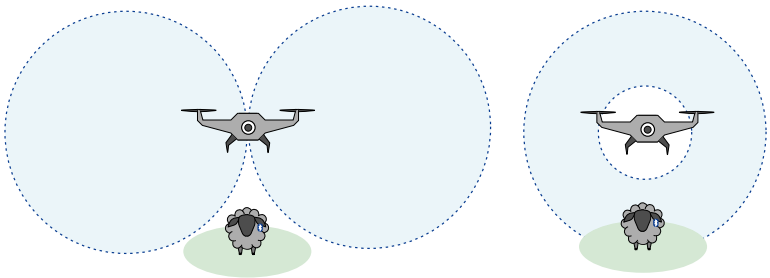

Figure 5.16: Simplified illustration of using vertical (LHS) versus horizontal (RHS) polarization on a UAV

Figure 5.17 show the four different orientations used for the peripheral devices. Simple PCB antennas are usually implemented using a normal PCB trace or wire consisting of a thin conducting metal layer with a certain width and height in the PCB plane. A rule of thumb is that such antennas have the highest directivity perpendicular to the PCB surface because of the difference in width versus depth of the antenna. Moreover, the antenna is located on one side of the board, facilitating minimum obstruction of signal propagation on this side. Thus, the best case orientations depicted in the figure are characterized by the front side of the transmitting development kit facing the front side of the receiving development kit. The best case orientation using a horizontally polarized antenna is denoted H_{BC}

whereas the best case orientation using a vertically polarized antenna is denoted V_{BC}. Conversely, the horizontal worst case orientation, denoted H_{WC}, refers to the case where the peripheral development kit has been rotated 90° relative to the H_{BC} orientation. This results in both a reduced directivity and that the zenith of the antenna, where the gain is theoretically zero, is pointed in the direction of the receiver. Another important consideration is that PCBs are usually implemented with a ground plane which covers the entire board. This is detrimental for signal propagation of a PCB antenna as the ground plane would absorb the EM-waves. For this reason, PCB antennas are usually implemented with no ground plane surrounding the trace as shown in Figure 5.17. However, when placing the development kit with a vertically polarized antenna in the worst case orientation, denoted as V_{WC}, the ground plane will obstruct the signal in the direction of the receiver as can be seen in the figure.

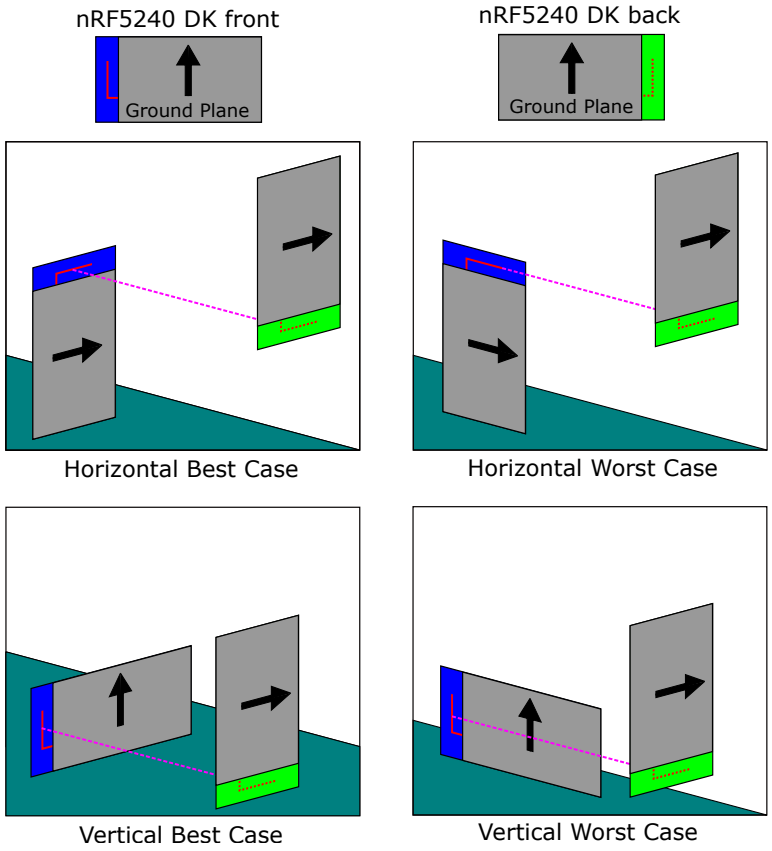

Figure 5.17: Illustration of the best case and worst case orientation of the peripheral devices (LHS device) with different polarizations and a horizontally polarized central (RHS) device.

In the field experiment, the two peripheral devices were initially placed in the H_{BC}

and V_{BC} orientation respectively. After completing the effective transmission range measurements, the devices were mounted with the H_{WC} and V_{WC} orientation and the sequence repeated. Afterwards, the linearly polarized horizontal (LPH) PCB antenna was replaced by the right hand circularly (RHC) cloverleaf antenna on the UAV and the experiment repeated. The cloverleaf antenna was mounted as shown in Figure B.3.

The central device was configured to continuously scan for advertising packets using SoftDevice S140. Upon receiving a packet, the source would be verified using the company specific identifier and the payload data stored on the device along with the RSSI value. In addition, a timer would be started whenever the first packet of a measurement sequence was received, which would trigger an interrupt after the measurement sequence was completed, allowing the device to safely store the payload along with the GPS coordinates from the GPS receiver on the micro SD Card card.

The source code for both the central and peripheral devices along with the raw and processed data can be obtained from [77].

5.2.2 Results

Linearly Polarized Antenna

Figure 5.18 and 5.19 show the measured PDR at each distance for each P_t value with the H_{BC} and V_{BC} orientation respectively. The distances are computed using the logged GPS position of the UAV and the peripheral devices and thus represent the effective transmission range not the actual distance between the devices. Notice that the distance between measurements vary somewhat and that the recorded distances along the abscissa differ slightly between the two plots as the UAV was not able to accurately position itself at $N \cdot 50\,\mathrm{m}$. However, the accuracy is close enough to facilitate a comparison between the two polarizations.

The results show that both the H_{BC} and V_{BC} orientation yield a high PDR at relatively long distances. However, the V_{BC} orientation surprisingly seems to outperform the H_{BC} orientation with marginally higher PDR values at similar distances. Both solutions seem to reliably deliver a PDR value of around 0.7 at the 700 m mark when using a P_t value of 3 and 4 dBm. The results seem to indicate that polarization mismatch does not pose such a significant problem as first assumed. However, notice that zero packets were received at the 50 m mark in the V_{BC} orientation. This is likely due to the disadvantage of the vertically polarized radiation pattern as discussed in Section 5.2.1.

Figure 5.20 and 5.21 show the measured PDR at each distance for each P_t value with the H_{WC} and V_{WC} orientation respectively. The results show worse performance

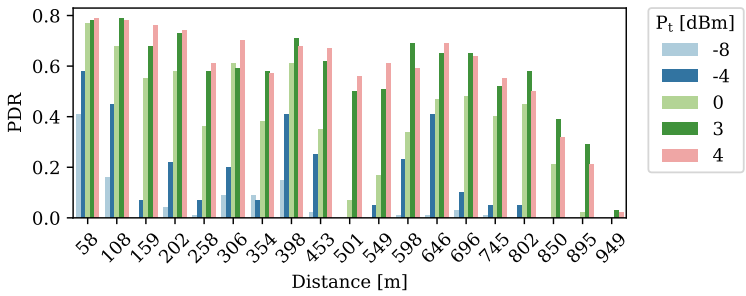

Figure 5.18: PDR for each P_t value and distance in the H_{BC} orientation.

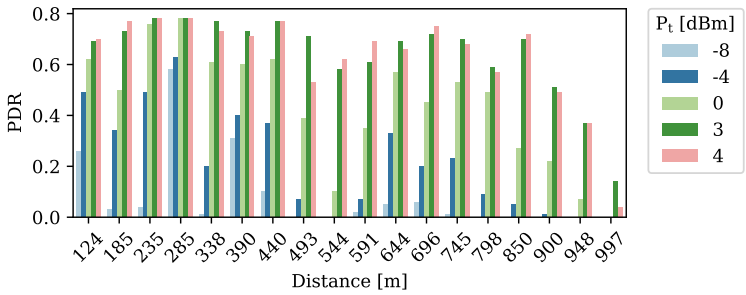

Figure 5.19: PDR for each P_t value and distance in the V_{BC} orientation.

for both orientations. However, the H_{WC} orientation still achieves a surprisingly good performance with a PDR of well over 0.7 at the 600 m mark with P_t values of 3 and 4 dBm. Despite this, the H_{WC} orientation generally exhibit a significantly higher degree of PDR fluctuation for each distance with PDR values going as low as 0.2 with the higher P_t values at the 450 m mark while abruptly approaching 0.7 at the following 500 m distance. This is likely due to constructive and destructive interference caused by ground reflections.

The V_{WC} orientation performed significantly worse in comparison. After the 100 m mark, the PDR decreases rapidly even for the higher P_t values. As previously noted, the polarization mismatch does not seem to result in a significant reduction in PDR performance and effective transmission range. The poor performance is thus likely a result of the ground plane on the development kit causing signal fading.

Generally, the result seem to indicate that the implemented PCB antenna on the nRF52852 DK have a higher degree of omnidirectionality than first assumed and that polarization mismatch is not detrimental for the performance of the system. However, the results also indicate that the system is susceptible to multipath propagation. Indeed, the problem seem to manifest more clearly for lower transmission powers in general. For instance, note that in Figure 5.18, the PDR drops below 0.1

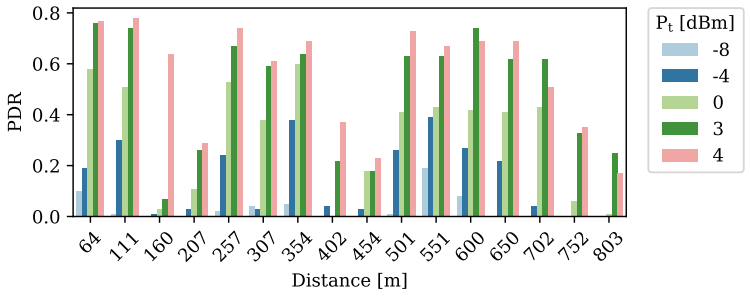

Figure 5.20: PDR for each P_t value and distance in the H_{WC} orientation.

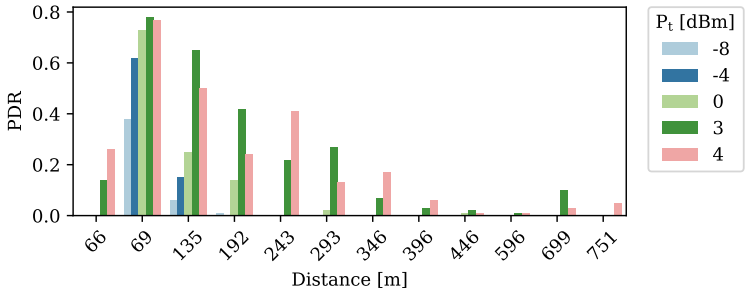

Figure 5.21: PDR for each P_t value and distance in the V_{WC} orientation.

at the 500 m mark when using 0 dBm and that no packets are received for lower P_t values. In contrast, 3 and 4 dBm achieves a PDR above 0.5 at the same distance. Moreover, in the H_{WC} orientation, the directivity is likely lower in the direction of the UAV, as discussed in Section 5.2.1, causing a smaller signal power to be transmitted in that direction. As a result, the system is more susceptible to multipath fading.

Indeed, Figure 5.22 and 5.23 show the average received RSSI value at each distance and P_t value for the H_{BC} and H_{WC} orientation respectively. Observe that the RSSI values are generally lower than the H_{WC} orientation for the same P_t values and tend to fluctuate more as a result. Moreover, in the H_{BC} orientation, the 4 dBm value tends to be less susceptible to the fluctuation compared to the rest, although the effect is still present. Thus, it is likely necessary to use a P_t value of 3 dBm or larger in the implementation of the system to achieve a reliable effective transmission range beyond 400 m.

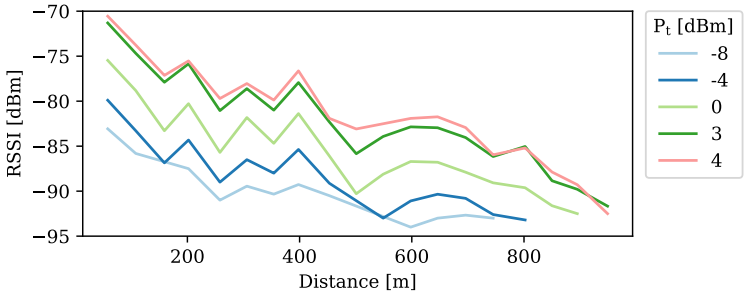

Figure 5.22: Measured average RSSI for each P_t value and distance in the H_{BC} orientation.

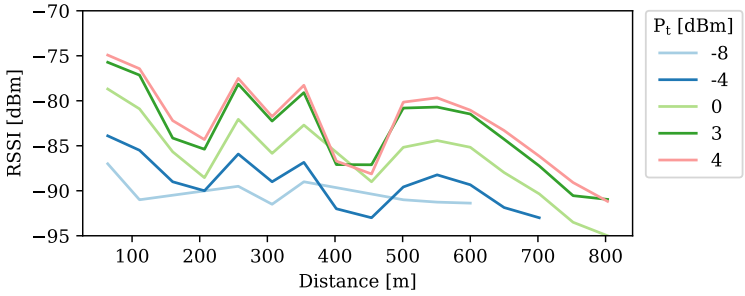

Figure 5.23: Measured average RSSI for each P_t value and distance in the H_{WC} orientation.

Circularly Polarized Antenna

As described in Section 3.1.2, a CP antenna can receive transmissions from an LP antenna with a penalty in received signal strength of −3 dBm. As polarization seems to be less problematic than anticipated, the use of a CP antenna should only result in the signal being more susceptible to multipath fading. Figure 5.24, 5.25, 5.26 and 5.27 show the measured PDR for each P_t value and distance in the H_{BC}, V_{BC}, H_{WC} and V_{WC} orientation respectively. The results show a rather poor performance of the cloverleaf antenna in all the orientations. Here the multipath fading effect is made even more apparent with fluctuation of the PDR values.

In conclusion, the circularly polarized cloverleaf antenna resulted in an overall worse performance compared to using the onboard PCB antenna of the development kit.

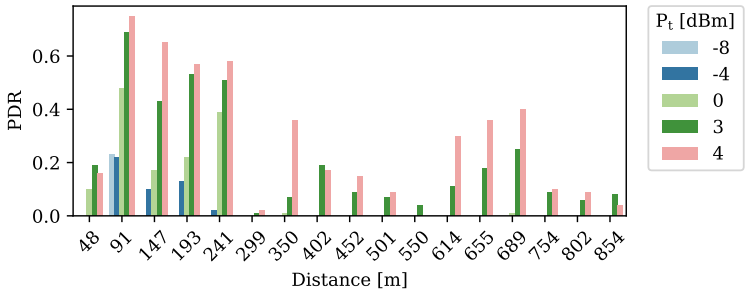

Figure 5.24: PDR for each P_t value and distance in the H_{BC} orientation.

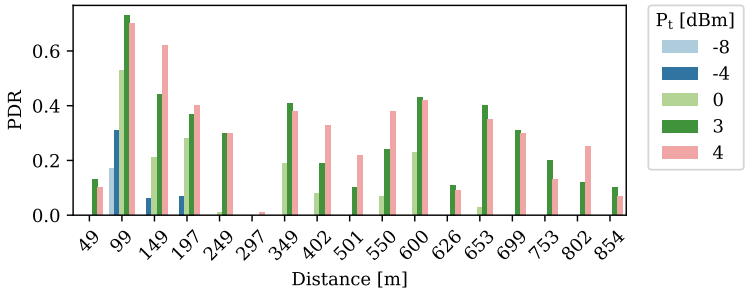

Figure 5.25: PDR for each P_t value and distance in the V_{BC} orientation.

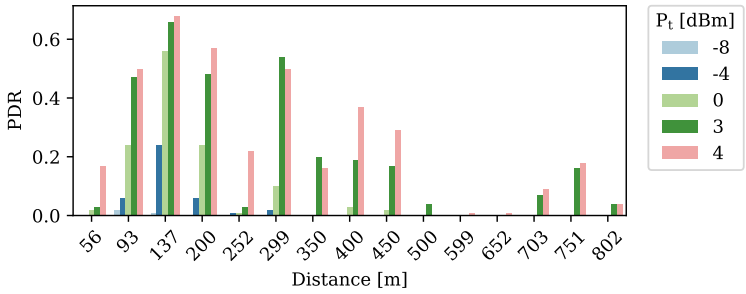

Figure 5.26: PDR for each P_t value and distance in the H_{WC} orientation.

Propagation Models

With the experiment conducted using the UAV, the propagation models considering the height difference between the devices described in Section 3.1.3 can be meaningfully compared to the results. As discussed above, the system seem to suffer from multipath fading to a large extent. Exactly this phenomenon is considered in the two ray ground reflection propagation model described by Eq 3.15. Using

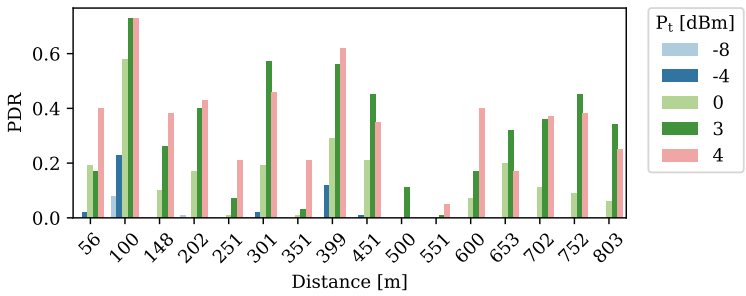

Figure 5.27: PDR for each P_t value and distance in the V_{WC} orientation.

$G_{los} = G_{ref} = 1$, $\lambda = 0.125\,\text{m}$, $h_t = 0.7\,\text{m}$, $h_r = 100\,\text{m}$ and a typical value for the relative permittivity in partially wet soil, $\epsilon_r = 9$ [78], the expected RSSI can be plotted for each distance. Figure 5.28 and 5.29 show the measured PDR value for $P_t = 0\,\text{dBm}$ at each distance compared to the two ray ground reflection model for the LP H_{BC} and LP V_{BC} orientations. Figure 5.30 show a similar plot with the device in the H_{WC} orientation using the CP antenna and $P_t = 4\,\text{dBm}$.

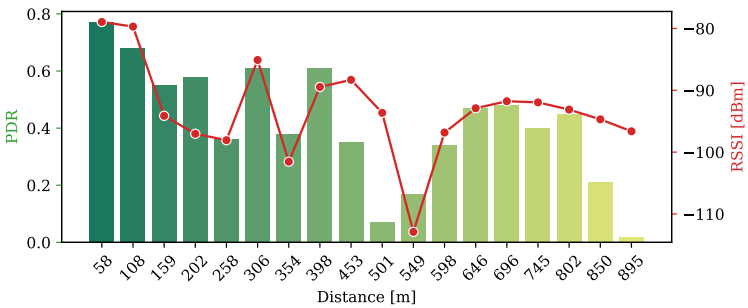

Figure 5.28: PDR with $P_t = 0\,\text{dBm}$ for each distance in the LP H_{BC} orientation compared to the expected RSSI value using the two ray ground reflection model.

The figures indicate a clear relationship between expected RSSI value and experimentally obtained RSSI value at a given distance and transmission power.

To evaluate the accuracy of using RSSI measurements for distance estimation, the log distance path loss with multipath fading model, the two ray ground reflection model and the Egli model can be plotted using the same parameter values as described above along with the average measured RSSI values for each distance. Figure 5.31 show this for the H_{BC} orientation with a LP antenna and $P_t = 0\,\text{dBm}$. Here, the two ray ground reflection model seems to accurately predict the increase and decrease in RSSI value. The multipath log distance model seems to be a good approximation of the lowest values in the two ground reflection estimations. However, the estimated value seems to be overly pessimistic compared to the measured

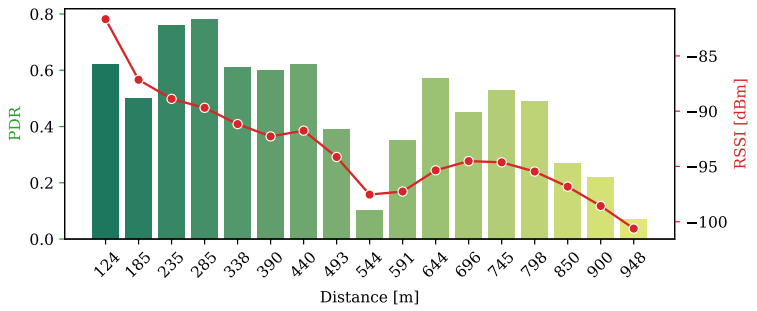

Figure 5.29: PDR with $P_t = 0\,\text{dBm}$ for each distance in the LP V_{BC} orientation compared to the expected RSSI value using the two ray ground reflection model.

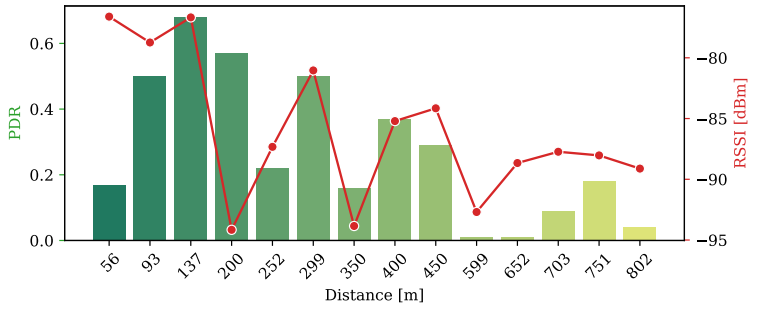

Figure 5.30: PDR with $P_t = 4\,\text{dBm}$ for each distance in the CP V_{BC} orientation compared to the expected RSSI value using the two ray ground reflection model.

values. The Egli model seems to follow a similar curve as the multipath log distance model, but with higher RSSI values in general.

On the other hand, the two ray model does not necessarily achieve such accurate estimation results in other cases. Figure 5.32 show the same plot with a H_{BC} orientation, but using the CP antenna and $P_t = 4\,\text{dBm}$. While the measured RSSI value better overlap with the predicted value range, the prediction of peaks and valleys is less accurate.

Figure 5.33 and 5.34 show a similar plot with a V_{BC} LP and V_{WC} CP orientation and a P_t value of 4 dBm. Observe that the oscillation of the two ray ground reflection model is significantly reduced when using vertical polarization. For the V_{BC} LP case, the measurement seem to closely follow the shape of the two ray ground reflection estimation curve. However, the measured RSSI value is generally significantly higher than the estimation. As a result of the decrease in oscillations, the multipath log distance model seems to more accurately reflect the more precise two ray ground reflection model. The Egli model seems to be less precise for

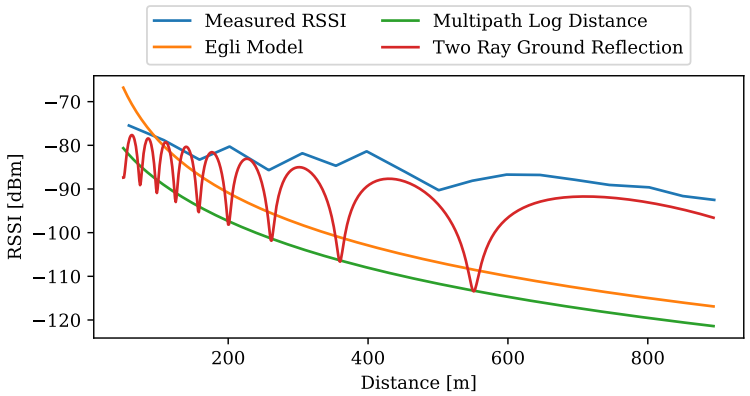

Figure 5.31: Measured RSSI values compared to the propagation models that consider height difference of the antennas, here with a H_{BC} LP orientation and $P_t = 0\,\text{dBm}$.

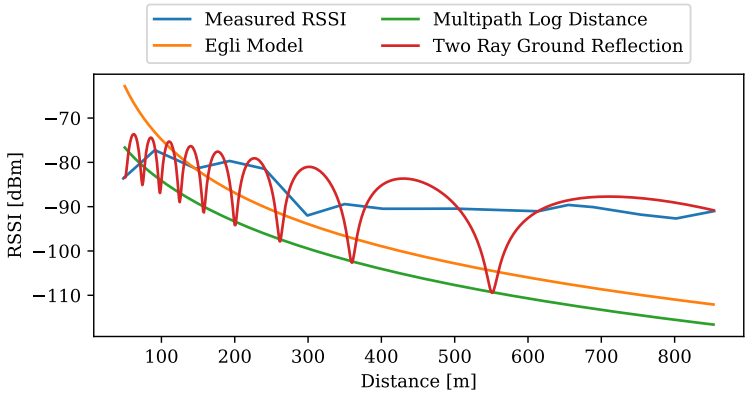

Figure 5.32: Measured RSSI values compared to the propagation models that consider height difference of the antennas, here with a H_{BC} CP orientation and $P_t = 4\,\text{dBm}$.

vertically polarized signals. In the V_{WC} CP plot, the measurements coincide with the two ray ground reflection model to a high degree, both in terms of the shape of the curve and the predicted values.

Finally, Figure 5.35 show another similar plot with a V_{WC} orientation and the LP antenna with a P_t value of 0 dBm. Here, the measured RSSI value seem to correspond closely to the multipath log distance model.

In conclusion, the two ray ground reflection model show a high degree accuracy when it it comes to predicting the overall shape of the graph for the measured

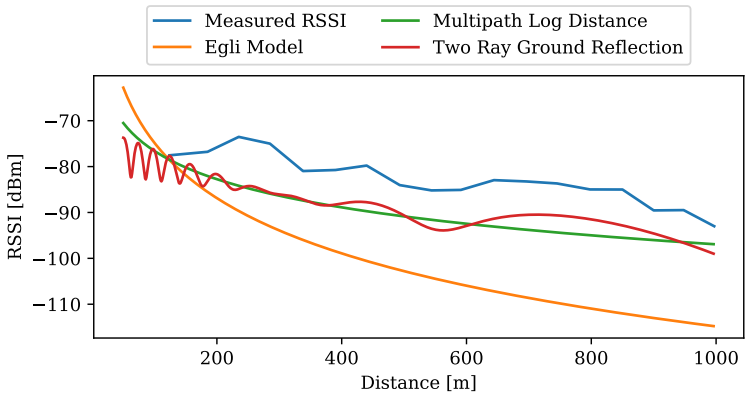

Figure 5.33: Measured RSSI values compared to the propagation models that consider height difference of the antennas, here with a V_{BC} LP orientation and $P_t = 4\,\mathrm{dBm}$.

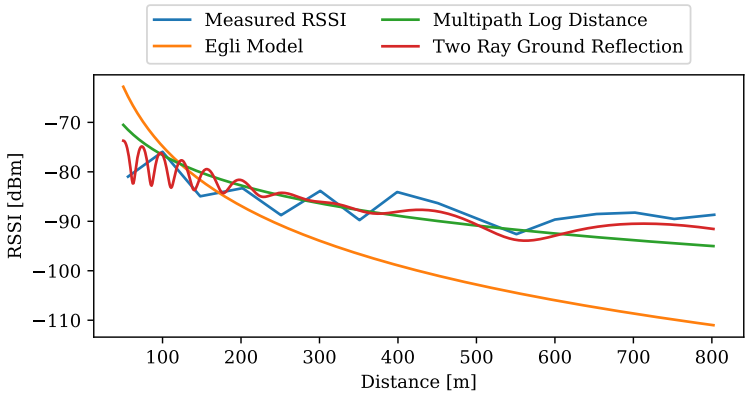

Figure 5.34: Measured RSSI values compared to the propagation models that consider height difference of the antennas, here with a V_{WC} CP orientation and $P_t = 4\,\mathrm{dBm}$.

RSSI values at a given distance. However, depending on the orientation of the transmitting device, the actual RSSI value can differ significantly. Moreover, the accuracy of the model further implies that using RSSI for distance measurements in such a system will yield inaccurate results because one measurement can correspond to multiple distances. However, this effect can be reduced by using a vertically polarized transmitting antenna. Thus, if RSSI-based distance measurements should be performed, the best approach is likely to use the multipath log distance model with a calibrated offset and a vertically polarized transmitting antenna, since it yields a single distance per measured RSSI value.

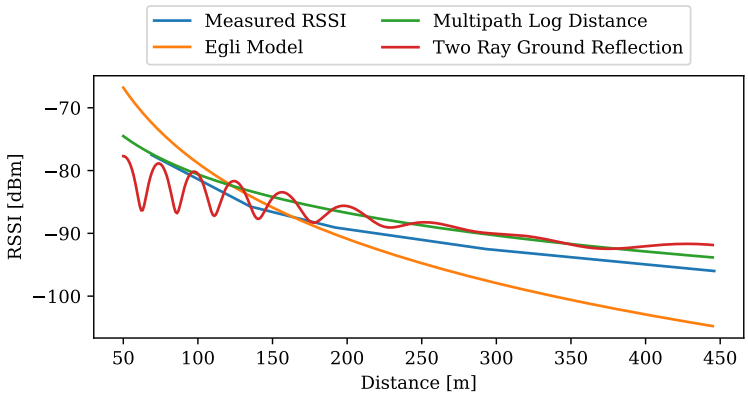

Figure 5.35: Measured RSSI values compared to the propagation models that consider height difference of the antennas, here with a V_{WC} LP orientation and $P_t = 0\,\text{dBm}$.

System Parameters

As previously stated, the use of the CP cloverleaf antenna resulted in an overall worse performance of the system. Thus, the onboard LP PCB antenna will be used going forward. Both the H_{BC} and V_{BC} orientation resulted in a relatively high effective transmission range. However, the V_{WC} orientation suffered a much lower performance compared to the H_{WC} orientation. It is certainly possible to design an ear tag using a vertically polarized PCB antenna that will not suffer from ground plane interference like the V_{WC} orientation was subjected to in this experiment. This would, however, require a larger designated antenna area area without a ground plane which would increase the overall size of the PCB, as shown in Figure 5.36. It seems that a better approach is to use a horizontally polarized antenna with an L-shape, where an added benefit is a larger degree of omnidirectionality, making the system less vulnerable to the orientation of the ear of the sheep. Finally, the use of a horizontally polarized antenna eliminates the problem with reduced directivity towards the sky when using a vertically polarized antenna.

Based of the presented results, an effective transmission range of $r_{eff} = 600\,\text{m}$ with an expected $PDR = 0.7$ for an RF transmission power of $P_t = 3\,\text{dBm}$, is selected for this system. As previously discussed, the lower P_t values seems to be too susceptible to multipath fading while a P_t value of 4 dBm and 3 dBm yielded similar results. When optimizing for a low power consumption, the natural choice is thus to use 3 dBm. While the system can achieve considerably longer transmission ranges in practice, a more conservative value for r_{eff} is chosen to ensure an optimal coverage of the searching area.

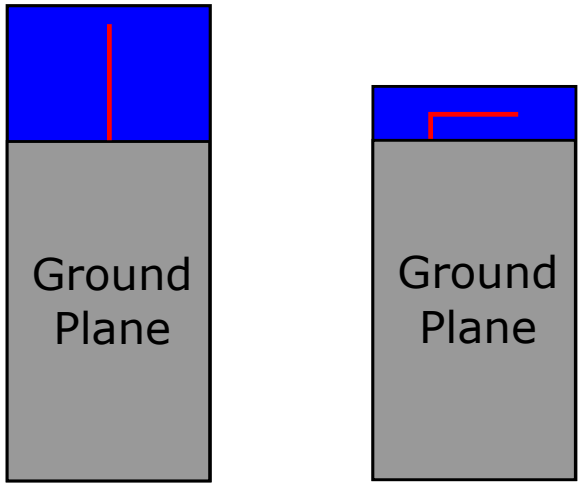

Figure 5.36: Illustration of the required PCB size of a horizontally (LHS) and vertically (RHS) polarized PCB antenna.

5.3 Round Trip Timing Accuracy

Having established the general performance of the system using certain parameters and system configurations, an investigation related to using a round trip timing based scheme for AoA distance measurements was conducted. By transmitting and receiving N round trip timing packets, a single distance measurement can be made. This amount is henceforth referred to as N_{RTT}. The goal of the investigation was to determine the accuracy of the distance measurements for several different values of N_{RTT} and, based on the results, optimize for low energy consumption by determining the lowest value for N_{RTT} to reduce energy consumption while still maintaining an acceptable measurement accuracy. The methodology and results of this investigation are presented in this section.

5.3.1 Methodology

The experiment was set up in a similar fashion to the previous investigation. Thus, the same hardware was used to conduct the investigation. The peripheral device was placed in a H_{BC} orientation at the same location as before with a height of 0.7 m above the ground. The device was configured to start advertising *connectable* undirected advertising packets upon a button press event from the external panel, until either a connection was established or a timer timed out. The advertising interval was set to the minimum value of 20 ms to facilitate a fast connection and thus measurement. Finally, a P_t value of 3 dBm was used. The parameter settings

or values used is shown in Table 5.4.

Table 5.4: Combinations of parameter values in the round trip timing accuracy investigation.

Parameters	Values
P_t [dBm]	3
PHY Mode	Coded
Advertising Interval [ms]	20
Peripheral Orientation	H_{BC}
Peripheral Height [cm]	70
Transmission Distance [m]	50, 100,..., 800
UAV Height [m]	100
Central Antenna Polarization	LPH
N_{RTT}	16, 32, 64, 128, 256, 512, 1024
RTT*Series* per Distance	5
Min Connection Interval [ms]	100
Slave Latency [connection events]	2
Supervision Timeout [ms]	4000
Timer Frequency [MHz]	16

The quadcopter drone was equipped with a central device and mounted such that the PCB antenna was horizontally polarized. As with the previous experiment, the UAV used a pre-planned path to autonomously hover at progressively larger distances away from the peripheral device, with 50 m increments, until a distance of 800 m was reached. The UAV used the same altitude of 100 m as before and travelled along the same path as in the previous experiment. The central device was configured to continuously scan for advertising packets and ensure a match of the company specific identifer.

Once an advertising packet was received, the device would transmit a connection requests until a connection was established or a timer timed out. The timer was used to ensure that the central device would not be stuck in an inescapable state if an error occurred. The device was configured to use a connection interval of 100 ms to speed up the communication and thus measurement series. The two following values were chosen somewhat arbitrarily, however the a slave latency of 2 connection events and a supervision timeout of 4 s was used to allow for some packet delivery failure tolerance. Upon establishing a connection, a distance measurement was conducted using 7 different N_{RTT} values in an RTT *series*. From here, the RTT series was repeated 5 times before the UAV was moved to the next location.

A user specific GATT service that facilitated the RTT measurements was implemented on both the slave and master device. In short, upon establishing a connection, the master device would use the service as a client while the slave device acted as a server. The client would then request to use a specific N_{RTT} value

and to enable the RTT measurement through a single connection event. Upon receiving an acknowledgement from the slave device, both devices would terminate the connection. To enable the usage of the radio without the BLE protocol, the SoftDevice was disabled entirely and a bare bones program would handle the measurement. It was also decided to use a single predetermined data channel instead of an advertising channel to minimize interference from other peripheral devices.

During an RTT measurement, the ear tag device would start continuously scanning for RTT packets on the determined channel. The device would additionally enable certain shortcuts in the radio hardware to significantly reduce the dwell time. That is, certain hardware interrupts were enabled to notify the device of the packet being received before the precessing of the packet is complete. This allowed the device to retransmit the packet as soon as the CRC was completed and the transmission source verified. However, in retrospect, this use of the shortcuts introduced jitter in the sequence as the interrupts were not triggered deterministically. For each received RTT packet or upon reaching a timeout from a timer, a counter was incremented and compared to the agreed upon N_{RTT} value. When this value was reached, the device would restart the SoftDevice.

After disabling the SoftDevice, the UAV device would wait for a predetermined amount of milliseconds and then start transmitting RTT packets. Using the same hardware shortcuts, an interrupt would be triggered whenever the payload of the packet had been transmitted. Using the event system of the SoC, a timer hardware peripheral was started upon receiving the payload interrupt event without involving the CPU. Again, this payload interrupt was not deterministic and caused jitter in terms of when the timer was started. However, this was mitigated by clearing or restarting the timer upon receiving an end event, indicating that the CRC bytes had been transmitted. According to the nRF52840 product specification [65], using this configuration ensures that the timer is cleared after a single system clock tick. The timer was configured to run on the internal 32 MHz RC oscillator on the SoC as the nRF52840 DK does not feature a high frequency external crystal oscillator. This results in a timer frequency of 16 MHz. The device would then start scanning for a reply from the ear tag. Upon receiving an address interrupt, indicating that the device had received the address of the packet, the timer would be stopped and captured at an end interrupt issued after the CRC was completed. This also introduced timer jitter as the address interrupt is not triggered deterministically.

To increase the accuracy of the measurements, two devices were placed as close as possible and set up to continuously perform RTT. From here the average number of clock ticks to perform a single round trip transmission was recorded and an offset was found. During a real RTT measurement, the captured timer value would be subtracted by the predetermined offset to find the RTT time described in Section 3.2 and the values stored in a buffer. After completing N_{RTT} measurements, the average value of the buffer was calculated.

An FSM was then implemented on both devices to facilitate the measurements

of different N_{RTT} values in several RTT series. At start-up, the ear tag device would start in an idle mode. Upon a button press from an external button panel, it would start advertising until a connection had been established and a RTT measurement using N_{RTT} packets had been completed. From here the device would automatically restart the advertising. When a connection was established and then terminated *without* enabling the RTT service, the device would go back to an idle mode so that the UAV could change positions. The state of the device would be communicated through the onboard LED interface of the development kit to ensure that the UAV could proceed to the next location or that an error occurred allowing for a new measurement attempt.

The UAV device would the continuously scan for advertising packets. After a connection had been established, the UAV would perform an RTT measurement for the first N_{RTT} value and then continue scanning. The state machine would then change the N_{RTT} value to the next value in an array and the procedure would be repeated for the RTT series. Upon completing 5 such series, the UAV device would initiate a final connection and terminate it without enabling the RTT service, allowing the ear tag device to go back to a idle state.

A weakness with this implementation was that a failed connection would stop the measurement for that distance. This resulted in having to perform several measurement for the some of the distances and not all measurement series were completed as a result. Another weakness with the implementation was that it only allowed for using a single peripheral device, as the central device would have to wait for the next advertising event to transmit a connection request. If a peripheral device A transmits an advertising packet first and another peripheral device B transmits an advertising packet shortly thereafter, the central device would receive the packet from A and try to connect to it. When the measurement is completed, peripheral A would start advertising at the same time as the central starts scanning, meaning that the packet from B is never received. Finally, another weakness is that both devices must disable and re-initialize the SoftDevice each time an RTT measurement is conducted. Re-initializing the SoftDevice is generally costly in terms of power consumption and will decrease the battery lifetime of an ear-tag. How these issues can be mitigated is addressed in Section 5.4.

Finally, for each measurement series, the GPS coordinates of the UAV was stored on the micro SD Card card along with the measured number of timer ticks for each N_{RTT} with the RTT series number. The number of received RTT packets was also stored to ensure measure the PDR. The source code for both devices with raw and processed data is available in [79].

5.3.2 Results

Using Eq. 3.20 with $f_{clk} = 16\,\text{MHz}$ and $c = 299\,704\,645\,\text{m/s}$, the resolution of the distance measurements was determined to be $MPT = 18.73\,\text{m}$. Ideally, the timer measuring the RTT should use a much higher frequency to increase this resolution and a more reliable crystal oscillator. However, the nRF52840 timer peripheral is not designed for higher clock frequencies than running at 16 MHz [65].

Most of the RTT measurements surprisingly achieved a PDR between 0.9 and 1.0, where a majority achieved a PDR above 0.95. This is likely due to the fact that only one transmission channel was used. Measurements achieving a PDR below 0.8 was discarded. This is because a complete implementation of the system would ideally retry an RTT measurement whenever the PDR is too low.

Using the recorded three-dimensional GPS coordinates of the peripheral device and the UAV, the true distance between the devices was calculated for each measurement. That is, the true distance is measured using the height difference between the devices in addition to the longitude and latitude difference. Each distance measurement was thus performed with an individual recorded true distance that would somewhat vary even though the UAV was attempting to hover at the same location. Note that the true distance measurement also has an inaccuracy related to the inaccuracy of the GPS receiver used. With a guaranteed accuracy of 3 m with a 50 % CEP, the true distance is potentially inaccurate with ±6 m for 50 % of the measurements. However, the true distance will be used as measured to evaluate the performance of the RTT distance measurements.

Since the true distance varies for similar measurements, the data was combined using distance bins. That is, the error between the RTT distance measurement and the true distance was first calculated by subtracting the true distance from the measured RTT distance, and then grouped according the the transmission distances showed in Table 5.4. The RTT distances were calculated using Eq. 3.23. Figure 5.37 show the distribution of the error at each N_{RTT} value at each distance bin using a boxplot. The results show that the error tends to be bounded within ±10 m for most of the measurements and N_{RTT} packets.

Figure 5.38 show the arithmetic mean error for each N_{RTT} value at each distance bin. Indeed, on average, the error tends to be relatively small and falls between ±5 m. However, in the 140 m bin and bin values larger than 500 m, the error tends to be larger with ±10 m. Moreover, there seems to be a trend where the system overestimates the distance in shorter ranges and underestimates at larger distances. The reason for this is largely unknown. However, an error significantly smaller than the MPT resolution is achieved in most cases. Finally, it does not seem to be a clear relationship between increasing the N_{RTT} value and the accuracy of the measurement. For instance, the N_{RTT} value of 16 generally performs better than the other cases for distance bins lower than 250 m, but then show a significantly worse performance for longer ranges. In the other extreme, using 1024 packets, the

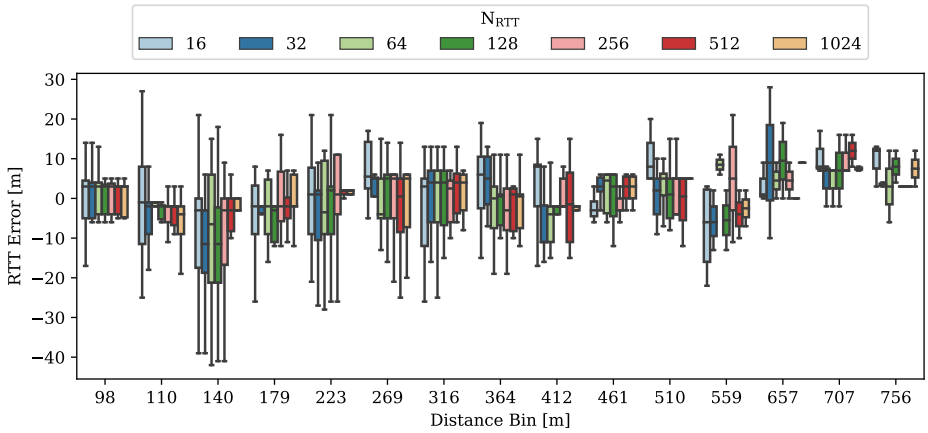

Figure 5.37: Boxplot showing the distribution of RTT errors for different values of N_{RTT} at each distance bin.

error is sometimes lower than the other cases and larger at other times.

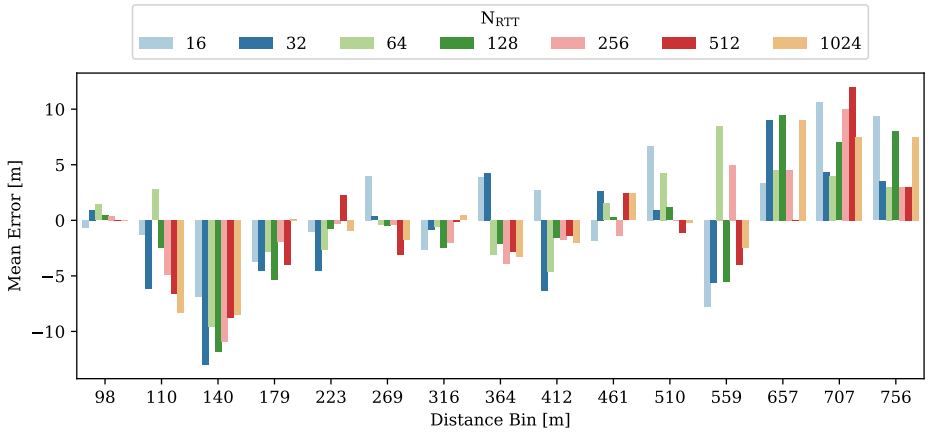

Figure 5.38: Mean RTT error for different N_{RTT} values at each distance bin.

Figure 5.39 show the distribution of error for all distance bins combined for each RTT value. The red mark show the mean value. The figure show that the error range tend to be smaller with larger N_{RTT} values. However, this reduction in error is less than expected with diminishing returns after increasing N_{RTT} from 16 to 32 packets. The jitter in the hardware adds random noise to the measurements, where the impact of this randomness should be reduced when increasing the number of measurements and computing the average. However, a significant design flaw

was discovered after the experiment was completed. When computing the average number of ticks for a single RTT measurement using N_{RTT} packets, the tick value was cast to an integer instead of a float value. Casting from a float to an integer rounds the value down to the nearest integer. Thus, for instance, if an average tick value of 10.98 was measured, the stored value would become 10. That is the difference of measuring a distance of approximately 103 m versus 94 m. This is also likely the reason that the vast majority of outliers reside on the negative error side, meaning that the measured RTT distance is smaller than the true distance.

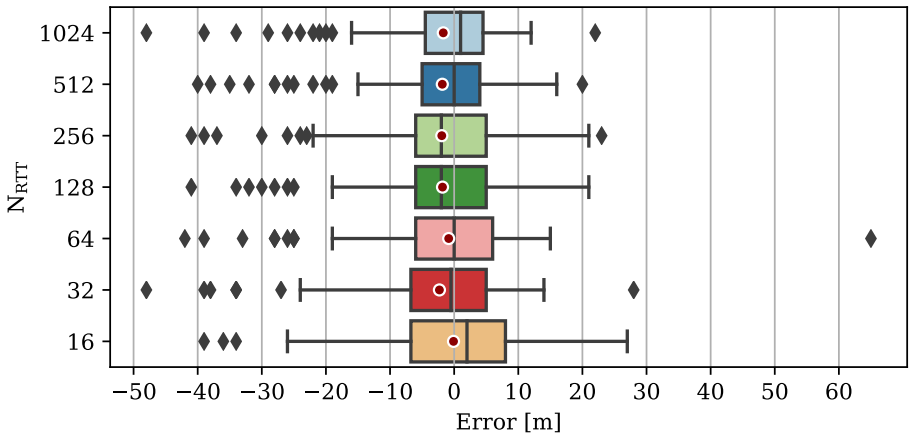

Figure 5.39: Boxplot showing the distribution of RTT errors for all the distances combined for different values of N_{RTT}.

In conclusion, the RTT measurements seem to perform relatively well despite of the implementation flaws. On average, the error was smaller than the MPT resolution for all distances and all N_{RTT} values. Moreover, the measured error is also uncertain due to the uncertainty of the true distance measurement using the GPS. Despite of this, performing distance measurements with a ± 10 m accuracy should yield an acceptable multilateration-based localization accuracy for finding sheep. However, the true accuracy of such a scheme and the impact of increasing N_{RTT} can not be determined based on the results because of the rounding error outside the control of the author. Due to time constraints, the experiment could not be repeated when the implementation flaw was discovered. As a result, it was determined to use $N_{RTT} = 64$ in the final investigation where multilateration was performed. This value was chosen because it had a lower standard deviation compared to the $N_{RTT} = 32$ case and the median value was zero error. However, it is likely that using a lower value would be feasible with a better implementation of the system, where the rounding error is removed, the random jitter reduced and the timer frequency increased.

5.4 Multilateration Performance

Up until this point, the experiments have been conducted with practically stationary devices. However, in the more dynamic and realistic scenario of a complete system, the UAV would be moving continuously as it follows it designated search pattern. Thus, the last field experiment aimed to evaluate the distance measurement performance for multilateration-based localization with a continuously moving quadcopter drone. While a detailed evaluation of the multilateration localization technique accuracy is considered out of scope for this thesis, a final accuracy comparison between an RSSI- and RTT-based distance measurement method is presented along with a simple multilateration plots, demonstrating the accuracy to some degree.

5.4.1 Methodology

The same hardware was used to conduct this experiment as described in the previous sections. A peripheral device was placed in the middle of the field used in the previous investigations and was configured to periodically transmit connectable undirected advertising packets. The UAV was equipped with a horizontally polarized central device, configured to continuously scan for advertising packets. Upon receiving an advertising packet, an RTT distance measurement was performed using the RTT service. The UAV was then configured to travel along a predetermined path with a constant speed while performing the distance measurements. The intent of the experiment was originally to place the peripheral device in various locations in the field and investigate the effect of different horizontally polarized antenna orientations relative to the drone path on the estimated distance and localization accuracy.

Table 5.5 show the combination of parameters used in the experiment. It shows that the same P_t value, PHY mode, peripheral height, UAV height and UAV antenna polarization was chosen as before, due to the reasons outlined in the previous sections of this chapter. While a real implementation of the system would require a significantly lower advertising interval in practice, it was decided that using an advertising interval of 1 s could be beneficial to increase the amount of RTT measurements being performed and thus increase the amount of data for analyzing RTT and RSSI distance measurement accuracy. Moreover, several samples could be removed in post processing to determine the relationship between number of measurements, GDoP and localization accuracy (which is out of scope for this thesis). Finally, a more realistic trial of the system using a much wider search pattern over a large area could not be accomplished due to the size of the field and regulations limiting where the UAV can be operated.

It was discovered during the experiment that a significantly lower amount of dis-

Table 5.5: Combinations of parameter values in the multilateration investigation.

Parameters	Values
P_t [dBm]	3
PHY Mode	Coded
Advertising Interval [ms]	1000
Peripheral Height [cm]	70
Peripheral Positions	A, B
Peripheral Antenna Orientation [°]	90, 0
Peripheral Antenna Polarization	LPH
UAV Height [m]	100
Central Antenna Polarization	LPH
Central Antenna Orientation	Perpendicular, Parallel
Search Sequences	7
N_{RTT}	64
Drone Speed [m/s]	5, 10
Min Connection Interval [ms]	7.5
Connection Request Timeout [ms]	1300
Slave Latency [connection events]	0
Supervision Timeout [ms]	4000

tance measurements were performed during the search than anticipated. In the attempt to rectify this, the experiment was conducted in a somewhat unsystematic fashion. While the distance measurements themselves were performed correctly with a very high overall PDR, the relatively low volume of distance measurements lead to the assumption that the system had problems establishing or maintaining a connection. Thus, during the experiment, the drone speed was changed from 10 m/s to 5 m/s to measure whether the drone speed had an impact on the amount of measurements.

The peripheral device was additionally moved from a position denoted as A to another position denoted as B on the field as shown in Figure C.1 in Appendix C. The figure also show the drone path used by marking the logged GPS locations on a map. The peripheral device was initially placed in a 90° orientation and placed in a 0° orientation in the final measurement as shown on the figure. Finally, it was discovered that the central device antenna had been mounted with an perpendicular orientation relative to the drone path. Recall from Section 5.2 that this would be the worst case orientation of the antenna when the peripheral device is not strictly aligned with the search pattern path. Thus, the orientation of the device was changed to a parallel antenna relative to the drone path. Table 5.6 show the different configurations for the seven different tests that were conducted.

The flight distance of the parallel search pattern was approximately 900 m which should ideally yield 90 and 180 RTT measurements with a UAV speed of 10 and

Table 5.6: Test set-up for the different multilateration tests.

Test Number	Peripheral Position	UAV Speed [m/s]	UAV Antenna Orient-ation	Ear Tag Antenna Orient-ation [°]	Number of RTT measure-ments
1	A	10	Per	90	33
2	A	10	Per	90	26
3	A	5	Per	90	49
4	B	5	Per	90	45
5	B	5	Par	90	68
6	B	10	Par	90	51
7	B	10	Par	0	33

5 m/s respectively. Notice that the results show a significantly lower value. When the UAV speed was halved for measurement number 3, the number of measurements doubled which indicated that the problem persisted. It seems that changing the position from A to B did not significantly affect the number of measurements as seen on measurement 3 and 4. However, using the parallel orientation of the UAV antenna in measurement 5 seemed to increase the number of packets to a great extent. After this was achieved, the UAV speed was increased to its previous value in measurement 6, which yielded relatively good results. Finally, one last test was completed where the orientation of the ear tag antenna was set to 0°, where the number of RTT measurements was reduced once more. This decrease in RTT measurements was expected due to the reduced directivity of the ear tag antenna in the direction of most of the UAV search path. After test number 7 was completed, the UAV ran out of battery and due to time constraints the investigation could not be repeated in a more controlled manner.

It was discovered after the tests were performed that some of the connection parameters were configured differently from the previous experiment, which could have lead to some of the connection problems. Notice that the minimum connection interval was set to 7.5 ms with a slave latency of 0 connection events with a supervision timeout of 4000 ms. This could have been too strict to maintain a connection or, if an unknown and unhandled connection error occurred such that the connection was lost, the supervision timeout was perhaps too long – resulting in several seconds where the devices had to wait before re-establishing the connection. Moreover, with an advertising interval of 1000 ms and a connection request timeout of 1300 ms, the central device would only attempt to transmit a connection request once, which, if the packet was not delivered, would result in a new sequence of scanning before attempting to establish another connection. Finally, the currently measured GPS data was transmitted from the GPS receiver with an interval of 1 s through an UART interrupt. This could potentially have interfered with the RTT measurements However, this part of the implementation was outside the control of

the author.

As discussed in Section 5.3, there was a rounding error present when computing the average time for an RTT measurement using N_{RTT} packets. This was rectified in this investigation. Instead of computing the average during run-time, the value for each individual round trip measurement was stored on the micro SD Card together with the measured RSSI for each RTT packet. This allowed for a more detailed analysis of the data. Moreover, a timer peripheral in hardware was used to measure the time between the last GPS data reception and the completion of an RTT measurement, denoted as Δt. Δt was stored together with the GPS data which contained the longitude, latitude, meters above sea level and the speed of the UAV measured by the GPS receiver.

The source code for both the central and peripheral devices along with the raw and processed data is available from [80].

5.4.2 Results

As with the results presented in Section 5.3, the PDR of the RTT measurements was mostly measured to be greater than 0.95. The measurements with a PDR below 0.8 was discarded.

The true distance between the UAV and ear tag was found using the GPS data and Δt. The measured UAV speed was used with the Δt value to estimate the distance travelled since the last GPS data was received. From here, the previous and following GPS coordinates was used as a initial and terminus point to create a list of equally spaced GPS coordinates between the two locations. The true location of the UAV at the time of the RTT measurement was then interpolated by finding the distance between the initial point and all other points in the list before finding the closest match to the estimated distance traveled. The distance between the measured GPS position of the ear tag and the estimated location of the UAV was then computed and is denoted as the true distance. However, as previously mentioned in Section 5.3, this true distance is also subject to inaccuracies caused by the measurement uncertainty of the GPS receiver.

RTT Distance Measurements

Having stored each individual RTT value for each RTT measurement, an investigation into which statistical approach would yield the most accurate distance measurement was conducted. That is, given a set of distances measured using RTT for a single UAV location, whether the arithmetic mean, geometric mean, harmonic mean, median, median grouped, or most common value would yield the least erroneous result. These methods was used to compute the estimated distance

and the root mean square (RMS) error was found using the true distance for each measurement series, as shown in Figure 5.40. The results show that for all measurement series, using the harmonic mean yielded the smallest RMS error. Thus, it is likely beneficial to use the harmonic mean when finding the average distance using RTT measurements. Moreover, all the methods for computing the average yielded better results than the median and most common value approaches. However, all methods resulted in a significantly smaller RMS error than the MPT resolution. Finally, the system generally show an acceptable performance in terms of distance measurement accuracy, with an RMS error below 7.5 m for all test numbers when using the harmonic mean.

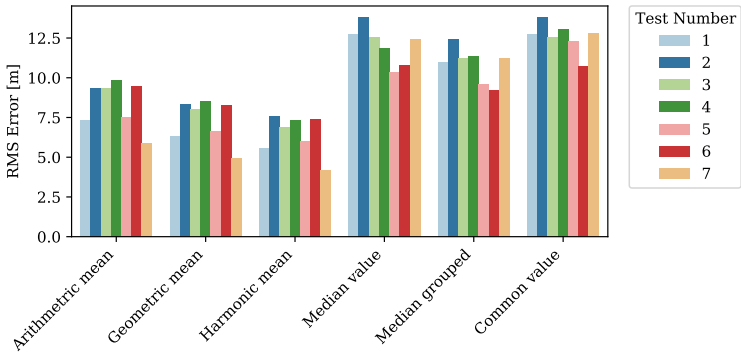

Figure 5.40: RMS error for each test number using different statistical methods.

Interestingly, the RMS error differ with a few meters for the different test numbers. However, looking at Table 5.6, no connection between the peripheral position, UAV speed, UAV antenna orientation or number of RTT measurements can be discerned. All though test number 7 was the only time the orientation of the ear tag was changed and has the lowest RMS error, the sample size is obviously too small to make any conclusions. Some of the test runs managed to perform distance measurements at longer distances than others. Because of this, it was investigated whether distance measurements performed at longer distances lead to any significant changes in performance. Figure 5.41 show the harmonic mean RMS error for all the measurement series in distance bins of 50 m. As the figure shows, the difference is negligible. In conclusion, it seems like the accuracy of the RTT distance measurement scheme is relatively robust to factors such as UAV speed, distance range and antenna orientation.

Finally, Figure 5.42 show a boxplot of the error, computed using harmonic mean and the true distance, for each test number. The plot show that there are significantly fewer outliers in these results compared to the results in Figure 5.39 in Section 5.3. Moreover, comparing these results to the $N_{RTT} = 64$ case in the previous section, the error spread is somewhat smaller with the interquartile range generally bounded within approximately -2.5 to 7 m. This is likely due to the fact

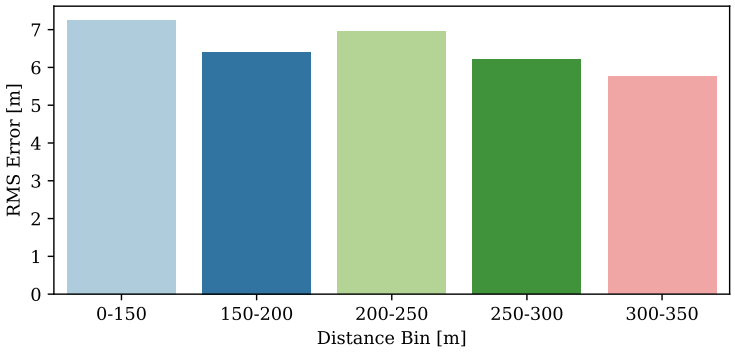

Figure 5.41: RMS error several distance bins using harmonic mean.

that the rounding error issue was resolved. Moreover, there seems to be a bias towards positive errors, meaning that the system tend to underestimate the distance by a few meters. This could be the results of a systematic inaccuracy regarding GPS receiver inaccuracy.

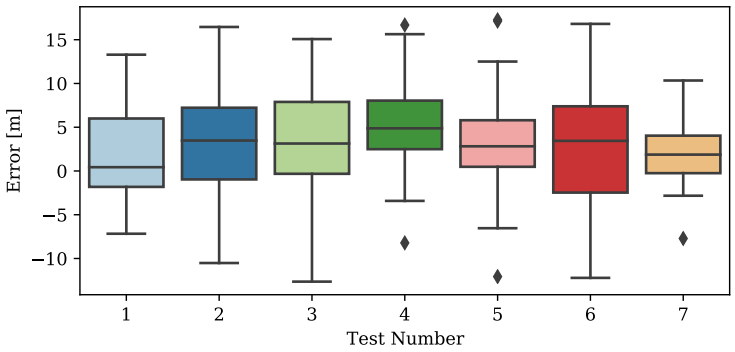

Figure 5.42: Boxplot of the error, calculated by subtracting the true distance from the measured distance, for each test number.

However, if the recorded GPS position of the ear tag is inaccurate in either longitude or latitude, one would expect the error to shift from positive to negative values or vice versa as the UAV moves around the device. Figure 5.43 and 5.44 show the sequence of errors in the order of when the RTT measurement was conducted for test number 3 (using position A) and 5 (using position B). The cyan-color stapled lines mark the turing points of the UAV. The results for test number 3 indicate that the recorded GPS position of the ear tag at position A might have an error. The results for test number 5 indicate that the recorded GPS position of the ear tag at position B is likely correct to a large degree. Similar results were present for the two positions with the other test numbers. However, another source of the

error could be the estimation of the UAV position as well.

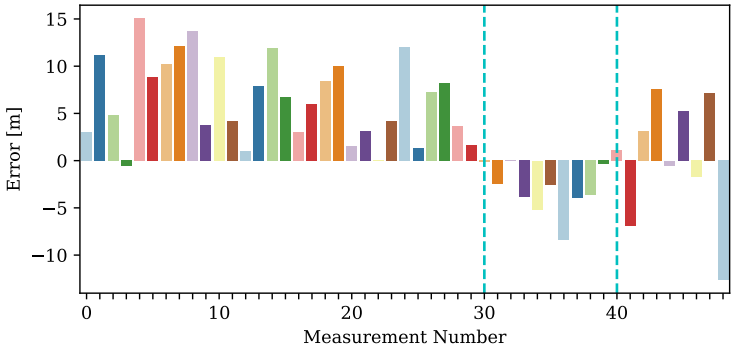

Figure 5.43: Sequence of errors for test number 3 in the order of when the RTT measurement was conducted. The cyan-color stapled lines mark the turing points of the UAV.

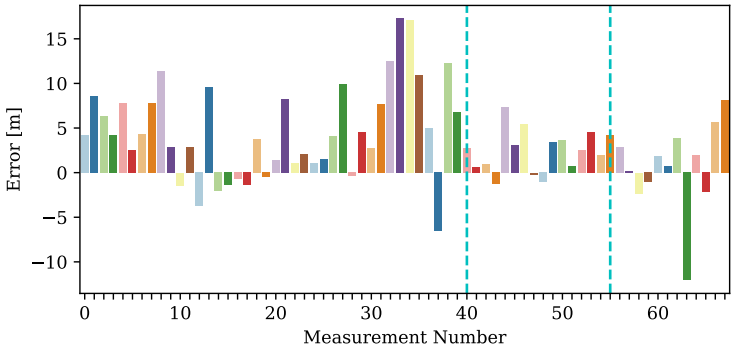

Figure 5.44: Sequence of errors for test number 5 in the order of when the RTT measurement was conducted. The cyan-colored stapled lines mark the turing points of the UAV.

Another source for the tendency to over-estimate the distance could be the offset subtracted from the measured RTT clock ticks. The jitter in the hardware would make calibrating this value to always be correct impossible. However, if this value is too low on average, the estimated distance would tend to be longer than the ground truth.

RSSI Distance Measurments

Due to the reasoning provided in Section 5.2, the log distance path loss with multipath fading model was used to estimate the distance. However, as was demonstrated, the model often estimated a too low value compared to the measured value. Thus an offset was added to the model. Figure 5.45 show the RMS error between the estimated distance and true distance when using 0, 5, 10, 15 and 20 dBm offset on the log distance path loss with multipath fading model. The RSSI distance was calculated using the arithmetic mean values from a single RTT measurement. Other types of averages yielded no significantly better performance while the minimum and maximum values yielded a worse performance. The figure show that an added offset of 15 dBm yielded the lowest RMS error. However, the error is still rather large overall. Using other propagation models yielded a worse overall performance. In conclusion, the RSSI-based distance measurements had a significantly worse performance than the RTT-based approach with a tenfold increase in RMS error.

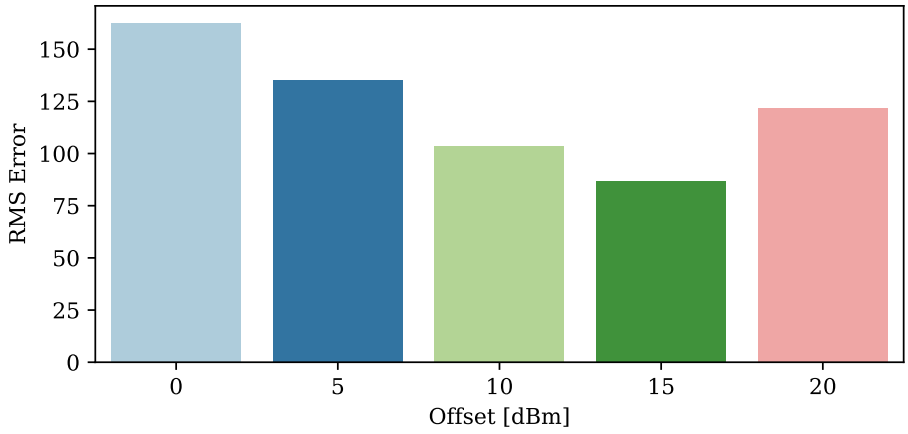

Figure 5.45: RMS error for RSSI-based distance measurements when using different offsets in the log distance path loss with multipath fading model.

Multilateration

Having measured the distances between the UAV and the stationary ear tag at several different known locations it is possible to perform multilateration to estimate the location of the device as discussed in previous chapters. However, as mentioned previously, detailed analysis of the localization performance is out of scope for this thesis as the work was predominantly aimed towards investigating the performance of radio based distance measurements. Despite this, it is still interesting to show

some multilateration plots based on the measurements to get an indication of the performance.

Figure 5.46 show the GPS position as blue markers for each RSSI-based distance measurement in test number 7, using the log distance path loss with multipath fading model and an added offset of 15 dBm. For each distance measurement, the estimated distance is plotted as the radius of a circle with the center on the GPS position. The GPS position of the ear tag is marked with a red marker. It is clear from the figure that the intersection of the circles does not clearly indicate a single position. However, some of the circles actually intersect at the true location of the ear tag, indicating that some of the distance measurements yielded accurate results. Moreover, by looking at the measurements, the location can likely be narrowed down to a smaller area compared to just using the effective transmission range as the radius. Despite this, the performance can generally be considered rather poor. Similar plots for test number 1-6 is shown in Appendix C and exhibit similar properties.

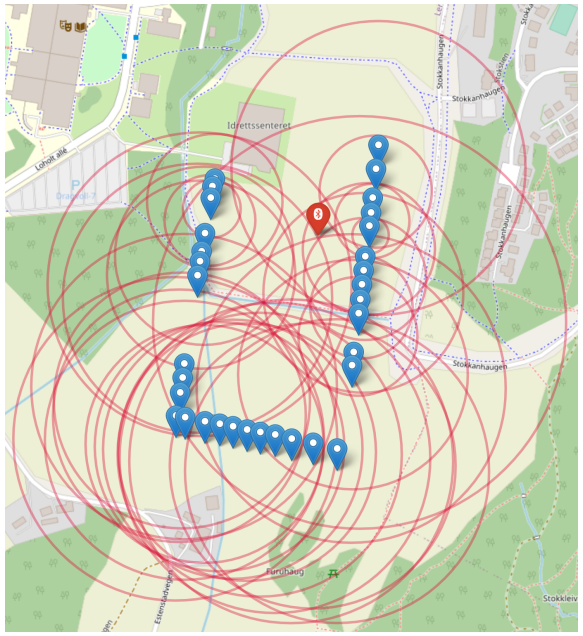

Figure 5.46: Multilateration using RSSI-based distance measurement for test number 7.

Figure 5.47 and 5.48 show a similar plot with RTT-based distance measurements for measurement number 7 and 5 respectively. Plots for measurement number 1-4 and 6 is also shown in Appendix C. From the plot it is clear that the circles intersect closely to the true position of the ear tag. The results indicate that using a BLE-enabled UAV for round-trip AoA-based multilateration localization scheme

is likely feasible for locating sheep.

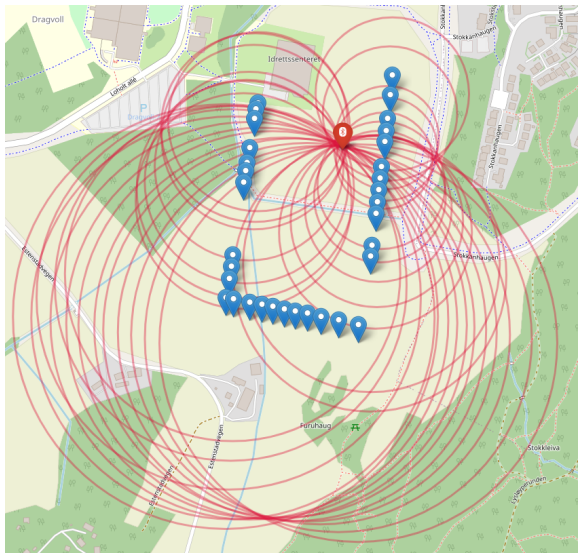

Figure 5.47: Multilateration using RTT-based distance measurement for test number 7.

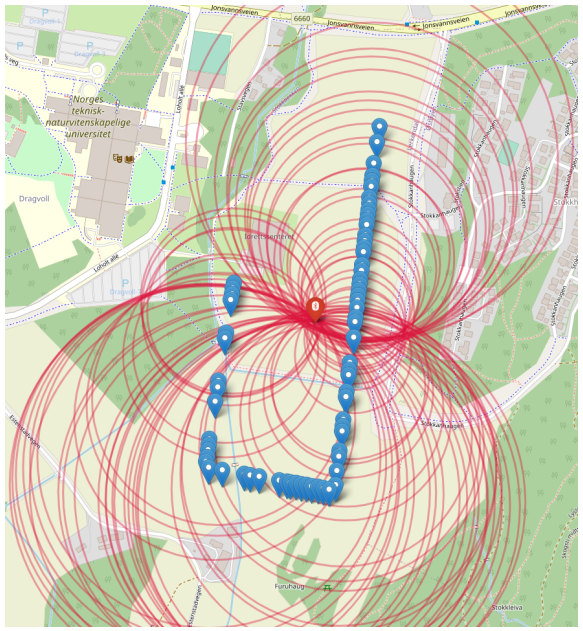

Figure 5.48: Multilateration using RTT-based distance measurement for test number 5.

6 Results and Discussion

Section 6.1 provides a summary the results presented in Chapter 5 and discusses limitations of the investigations in addition to the overall performance of the proposed system. An estimation of the expected battery lifetime of the ear tags with different advertising intervals is provided in Section 6.2.

6.1 System Performance

The preliminary investigation showed that use of coded PHY generally outperformed the LE PHY implementation by providing significantly higher PDR values at lower P_t values. The field experiments did not fascilitate identification of a maximum range of PHY at higher P_t values in a LOS scenario due to the loss of LOS at distances above 1 km. However, the results indicate that the free space propagation model can predict the maximum range to great extent for P_t values.

It was also found that the indreased range when using coded PHY resulted in a large penalty in terms of device power consumption with an eight times increase when transmitting a single advertising packet compared to LE PHY. However, it could be argued that the power consumption measurement shown in Figure 5.9 does not accurately reflect the actual power consumption of coded PHY in a real implementation of the system. Notice that the current graph for LE PHY in Figure 5.8 show three distinct peaks which corresponds to transmitting the advertising packet on the three different advertising channels. In the case of coded PHY, four distinct peaks are present, with the last being wider than the first three. Recall from Section 3.3 that using coded PHY also enables use of extended advertising. Extended advertising enables an increase of the advertising packet payload from 31 bytes to 255 bytes by transmitting a header on the three main advertising channels that points to the larger payload on one of the data channels. Since the coded PHY mode transmits 1 byte for each data bit being advertised, the payload likely surpassed the 31 byte limit with the actual payload being transmitted on one of the data channels, as reflected by the current graph. Thus, the payload size should have been controlled for when performing the current measurements in order to get a more clear depiction of the difference in power consumption.

As the preliminary investigation was conducted on the ground, the results might not reflect the performance of using LE PHY when the receiver is mounted on a UAV. It could very well be the case that using LE PHY would ultimately be more beneficial in terms of a reduced power consumption on the tags, with the

penalty of a smaller effective range. On the other hand, a shorter transmission range would require the peripheral devices to transmit advertising packets more frequently, which could negate this benefit. In addition, the coded PHY mode is defined in the core specification to encode each payload bit with either 2 *or* 8 bits. Using the former mode could potentially prove to be an acceptable tradeoff between power consumption and effective transmission range. However, the devices deployed in the investigation did not support this mode.

A limitation with the PDR measurements in both the preliminary and aerial investigation is that the actual number of transmitted packets were not verified. Instead of configuring a specific number of packets to be transmitted before stopping the advertising, the deployed SoftDevice only allowed for specifying an advertising timeout. Thus, the number of advertising packets was calculated using the advertising interval and the specified timeout. As a result, the number of transmitted packers for each PDR measurement could have been higher or lower than the reported value which could have skewed the results.

The results of the preliminary and aerial investigation also show that a PDR value above 0.8 was never measured. On the other hand, for the RTT measurements, the PDR values was routinely measured to be significantly higher, with most cases achieving a PDR of 1.0. The main difference between these measurements was using three advertising channels in the first two experiments and a single data transmission channel in the latter. As mentioned in Section 3.3, the use of three advertising channels is specified in the core BLE specification to reduce interference from other devices. As a result, the central device must periodically switch between which channels to scan, which causes packets to be lost. However, for this application, it is could be the case that interference from other devices could be considered negligible as the sheep are located in areas with little infrastructure. Ear tags located in the same area could of course interfere with each other, however, considering that the system would use an advertising interval of several seconds and transmitting a single advertising packet takes a few milliseconds, the probability of transmission at the same time is considered rather low. Only having to transmit an advertising packet on a single channel would also significantly reduce the energy consumption of the ear tags.

The performance of the onboard PCB antenna on the ear tag with different orientations and polarizations was evaluated by equipping the central device with both a PCB antenna and a circularly polarized antenna in the aerial investigation. The PCB antenna generally outperformed the cloverleaf antenna in all orientations, for reasons largely unknown. The relatively cheap cloverleaf antenna could have had a design flaw, causing it to have a poor performance in general. Another possibility is that the polarization mismatch between the LP transmitter and CP receiver lead to an attenuation of the signal strength by $-3\,\mathrm{dBm}$ as predicted by the theory in Section 3.1. As the results show that lower signal strengths are more susceptible to multipath fading in general, the performance could have been reduced for this reason alone.

Moreover, the results also show that the performance of the onboard PCB antenna was generally unaffected by polarization mismatch, leading to the author to hypothesize that the antenna could not be considered to have the same characteristics as a theoretical quarter wavelength monopole antenna. Thus, if the PCB antenna has a higher degree of omnidirectionality than first assumed, the polarization mismatch with the cloverleaf antenna could potentially not be a factor. how the implementation of the PCB antenna affects the polarization is not well understood. For instance, it could be the case that the signal is LHC polarized while the cloverleaf antenna was RHC polarized, leading to a low PLF value and causing the signal strength to be reduced by several dBm. The orientation of the cloverleaf antenna on the drone could also have impacted the results. In conclusion, the radiation pattern of the antennas should ideally have been characterized along with the polarization of the signals to better understand how this affects the performance of the system.

While the performance of the onboard PCB antenna yielded acceptable results, it could have been beneficial to test multiple antenna designs, both on the UAV and the ear tags. There is a high probability that there exists antenna designs more suited for this application. Despite this, it was concluded that, for this implementation of the system, a horizontally polarized PCB antenna will likely yield the best performance on the ear tag when considering that a vertically polarized antenna theoretically has zero directivity towards the sky and that the UAV is above the tag. Moreover, to ensure that a vertically polarized antenna is not blocked by the ground plane on the PCB, the size of the ear tag would have to be increased – for this type of antenna implementation. It was also suggested that using a horizontally polarized antenna oriented in a parallel direction relative to the direction of travel of the UAV is likely the best alternative when using this antenna implementation. However, this assumption was not tested directly due to time constraints.

As previously stated, the results of the initial and aerial investigation show that the performance of the system was affected by multipath fading to a large degree, as predicted by the two ray ground reflection model. When using the model to calculate the predicted signal strength for a specific set of parameters, it showed that using vertical polarization should theoretically yield less fluctuation due to constructive and destructive interference. However, the validity of this was not tested. It could thus have been beneficial to run simulations in an attempt to find the optimal UAV height with different antenna designs and orientations while optimizing different parameters to reduce the impact of multipath fading. As the interference is directly affected by the height difference, it could also be interesting to investigate whether dynamically and periodically changing the UAV altitude during a search would increase the probability of receiving an advertising packet. Another option could be to use a circularly polarized PCB antenna on the ear tag since the reflected signals will be changed to the opposite *sense*, as described in Section 3.1, and the effects of multipath propagation reduced.

Generally, the results showedthe system was less affected by multipath fading when

using higher Pt values. Because of this, it was suggested that a conservative r_{eff} value of 600 m with a PDR of 0.7 could characterize the performance of the system when using a P_t value of 3 dBm. However, this value could likely be improved upon to a large degree if suggestions such as using alternative antenna designs, advertising on a single advertising channel and reducing multipath fading effects are implemented.

The system was tested in a LOS environment for all the experiments. This is generally considered an unrealistic scenario in many cases if the system is deployed as envisioned. The presence of vegetation and other obstacles can cause shadowing effects and severely reduce the performance of the system, both in terms of the effective range and the distance measurement accuracy. Moreover, depending on the orientation of the sheep relative to the UAV, the head of the sheep could also block the LOS. Thus, to achieve a more accurate evaluation of the performance, the experiments should ideally have included scenarios where the device is placed in vegetation, under the cover of trees in a forest or using other obstacles in the LOS. Because of this, the overall performance of the system can not be properly evaluated based on the presented results alone.

The accuracy and feasibility of using RSSI measurements for distance estimation was investigated in Section 5.1, 5.2 and 5.4. The results show that even for a stationary system with identical conditions, the RSSI measurements varied greatly between transmissions. It was therefore concluded that it is likely necessary to perform several RSSI measurements to increase the accuracy of the distance measurement. However, the results also showed that the measured RSSI value at a given distance is highly dependent on the orientation of the transmitting device. This could be detrimental for the performance in this scheme, as the ear tags is subject to constant orientation changes when mounted on a sheep.

More importantly, the two ray ground reflection model seemed to predict fluctuation of the RSSI signal with relatively high precision for some of the measurements. This confirmed that the measured RSSI values are greatly affected by multipath fading. As a result, a single measured RSSI value can correspond to multiple distances due to the nature of the two ray ground reflection model. The results also show that the log distance path loss with multipath fading model can be used to approximate the two ray ground reflection model, where one RSSI value corresponds to a single distance. Moreover, based on the results, it was suggested that the resulting RSSI-distance curve could be calibrated by adding an offset.

Thus, after measuring the RSSI values from packets transmitted during the multilateration investigation and finding the average value for each position, a distance was estimated using different offsets. It was found that an offset of 15 dBm yielded the lowest overall RMS error, with an RMS uncertainty slightly above 80 m. Using the other radio propagation models presented in Section 3.1 yielded an overall worse performance. It was then shown through multilateration plots that the large error resulted in no clear location estimate for the ear tag. However, it is likely

that this scheme would still be more accurate in terms of localization than a system that only uses a fixed r_{eff} value to draw the circles. Finally, another drawback of using RSSI-based distance measurements is that according to the datasheet of the nRF52840 [65], the measured RSSI value can only be considered accurate within a range of -90 to -20 dBm with a typical uncertainty of ± 2 dBm. As an example, using Friis transmission equation, this means that distance measurements would not be valid for distances above approximately 400 m. Moreover, the uncertainty of the measurement with ± 2 dBm could result in an uncertainty of several meters.

The accuracy of the RTT ToA based distance measurements were investigated in Section 5.3 and 5.4. Here, the RTT scheme was implemented by using a user defined GATT service, where a distance measurement could be initiated after a BLE connection was established. However, performing the RTT measurement could not be facilitated through the BLE protocol and the SDR had to be used directly instead. This was achieved by disabling the SoftDevice, which acts like the BLE operating system as described in Section 3.3, so that the radio could be controlled directly.

For each completed measurement, the SoftDevice had to be re-initialized which consumes a certain amount of power. More importantly, this approach meant that a new connection would have to be established each time a distance measurement was performed. Thus, even after the device on the UAV had detected an advertising packet for the first time, the distance measurements could only be performed at half the rate of the advertising interval, since the central device must wait for the next advertising event to issue a connection request. While this can be considered less than ideal, the main issue of this approach was that the system could only perform distance measurements with one device even though several devices was within coverage. That is, the first advertising packet received would initiate a connection request and after the distance measurement was completed, the same device would with a high probability be the first device to transmit a new advertising packet, restarting the sequence until the device is out of range. This could have been mitigated by blacklisting the device for the duration of one advertising period to check if other peripheral devices are present. That is, avoid connecting to the device once an advertisement is received. However, this would also decrease the rate of distance measurements by a factor of two. It could also create a state where peripheral A and B is alternately blacklisted and connected, while peripheral C is never discovered.

A better approach is likely to use the so called Timeslot API in the SoftDevice. This enables the use of periodic timeslots ranging from 100 µs to 128 s where the SoftDevice render full control over the radio and other restricted hardware peripherals to the user. In this way, the SoftDevice on the central/master device can maintain an established connection with a slave while scanning for advertising packets from other peripherals in the meantime. From here, several slaves can be connected to the master simultaneously. Moreover, the master device can use the GATT service through the connection to initiate an RTT measurement where both

the slave and master request a timeslot window equal to the duration of an RTT measurement. An RTT measurement can then be performed with free access to the radio hardware. Once the measurement is completed, the SoftDevice on the master reestablish control over the radio and continues to both maintain the connection with the slaves and scanning for other peripherals. Likewise, the SoftDevice on the slave continues to maintain the connection. Using a round robin scheduling scheme, the distance measurements can be alternately performed with each connected slave as often as the connection parameters allow until the slave is out of range and the connection is lost.

Another issue with the implementation was that the radio interrupt shortcuts were used to reduce the dwell time between receiving an RTT packet and retransmitting it. While it is beneficial to decrease the dwell time to facilitate faster distance measurements, the implementation introduced unnecessary random jitter in the hardware, as discussed in Section 5.3. This jitter likely led to an increase in measurement inaccuracy as the offset subtracted from the number of clock ticks would therefore be higher or lower than the true value in many cases. The development of an RTT measurement scheme using the Timeslot API and reduced hardware jitter was nearly completed at the end of the experimental stage of this thesis. However, due to time constraints, the solution could not be properly tested and the performance is thus not evaluated here. However, it is likely that such a scheme would be a more acceptable approach for a precision localization mode using multilateration.

The round trip timing accuracy presented in Section 5.3 was performed with a rounding error in the implementation. For this reason, the relative performance of increasing the number of packets (N_{RTT}) for each distance measurements could not be determined. Despite this, the measurements still showed a decrease in error as the value was increased so that the smallest value of 16 yielded the largest errors on average. However, there seemed to be a diminishing return for doubling the number of packets. As a result, an N_{RTT} value of 64 was chosen as a tradeoff between accuracy and low power consumption for the subsequent investigation. However, it is likely that using a lower value could yield an acceptable accuracy without the rounding error and less jitter. Indeed, considering the Timeslot API implementation, it may prove beneficial to use a lower number despite a lower accuracy if that enables more frequent distance measurements while maintaining a connection with in increased amount of slave devices due to a shorter timeslot window required.

In a future implementation of the system, it would also be beneficial to use a more accurate external crystal oscillator to reduce jitter stemming from the clock itself. Increasing the frequency of such an oscillator would further increase the resolution of the RTT measurement significantly, which would likely allow for a smaller N_{RTT} value with a higher accuracy. However, this would require external hardware or the use of another BLE SoC as the maximum frequency of the timer is limited to 16 MHz. However, it would be necessary to further investigate whether the use of an external timer would result in an introduction of more jitter which could

effectively eliminate the added benefit.

The accuracy of the implemented RTT distance measurement scheme was then tested using a moving UAV that followed a search pattern seven times, where the rounding error was removed by storing the individual sample values. This investigations had several limitations as discussed in Section 5.4. In short, the number of RTT measurements were significantly lower than anticipated and several changes to the experimental setup was done in a somewhat unsystematic fashion to attempt to rectify this issue during he investigation. The cause of this issue is still unknown, however the results show that the accuracy of the RTT measurements themselves were largely unaffected by the different experimental setups. Especially the UAV speed did not seem to affect the accuracy. However, the sample size is likely too small to comment on this with any certainty.

The results also showed that the accuracy was not significantly different for longer distances compared shorter distances. The RMS error was calculated for each test number using several statistical approaches to find the estimated distance. It was found that using the harmonic mean yielded the lowest RMS error, where an RMS uncertainty of approximately 4 m and 7.5 m was achieved in the best and worst case respectively. However, it is not known why using the harmonic mean achieves the best results as it is typically applied to find the average of rates, such as the average speed used when travelling between two points.

The computed RMS error values is also subject to an uncertainty due to the potentially inaccurate GPS position measurement for both for the tag and UAV location, affecting the estimated true distance value. The accuracy of the receiver is listed as 3 m CEP with a 50 % probability. This means that determining the so called true distance between these two points could potentially lead to an error bound within ± 6 m with a probability of 25 %, where the error could be larger 75 % of the time. Thus, with an average estimated RMS error of 6.42 m, it is difficult to distinguish contributions from the RTT measurement uncertainty and GPS uncertainty. However, looking at the errors for each individual RTT measurement in a sequence, it is probable that at least one of the assumed true tag positions is somewhat inaccurate, which could have inflated the estimated RMS error values. A full implementation of the system could use a higher precision GPS receiver, however there is a penalty in terms of increased system costs when increasing the precision of the receiver. At any rate, it would be interesting to measure the RMS error with a more precise system to more accurately evaluate the accuracy of the RTT distance measurements.

The area where the multilateration experiment was conducted was generally too small to simulate a real implementation of the system, as the established effective transmission range was approximately equal to the length of the field. As a result, no distance measurements were conducted above a true distance of 400 m. Although RTT measurements were conducted on longer distances in the investigation presented in Section 5.3, the UAV was stationary and the system suffered

from the rounding error as previously mentioned. It is thus not possible to discuss the accuracy of the distance measurements with a moving UAV at distances above 400 m. Moreover, no distance measurements were performed as shorter ranges than approximately 100 m. It would be interesting to evaluate the performance of the system at such a close range. It is likely that the accuracy would be lower as the distance approaches the MPT resolution and would thus likely require a higher N_{RTT} value. Moreover, the system should ideally have been tested with the Timeslot API implementation and using multiple peripheral devices. Despite this, the results show that the RTT-based distance measurements could likely be used in a multilateration scheme for precision localization of sheep. However, a detailed analysis of the localization performance is, as mentioned multiple times, out of scope for this thesis.

The coarse localization scheme proposed in Chapter 4 was never properly tested. Although the results indicate that such a scheme should be possible to implement, a field trial using a search pattern with multiple ear tags over a vast geographic area would be necessary to confirm this claim and more importantly evaluate the localization accuracy of such an implementation. It could also be beneficial to test this with a smaller P_t value, such as 0 dBm, to reduce the effective transmission distance and increase localization accuracy with an added benefit of lower ear tag power consumption and a higher cost in UAV energy consumption to cover the same area. The system was never tested at any other altitudes than 100 m and it would also be interesting to verify the performance using a fixed wing drone. Moreover, such a test could be used to verify the validity of the advertising interval models proposed in Section 3.4.

It is also worth discussing that using BLE for this system has certain advantages and disadvantages. The main advantage is that it allows the system to easily communicate with other devices due to the multitude of BLE enabled devices throughout the world. Moreover, using a predefined protocol optimized for low power consumption allows for an easier implementation of the system. However, using the protocol also limits how the system can be implemented. For instance, doing RTT measurements with the protocol was quite difficult. It could thus be beneficial to utilize the SDR on the SoC directly and increase the efficiency of the system by removing the necessity of establishing BLE connections since the application is a very specific use case. On the other hand, this would significantly increase the difficulty of implementing the system and the easy interface to other devices would be lost. Finally, it would also be interesting to compare the performance to other radio and UAV-based localization schemes.

6.2 Advertising Interval and Battery Lifetime

Using the established effective transmission range $r_{eff} = 600\,\text{m}$ with a PDR of 0.7 from Section 5.2, the advertising interval for this implementation can be estimated using different values for both the distance between parallel lines (d_s) and UAV speeds (s_{uav}). Table 6.1 shows some minimum advertising interval (T_{Amin}) values and worst case position advertising values (T_{wc}) using Eq. 3.26, 3.27 and 3.28 from Section 3.4. All the values are rounded to the nearest integer to increase readability.

Table 6.1: Different advertising intervals depending on drone speed and parallel search pattern distance with a given effective transmission range.

r_{eff} [m]	PDR	s_{uav} [m/s]	d_s [m]	T_{Amin} [s]	T_{wc} [s]
600	0.7	20	$0.9r_{eff}$	26	5
			$0.8r_{eff}$	36	6
			$0.7r_{eff}$	43	7
			$0.6r_{eff}$	48	8
			$0.5r_{eff}$	52	9
600	0.7	10	$0.9r_{eff}$	52	9
			$0.8r_{eff}$	72	13
			$0.7r_{eff}$	86	15
			$0.6r_{eff}$	96	17
			$0.5r_{eff}$	104	18
600	0.7	5	$0.9r_{eff}$	105	18
			$0.8r_{eff}$	144	25
			$0.7r_{eff}$	171	30
			$0.6r_{eff}$	192	34
			$0.5r_{eff}$	208	36

The estimates show a clear tradeoff between search efficiency (and possibly UAV battery lifetime), by using faster UAV speeds and a lower degree of coverage overlap, and ear tag energy consumption due to an increase in the required advertising interval. However, note that the maximum advertising interval set by the BLE core specification is 10.24 s [64]. While it is possible to increase this value in practice, the resulting implementation would not be in accordance with the specification.

Recall from Section 3.3 that the BLE protocol is designed so that a connection request is transmitted on the next advertising event. Using a longer advertising interval will therefore significantly increase the time between an advertising packet is received and a connection is established to perform a distance measurement. If the implementation requires a new connection to be established between distance measurements for the same device, it could lead to a severe penalty in the amount of distance measurement that could be performed when the UAV is within coverage

of the device. This could be mitigated by increasing the advertising interval on the peripheral device for a predetermined amount of time after the first connection is established, before resetting to the normal interval. This would allow the central device to establish connections at a faster rate whenever in coverage without significantly increasing energy consumption the rest of the time. However, an alternative is to implement the system using the timeslot API, as discussed above, where a connection is maintained between RTT measurements, eliminating the problem. Despite these results showing that a relatively high advertising interval would be feasible, it is important to emphasize that no experiments were performed to verify the validity of this model.

It is possible to estimate the average current consumption for different advertising intervals using the online power profile tool provided ny Nordic Semiconductor [81]. The tool does not offer support for the nRF52811 SoC suggested for the implementation of the ear tag. It does, however, support power estimations for the nRF52810 SoC which is very similar in terms of implementation [82]. The main difference is that the long range mode or coded PHY is not supported by the device. Thus, the power profiler tool does not support the long range mode either. However, this can be simulated by multiplying the payload variable with eight in the calculator. Thus, if we assume a payload of 31 bytes (the maximum allowed by the profiler) an semi-accurate estimate should be obtainable. Here, it is assumed that no additional payload is transmitted on a data transmission channel using extended advertising.

Note that if more information must be transmitted in the full implementation of the system, the payload should be decreased to the smallest value possible, where the UAV central device would issue a scan request for the rest of the information whenever in range to facilitate a lower average power consumption. Finally, the profiler does not support using a P_t value of 3 dBm, so 4 dBm was used instead. Thus, it is fair to say that the values presented in Table 6.2 is likely an overestimation of the average power consumption for the ear tags using connectable undirected advertising packets with different advertising intervals. The table also show the expected estimated battery lifetime of the system if the periodic advertising is never stopped and if a standard and relatively cheap 3 V, 225 mAh capacity CR2032 coin cell battery is used to power the system [83]. Note that the lifetime is a simple estimate where the capacity is divided by the current consumption and will be subjected to variation depending on several factors such as battery age, temperature and discharge rate in practice.

In conclusion, assuming the estimated power consumption numbers are accurate, an implemented ear tag can reasonable be expected to have a battery lifetime of several years depending on the advertising interval. The consumption will increase when localization is performed, however considering the relatively rare occurrence of this in the proposed system, the associated consumption is likely negligible. Moreover, if the system only advertises on a single channel, the energy consumption would be reduced to approximately one third of the reported values, as using the radio is the main source of the power consumption, further increasing the battery lifetime.

Table 6.2: Estimated battery lifetime of the ear tag using a 225 mAh coin cell battery and different advertising intervals.

Advertising Interval [s]	Average Power Consumption [µA]	Battery Lifetime [days]	Battery Lifetime [years]
1	16	586	1.61
2	8.8	1065	2.92
3	6.2	1512	4.14
5	4.2	2232	6.12
7	3.3	2841	7.78
9	2.8	3348	9.17
10.24	2.6	3606	9.88

Finally, if a start-up date is used, as described in Chapter 4, where the device remains in a low power sleep state throughout most of the year and at night, the lifetime will likely predominantly depend on the natural self-discharge rate of the battery as a result of entropy. However, the real battery lifetime of the system can only be obtained by implementing the ear tag PCB and measuring the power consumption.

7 Conclusion

The aim of the thesis was to evaluate the feasibility of using a UAV-enabled and BLE-based scheme to design and implement a low-cost system that perform localization of sheep over wide rangelands as proposed in Chapter 4. This was accomplished by first conducting a literary review on existing and proposed solutions concerning animal localization and performing several field trials to evaluate the performance of the implemented system. The field trials were conducted to investigate the relative performance of using the BLE long range mode compared to the normal BLE mode with different transmission parameters. Moreover, the transmission range of the system was investigated using different antenna orientations with both a linearly and circularly polarized receiving antenna on the UAV. An investigation into the accuracy and performance of using round-trip time of arrival measurements for distance estimation between devices was conducted. The performance of this scheme was compared to a received signal strength indicator distance estimation scheme for a multilateration based localization system.

Both a vision and radio based approach was evaluated in the literary review. It was concluded that vision based systems has the potential to become an effective and non-intrusive solution in future animal tracking systems, especially if the system is implemented using a UAV to cover large areas. However, the current cost of the technology required to accomplish precise vision based localization, while tracking multiple animals over wide areas, is currently too high to be feasible in many cases. Moreover, identifying individual animals is also a significant challenge that should be addressed if such systems are to be used in animal husbandry. One possible solution is to combine visual-based solutions with a more traditional radio based approach.

Several radio based animal tracking solutions were presented and discussed. The advantages and disadvantages of using GPS receivers on the animals in combination with long-range radio technologies was evaluated. It was concluded that using the more common technologies available with high bandwidth and data rates, such as GSM, would yield a system that is too costly in terms of energy consumption of the tracking devices. Moreover, using satellite communication would likely not be economically feasible for tracking sheep. Using an LPWAN technology, such as LoRa and NB-IoT, was identified as the best candidates for such an implementation.

Some commercially available systems for tracking sheep and other tracking solutions using LPWAN was evaluated. It was concluded that such solutions was generally very costly relative to the economic value of sheep due to the required battery size and the costs of using a GPS receiver and the LPWAN radio. This also made the solutions relatively bulky and could hinder the movement of the

animals. Lastly, the current lack of LPWAN infrastructure in rangelands could be detrimental to the performance of the system. It was concluded that a simpler and more cost effective system without the need for a GPS receiver that also required less infrastructure was desireable.

Various proposals using short-range radio for tracking animals was presented and evaluated. It was concluded that, for a sheep localization system, the use of stationary base stations was unfeasible due to the infrastructure costs. It was also determined that the use of one or several a UAV-based mobile base stations could be beneficial to reduce costs. Moreover, several short-range radio technologies was evaluated, including the us of the more traditional RFID and VHF-based systems. However, it was concluded that most of the solutions were either too costly in terms of energy consumption or had an insufficient transmission range. Moreover, some of the solutions required relatively large antennas to operate effectively. It was further suggested that using BLE could be a valid approach due to the inherent low energy consumption and comparatively long ranges offered by the long range mode. In addition, the low price and wide availability of BLE SoCs could significantly reduce the costs of the localization system while enabling an easy connection to smartphones and other devices. Finally, a small literature review regarding UAV data collection was presented. It was concluded that this work could help improve the full implementation of a sheep tracking system.

Based on the literary review, a novel and cost-effective system for sheep localization was proposed. The system consisted of using low-cost BLE ear tags on the sheep in combination with a BLE-enabled UAV equipped with a GPS receiver. The four fundamental radio localization approaches was evaluated for this system. It was concluded that the proposed system should offer two localization schemes. The first is a coarse localization mode that can be used to locate the majority of the sheep and should enable very low energy consumption of the tags. This is achieved by performing a combination of proximity based localization and exploiting the movement of the UAV to perform multilateration using fixed distances. The other mode is a precise localization scheme that use round-trip time of arrival measurements to estimate the distance between devices and perform multilateration at the cost of higher energy consumption. This mode is intended to assist the localization the remaining sheep that is otherwise difficult to find.

A preliminary investigation showed that the BLE long range mode significantly outperformed the normal BLE transmission mode in terms of range and packet delivery ratio when used on the ground. For this reason it was concluded that using the BLE long range is beneficial to cover larger areas and decrease the necessary advertising interval to reduce energy consumption on the ear tag. The aerial investigation using a UAV showed that the onboard PCB antennas of the deployed devices significantly outperformed the cloverleaf antenna that was tested. Moreover, the PCB antennas showed a high degree of robustness in terms of polarization mismatch. While several other antenna designs could ultimately prove to have a better performance, it was concluded that using the the PCB antennas was suffi-

cient to implemented the system. The system achieved a conservatively estimated effective transmission range of 600 m with a packet delivery ratio of 0.7 when using a UAV altitude of 100 m. It was also concluded that using a single advertising channel could be beneficial to further increase the expected packet delivery ratio, and thus the effective transmission range, in addition to reducing the power consumption of the ear tags.

The observed characteristics of the system was evaluated against several empirical and theoretical radio propagation models. Among these, the two ray ground reflection model had the highest prediction ability for the observed results. For this reason it was concluded that the proposed system is highly susceptible to multipath propagation fading, especially when using lower transmission powers. It was thus suggested that using a relatively high transmission power value was necessary to reduce this effect in the implementation of the system. Moreover, the multipath propagation effects severely compromised the accuracy of the RSSI-based distance measurements. It was found that using a log distance path loss with multipath propagation model with an offset yielded the lowest RMS error of approximately 80 m for the RSSI-based distance measurements. This high degree of inaccuracy makes the approach unsuited for precision localization using multilateration. However, it could potentially be implemented in the coarse localization scheme as an alternative to using fixed distances.

A round trip time of arrival measurement scheme was implemented, tested and evaluated. Despite several identified shortcomings with the implementation, the results showed a high degree of precision compared to the RSSI-based approach, with an RMS error of approximately 6.5 m. Implementing the suggested improvements of the system would likely yield a significantly lower RMS error while additionally reducing the energy consumption due to a reduction in the number of packets required to be transmitted. The results also showed that the implementation had a high degree of robustness in terms of using different UAV speeds and ranges. A system enabling the UAV to maintain a connection with multiple ear tags while simultaneously performing distance measurements was proposed, but could not be tested due to time constraints. Despite this, it was shown that the implemented system could be used to locate the true position of a single ear tag using with a relatively high degree of precision and accuracy using multilateration plots. Considering the size and possible movement of sheep the performance is considered sufficient for high precision localization.

Given the conservatively estimated effective range of the system and different UAV speeds, the required advertising interval of the ear tags was estimated. Using a power estimation tool, it was shown that these advertisement intervals would likely yield a battery lifetime of several years. It was concluded that implementing some of the energy conserving approaches that was suggested for the system, it is likely that the battery lifetime of the device is mostly limited by the natural self-discharge rate of the coin cell battery.

The inexpensive components required to implement the ear tags with a battery lifetime that would likely span the lifetime of a sheep, if not longer, significantly reduces cost of deploying the suggested system compared to existing solutions. Moreover, the low cost would allow each individual sheep to be equipped with the technology, ensuring that all of the livestock can be localized with either a coarse or high precision mode at the end of the season. The operating costs of the system is also significantly lower compared to existing solutions depending on infrastructure being installed and maintained. In this system, only a comparatively cheap UAV, equipped with a relatively low-cost module assisted by an already owned smartphone, is required to locate the sheep. While field trials with the fully implemented system using real sheep in a wide area was not conducted, the results show that the proposed solution has a promising future and high degree of feasibility for a low-cost, high precision sheep localization system.

8 Future Work

The implemented round trip time of arrival measurement scheme yielded overall acceptable results as concluded in Chapter 7. However, as discussed in Chapter 6, there are several measures that could be implemented to potentially improve the performance. The most important measure would be to implement and test the system using the Timeslot API. This would likely allow the system to perform distance measurements at a higher rate while maintaining a connection with multiple slaves and scanning for advertising packets. Such an implementation or an equivalent method would be absolutely necessary for the deploying the system. Implementing the system with less random jitter in the hardware would also likely increase the accuracy of the distance measurements. Using an external timer with a high precision and frequency crystal oscillator would also likely increase the accuracy of the distance measurements. From here, it could be interesting to optimize for the minimum number of packets being transmitted for a single distance measurement to reduce power consumption and still maintain an acceptable localization accuracy. Depending on the resulting power consumption, it could be feasible to only utilize the precise localization scheme.

An investigation into the possibility of using a single advertising channel to reduce power consumption and increase both the packet delivery ratio and effective transmission range is likely worthwhile. It should also be investigated whether the effects of multipath fading on the transmitted signals can be reduced to increase the effective transmission range. This could potentially be accomplished by using different UAV heights or testing different antenna designs. The radiation pattern of the antennas deployed should ideally be measured to optimize the performance of both the ear tags and the UAV module.

In addition to implementing the measures described above, a full prototype of the system should be developed to properly evaluate the performance. This include the development of the ear tags, the smartphone application and UAV module. From here, both the coarse and precise localization scheme should be tested using real sheep in wide areas featuring objects that can block the LOS. The system could also be tested using multiple UAVs. It would be especially interesting to verify the estimated battery life of the ear tags with a custom PCB using the intended device and a coin cell battery, especially if the start-up date feature is implemented. This would also allow the estimated advertising interval values to evaluated. It could also be interesting to see if the localization accuracy can be further increased by implementing a direction finding antenna to perform triangulation and evaluate the performance compared to the multilateration-based localization. Another alternative is to combine the two methods to potentially further increase localiza-

tion accuracy. It would also be prudent to investigate other use-cases where this solution can be applied.

From here the functionality of the system can be expanded upon. For instance, the ear tag could contain sensors that monitors the health of the sheep. An accelerometer or similar device could be used to periodically check the movement of the sheep. If no movement is detected in several consecutive measurements, the ear tag could advertise that the animal is likely deceased. The UAV system could also be expanded with a camera or other visual sensors to further aid with the localization. An investigation into using different UAV search patterns or even a dynamic autonomous search path could potentially reduce the energy consumption of both the UAV and ear tag or improve localization accuracy. Finally, it would be interesting to investigate the possibility of partially or fully automating the sheep relocation process. By deploying several coordinated UAVs equipped with speakers that can emit barking sounds, the drones could potentially herd the animals and direct them in the right direction.

Bibliography

[1] B. Chessa, F. Pereira, F. Arnaud, A. Amorim, F. Goyache, I. Mainland, R. Kao, J. M. Pemberton, D. Beraldi, M. Stear, A. Alberti, M. Pittau, L. Iannuzzi, M. Banabazi, R. Kazwala, Y.-P. Zhang, J. Arranz, B. Ali, Z. Wang, M. Uzun, M. Dione, I. Olsaker, L.-E. Holm, U. Saarma, S. Ahmad, N. Marzanov, E. Eythorsdottir, M. Holland, P. Ajmone-Marsan, M. Bruford, J. Kantanen, T. Spencer, and M. Palmarini, "REVEALING THE HISTORY OF SHEEP DOMESTICATION USING RETROVIRUS INTEGRATIONS," vol. 324, no. 5926, pp. 532–536. [Online]. Available: https://www.ncbi.nlm.nih.gov/pmc/articles/PMC3145132/

[2] "Conversation with Professor Svein-Olaf Hvasshovd," Department of Computer Science, Norwegian University of Science and Technology, 2020.

[3] K. Ren, J. Karlsson, M. Liuska, M. Hartikainen, I. Hansen, and G. H. Jørgensen, "A sensor-fusion-system for tracking sheep location and behaviour," vol. 16, no. 5, p. 1550147720921776. [Online]. Available: https://doi.org/10.1177/1550147720921776

[4] H. Bai, G. Zhou, Y. Hu, A. Sun, X. Xu, X. Liu, and C. Lu, "Traceability technologies for farm animals and their products in China," vol. 79, pp. 35–43. [Online]. Available: http://www.sciencedirect.com/science/article/pii/S0956713517300865

[5] E. A. Raizman, H. B. Rasmussen, L. E. King, F. W. Ihwagi, and I. Douglas-Hamilton, "Feasibility study on the spatial and temporal movement of Samburu's cattle and wildlife in Kenya using GPS radio-tracking, remote sensing and GIS," vol. 111, no. 1, pp. 76–80. [Online]. Available: http://www.sciencedirect.com/science/article/pii/S0167587713001451

[6] N. A. Molapo, R. Malekian, and L. Nair, "Real-Time Livestock Tracking System with Integration of Sensors and Beacon Navigation," vol. 104, no. 2, pp. 853–879. [Online]. Available: https://doi.org/10.1007/s11277-018-6055-0

[7] M. A. Olivares-Mendez, C. Fu, P. Ludivig, T. F. Bissyandé, S. Kannan, M. Zurad, A. Annaiyan, H. Voos, and P. Campoy, "Towards an Autonomous Vision-Based Unmanned Aerial System against Wildlife Poachers," vol. 15, no. 12, pp. 31 362–31 391.

[8] A. S. Voulodimos, C. Z. Patrikakis, A. B. Sideridis, V. A. Ntafis, and E. M. Xylouri, "A complete farm management system based on animal identification using RFID technology," vol. 70, no. 2, pp. 380–388. [Online].

Available:
http://www.sciencedirect.com/science/article/pii/S0168169909001392

[9] W. W. Cochran and R. D. Lord, "A Radio-Tracking System for Wild Animals," vol. 27, no. 1, pp. 9–24.

[10] S. Ward, J. Hensler, B. Alsalam, and L. F. Gonzalez, "Autonomous UAVs wildlife detection using thermal imaging, predictive navigation and computer vision," in *2016 IEEE Aerospace Conference*, pp. 1–8.

[11] L. F. Gonzalez, G. A. Montes, E. Puig, S. Johnson, K. Mengersen, and K. J. Gaston, "Unmanned Aerial Vehicles (UAVs) and Artificial Intelligence Revolutionizing Wildlife Monitoring and Conservation," vol. 16, no. 1, p. 97. [Online]. Available: https://www.mdpi.com/1424-8220/16/1/97

[12] D. Zhou, "Thermal Image-Based Deer Detection to Reduce Accidents Due to Deer-Vehicle Collisions," accepted: 2013-02-21T16:12:27Z. [Online]. Available: http://conservancy.umn.edu/handle/11299/144870

[13] H. Van Nguyen, M. Chesser, L. P. Koh, S. H. Rezatofighi, and D. C. Ranasinghe, "TrackerBots: Autonomous Unmanned Aerial Vehicle for Real-Time Localization and Tracking of Multiple Radio-Tagged Animals," vol. 36, no. 3, pp. 617–635. [Online]. Available: http://arxiv.org/abs/1712.01491

[14] W. Kim, Y. B. Cho, and S. Lee, "Thermal Sensor-Based Multiple Object Tracking for Intelligent Livestock Breeding," vol. 5, pp. 27453–27463.

[15] D. Doberstein, *Fundamentals of GPS Receivers: A Hardware Approach*. Springer Science & Business Media.

[16] GPS.gov: GPS Accuracy. [Online]. Available: https://www.gps.gov/systems/gps/performance/accuracy/

[17] Superaccurate GPS Chips Coming to Smartphones in 2018 - IEEE Spectrum. [Online]. Available: https://spectrum.ieee.org/tech-talk/semiconductors/design/superaccurate-gps-chips-coming-to-smartphones-in-2018

[18] M. K. Gaur, "Role of GPS in monitoring livestock migration," accepted: 2017-07-24T00:45:45Z. [Online]. Available: https://repo.mel.cgiar.org/handle/20.500.11766/7283

[19] J. G. Panicker, M. Azman, and R. Kashyap, "A LoRa Wireless Mesh Network for Wide-Area Animal Tracking," in *2019 IEEE International Conference on Electrical, Computer and Communication Technologies (ICECCT)*, pp. 1–5.

[20] K. Mekki, E. Bajic, F. Chaxel, and F. Meyer, "A comparative study of LPWAN technologies for large-scale IoT deployment," vol. 5, no. 1, pp. 1–7. [Online]. Available: http://www.sciencedirect.com/science/article/pii/S2405959517302953

[21] Anicare website. [Online]. Available: https://anicare.fi/en/

[22] Cellular iot ear tag tracks health and location of farmed reindeer and other herding animals. [Online]. Available: https://www.nordicsemi.com/News/2019/04/Cellular-IoT-ear-tag-Healtag-tracks-health-and-location-of-herding-animals

[23] Cellular iot monitoring of valuable livestock can mean the difference between boom and bust. [Online]. Available: https://www.nordicsemi.com/News/2019/07/Following-the-herd

[24] Shiip website. [Online]. Available: https://www.shiip.no/

[25] Telespor website. [Online]. Available: https://telespor.no/

[26] Findmy website. [Online]. Available: https://www.findmy.no/

[27] Smartbjella product specification website. [Online]. Available: https://smartbjella.no/produkt/

[28] H. Bayram, N. Stefas, and V. Isler, "Aerial Radio-Based Telemetry for Tracking Wildlife," in *2018 IEEE/RSJ International Conference on Intelligent Robots and Systems (IROS)*, pp. 4723–4728.

[29] N. Bulusu, J. Heidemann, and D. Estrin, "GPS-less low-cost outdoor localization for very small devices," vol. 7, no. 5, pp. 28–34.

[30] A. Bhavsar and H. Arolkar, "ZigBee based network architecture for animal health monitoring," in *2015 1st International Conference on Next Generation Computing Technologies (NGCT)*, pp. 398–402.

[31] G. Scheepers, R. Malekian, D. C. Bogatinoska, and B. R. Stojkoska, "A low-power cost-effective flexible solar panel powered device for wireless livestock tracking," in *2017 25th Telecommunication Forum (FOR)*, pp. 1–4.

[32] H. M. A. Fahmy, *Wireless sensor networks*. Springer, 2020.

[33] I. F. Akyildiz, W. Su, Y. Sankarasubramaniam, and E. Cayirci, "Wireless sensor networks: A survey," vol. 38, no. 4, pp. 393–422. [Online]. Available: http://www.sciencedirect.com/science/article/pii/S1389128601003024

[34] R. N. Handcock, D. L. Swain, G. J. Bishop-Hurley, K. P. Patison, T. Wark, P. Valencia, P. Corke, and C. J. O'Neill, "Monitoring Animal Behaviour and Environmental Interactions Using Wireless Sensor Networks, GPS Collars and Satellite Remote Sensing," vol. 9, no. 5, pp. 3586–3603. [Online]. Available: https://www.mdpi.com/1424-8220/9/5/3586

[35] ITU. Nomenclature of the frequency and wavelength bands used in telecommunications. [Online]. Available: https://www.itu.int/rec/R-REC-V.431/en

[36] S. Rerucha, P. Jedlicka, J. Hrabina, M. Cizek, B. Mikel, O. Cip, T. Bartonicka, and R. Helan, "Miniaturized GPS position logger for tracking of small mammals," in *2017 6th Mediterranean Conference on Embedded Computing (MECO)*, pp. 1–4.

[37] K. Kaneda and T. Maeda, "Position Measurement System Using a Drone for Tsushima Leopard Cats," in *2018 IEEE 7th Global Conference on Consumer Electronics (GCCE)*, pp. 691–693.

[38] C. G. Muller, B. L. Chilvers, Z. Barker, K. P. Barnsdale, P. F. Battley, R. K. French, J. McCullough, and F. Samandari, "Aerial VHF tracking of wildlife using an unmanned aerial vehicle (UAV): Comparing efficiency of yellow-eyed penguin (Megadyptes antipodes) nest location methods," vol. 46, no. 2, pp. 145–153. [Online]. Available: https://www.publish.csiro.au/wr/WR17147

[39] A. Karki, "Radio direction finding using pseudo-Doppler for UAV-based Animal Tracking." [Online]. Available: https://scholarworks.gvsu.edu/theses/968

[40] K. VonEhr, S. Hilaski, B. E. Dunne, and J. Ward, "Software Defined Radio for direction-finding in UAV wildlife tracking," in *2016 IEEE International Conference on Electro Information Technology (EIT)*, pp. 0464–0469.

[41] K. Townsend, C. Cufí, A. Davidson, and R. Davidson, *Getting Started With Bluetooth Low Energy*. 1005 Gravenstein Highway North, Sebastpol, CA 95472: O'Reilly Media, Inc, 2015.

[42] "Bluetooth market update 2020," Bluetooth Special Interest Group, Kirkland, Washington, U.S., 2020.

[43] S. Rashed and M. Soyturk, "Analyzing the Effects of UAV Mobility Patterns on Data Collection in Wireless Sensor Networks," vol. 17, no. 2, p. 413. [Online]. Available: https://www.mdpi.com/1424-8220/17/2/413

[44] C. Zhan, Y. Zeng, and R. Zhang, "Energy-Efficient Data Collection in UAV Enabled Wireless Sensor Network," vol. 7, no. 3, pp. 328–331.

[45] J. Liu, X. Wang, B. Bai, and H. Dai, "Age-optimal trajectory planning for UAV-assisted data collection," in *IEEE INFOCOM 2018 - IEEE Conference on Computer Communications Workshops (INFOCOM WKSHPS)*, pp. 553–558.

[46] C. Downey. Understanding Wireless Range Calculations. [Online]. Available: https://www.electronicdesign.com/technologies/communications/article/21796484/understanding-wireless-range-calculations

[47] A. Goldsmith, *Wireless Communications*. USA: Cambridge University Press, 2005.

[48] *ZigBee Wireless Networks and Transceivers.* Elsevier. [Online]. Available: https://linkinghub.elsevier.com/retrieve/pii/B9780750683937X00015

[49] A. Saakian, *Radio Wave Propagation Fundamentals.* Artech House.

[50] W. L. Stutzman and G. A. Thiele, *Antenna Theory and Design.* John Wiley & Sons.

[51] Polarization of antennas. [Online]. Available: http://www.antenna-theory.com/basics/polarization.php

[52] B. Blog Admin. Circular and Linear Polarization. [Online]. Available: https://www.linksystems-uk.com/circular-linear-polarization/

[53] J. A. Shaw, "Radiometry and the Friis transmission equation," vol. 81, no. 1, pp. 33–37. [Online]. Available: https://aapt.scitation.org/doi/full/10.1119/1.4755780

[54] T.-I. Kvaksrud, "Range measurements in an open field environment," *Texas Instrum. Incorporated, Dallas, TX, Design Note DN018*, p. 12, 2008.

[55] M. Malajner, K. Benkic, P. Planinsic, and Z. Cucej, "The Accuracy of Propagation Models for Distance Measurement between WSN Nodes," in *2009 16th International Conference on Systems, Signals and Image Processing*, pp. 1–4.

[56] M. Viswanathan and V. Mathuranathan, *Wireless Communication Systems in Matlab: (Black & White Edition).* Independently Published. [Online]. Available: https://books.google.no/books?id=zry5uwEACAAJ

[57] J. J. Egli, "Radio Propagation above 40 MC over Irregular Terrain," vol. 45, no. 10, pp. 1383–1391.

[58] J. A. del Peral-Rosado, R. Raulefs, J. A. López-Salcedo, and G. Seco-Granados, "Survey of Cellular Mobile Radio Localization Methods: From 1G to 5G," vol. 20, no. 2, pp. 1124–1148, Secondquarter 2018.

[59] L. Jayashree, S. Arumugam, M. Anusha, and A. Hariny, "On the accuracy of centroid based multilateration procedure for location discovery in wireless sensor networks," in *2006 IFIP International Conference on Wireless and Optical Communications Networks*, pp. 6 pp.–6.

[60] J. C. Hamann, "Exploring the mathematics of multilateration," *Department of Electrical and Computer Engineering, University of Wyoming*, 2007.

[61] K. Yu, I. Sharp, and Y. J. Guo, *Ground-Based Wireless Positioning.* John Wiley & Sons.

[62] J. O. Roa, A. R. Jiménez, F. Seco, J. C. Prieto, and J. Ealo, "Optimal placement of sensors for trilateration: Regular lattices vs meta-heuristic solutions," in *Proceedings of the 11th International Conference on Computer Aided Systems Theory*, ser. EUROCAST'07. Springer-Verlag, pp. 780–787.

[63] G. Mao, B. Fidan, and B. D. O. Anderson, "Wireless sensor network localization techniques," vol. 51, no. 10, pp. 2529–2553, mSC2010: 68M10 = Network design and communication in computer systems. [Online]. Available: https://zbmath.org/?q=an%3A1120.68021

[64] *Bluetooth Core Specification*, Bluetooth Special Interest Group Std. 5.2, 2019.

[65] "nrf52840 product specification," Nordic Semiconductor ASA, 2018.

[66] Bluetooth 5 Advertising Extensions. [Online]. Available: https://blog.nordicsemi.com/getconnected/bluetooth-5-advertising-extensions

[67] Intro to Bluetooth Generic Access Profile (GAP). [Online]. Available: https://www.bluetooth.com/bluetooth-resources/intro-to-bluetooth-generic-access-profile-gap/

[68] M. Woolley. Exploring Bluetooth 5 -Going the Distance. [Online]. Available: https://www.bluetooth.com/blog/exploring-bluetooth-5-going-the-distance/

[69] C. Gu, L. Jiang, and R. Tan, "LoRa-Based Localization: Opportunities and Challenges." [Online]. Available: http://arxiv.org/abs/1812.11481

[70] "Designing a quarterwave printed monopole antenna for 2.45 ghz," White Paper, Nordic Semiconductor ASA, January 2005. [Online]. Available: https://infocenter.nordicsemi.com/pdf/nwp_008.pdf?cp=12_18

[71] "nrf52811 product specification," Nordic Semiconductor ASA, 2018.

[72] "nrf5 sdk v16.0.0 documentation," Nordic Semiconductor ASA, 2019.

[73] "S140 softdevice specification," Nordic Semiconductor ASA, 2019.

[74] O. A. H. Henrik Nyholm. System on sheep github repository - preliminary investigation. [Online]. Available: https://github.com/h3nrikoo/system_on_sheep/tree/master/measurements/initial_range_test

[75] Trondheim kommune - public map and geographic data of trondheim. [Online]. Available: https://www.trondheim.kommune.no/tema/bygg-kart-og-eiendom/

[76] "Fgpmmopa6h gps standalone module data sheet," GlobalTop Technology. [Online]. Available: https://datasheetspdf.com/pdf/900723/GlobalTop/FGPMMOPA6H/1

[77] O. A. H. Henrik Nyholm. System on sheep github repository - drone investigation. [Online]. Available: https://github.com/h3nrikoo/system_on_sheep/tree/master/measurements/drone_range_test

[78] J. Rhebergen, H. Lensen, P. Schwering, G. Marin, and J. Hendrickx, "Soil moisture distribution around land mines and the effect on relative permittivity," *Proc SPIE*, 08 2002.

[79] O. A. H. Henrik Nyholm. System on sheep github repository - rtt investigation. [Online]. Available: https://github.com/h3nrikoo/system_on_sheep/tree/master/measurements/rttr_measurements

[80] ——. System on sheep github repository - multilateration. [Online]. Available: https://github.com/h3nrikoo/system_on_sheep/tree/master/v2

[81] N. Semiconductor. Online power profiler for ble. [Online]. Available: https://devzone.nordicsemi.com/nordic/power/w/opp/2/online-power-profiler-for-ble

[82] "nrf52810 product specification," Nordic Semiconductor ASA, 2019.

[83] Cr3220 coin cell battery specifications. Panasonic. [Online]. Available: https://industrial.panasonic.com/ww/products/batteries/primary-batteries/lithium-batteries/models/CR2032

A | Preliminary Investigation

Test set-up

Figure A.1: Photograph of the tripod test setup.

Map data

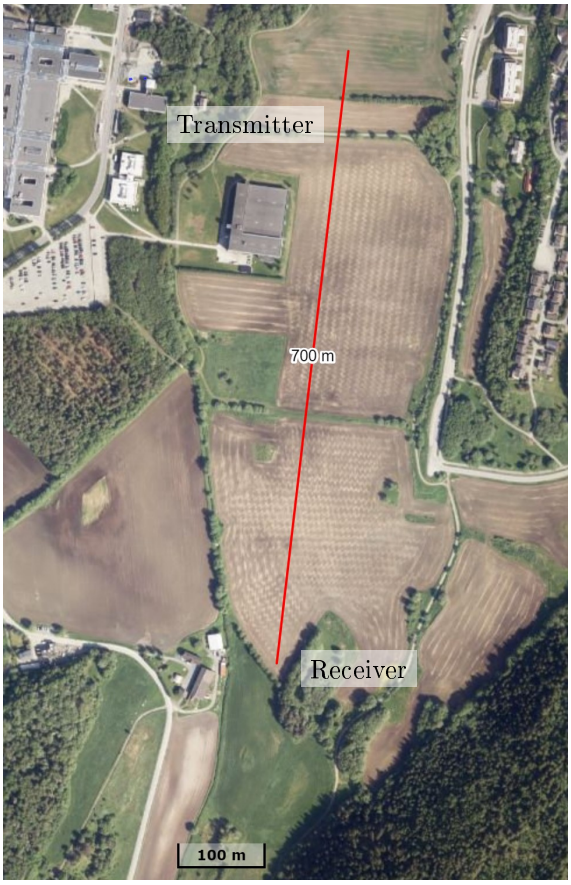

Figure A.2: Aerial photograph of the field used in the initial investigation measurements for the first 100 m to 600 m. Map and geographic data provided by [75].

Results

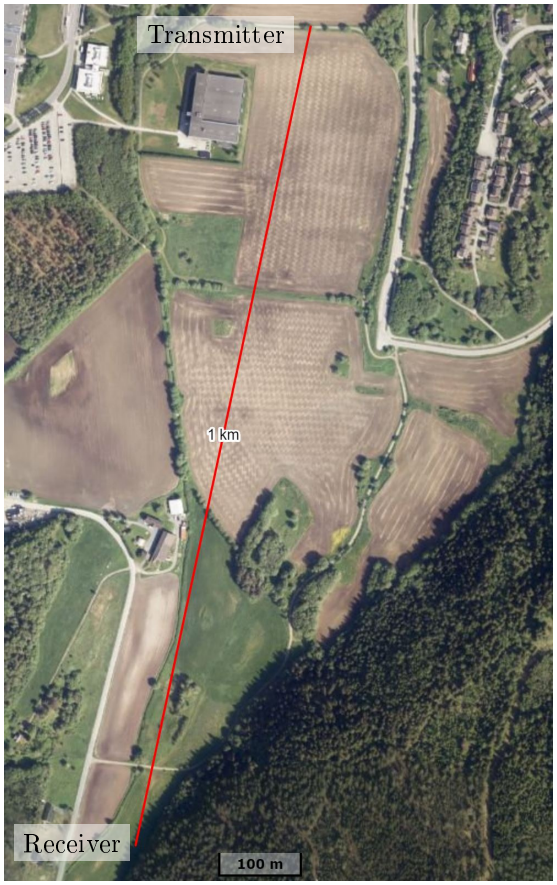

Figure A.3: Aerial photograph of the field used in the initial investigation measurements for the last 700 m to 1000 m. Map and geographic data provided by [75].

Figure A.4: Photograph of the field where the initial investigations were conducted at Dragvoll, Trondheim.

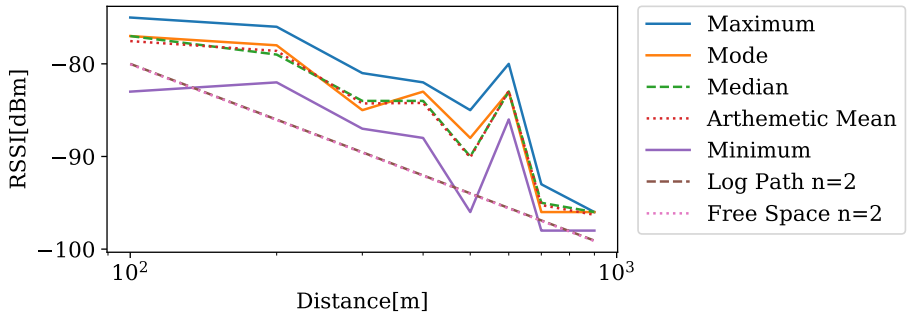

Figure A.5: Measured RSSI values at each distance for each angle with a height of 200 cm and $P_t = 0$ dBm versus the free space and log distance propagation models using attenuation constant $n = 2$.

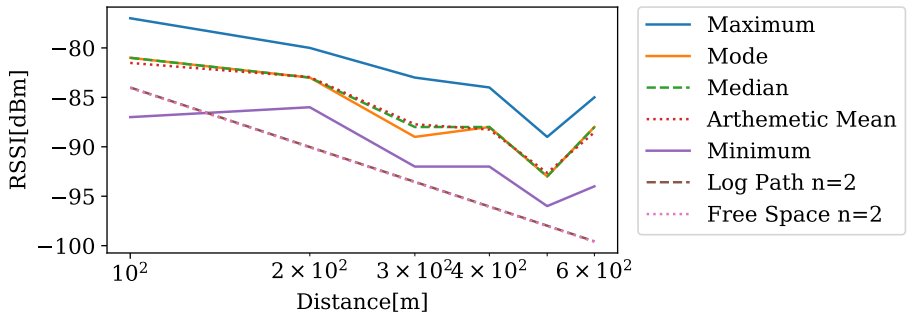

Figure A.6: Measured RSSI values at each distance for each angle with a height of 200 cm and $P_t = -4$ dBm versus the free space and log distance propagation models using attenuation constant $n = 2$.

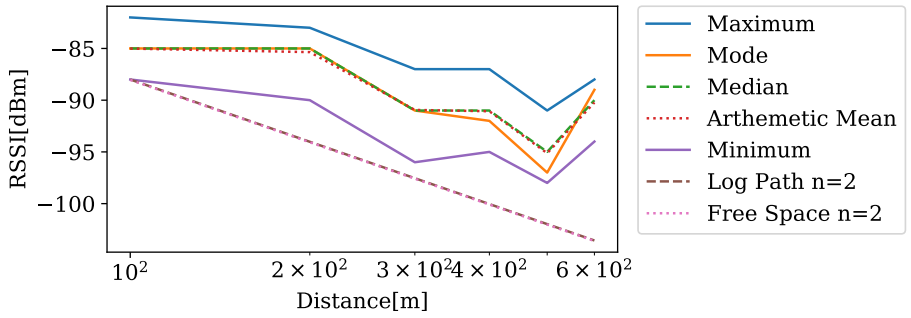

Figure A.7: Measured RSSI values at each distance for each angle with a height of 200 cm and $P_t = -8$ dBm versus the free space and log distance propagation models using attenuation constant $n = 2$.

B | Aerial Investigation

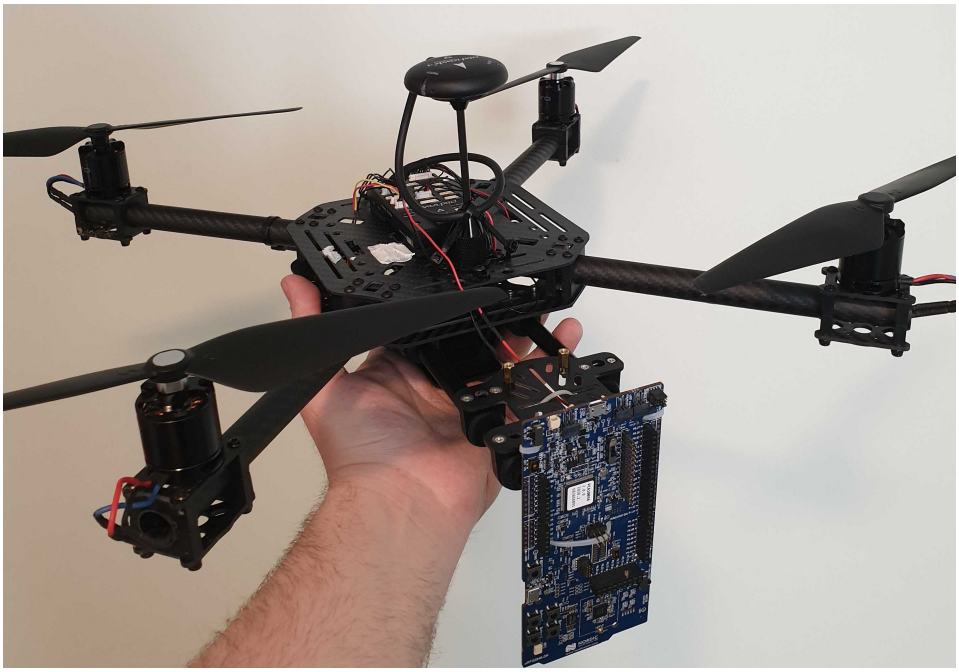

Figure B.1: Photograph of the quadcopter drone used in the experiments. The picture also show how the central device was equipped as the payload of the UAV.

Figure B.2: Photograph showing the circularly polarized cloverleaf antenna used as the receiving antenna on the UAV.

Figure B.3: Photograph showing the circularly polarized cloverleaf antenna connected to the central device and mounted on the quadcopter drone.

C | Multilateration

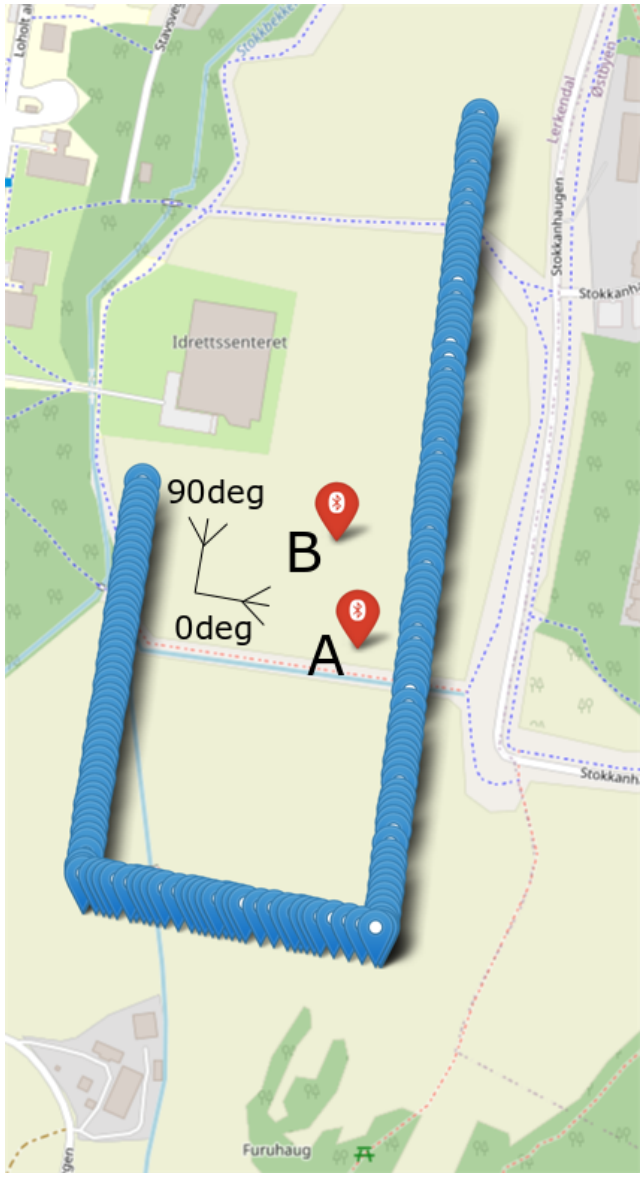

Figure C.1: Drone path in the multilateration investigation and the two locations tested A (bottom right) and B (upper left) marked in red.

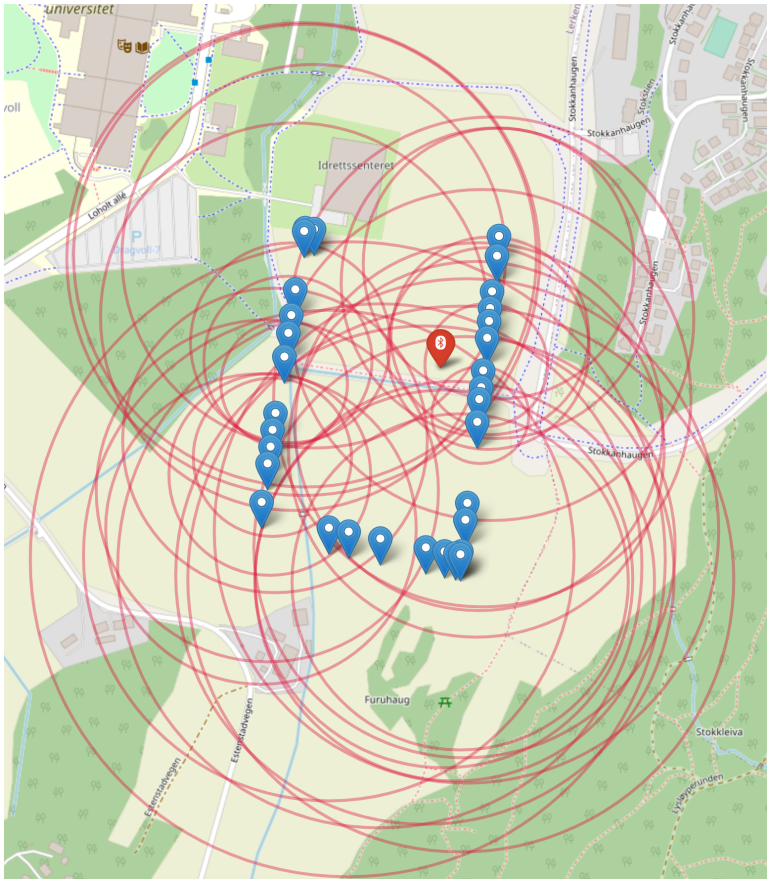

Figure C.2: Multilateration using RSSI-based distance measurement for test number 1.

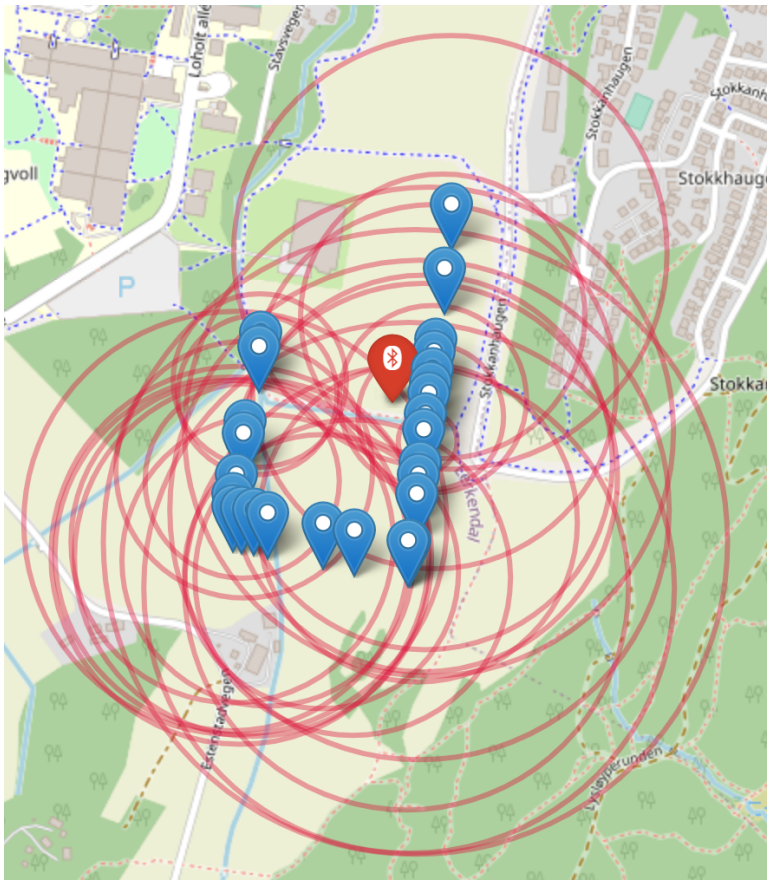

Figure C.3: Multilateration using RSSI-based distance measurement for test number 2.

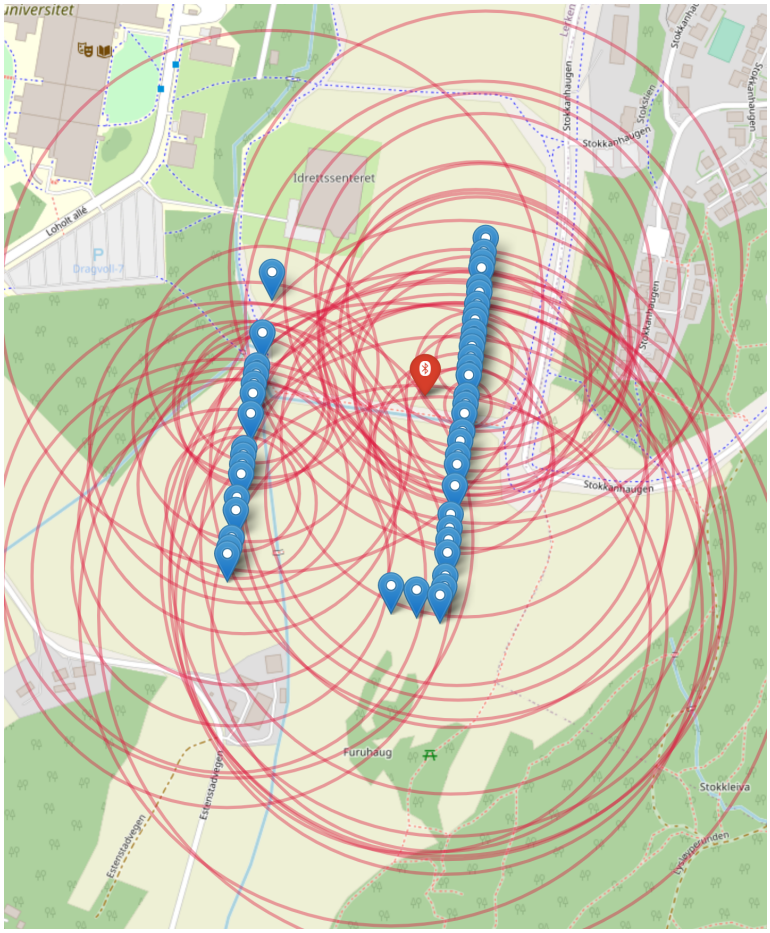

Figure C.4: Multilateration using RSSI-based distance measurement for test number 3.

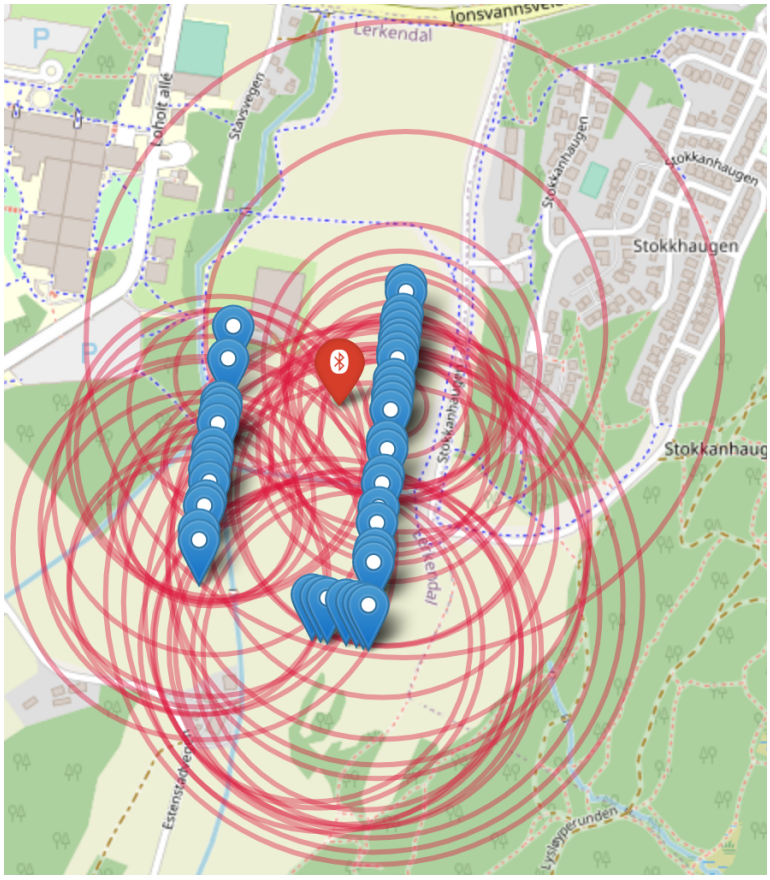

Figure C.5: Multilateration using RSSI-based distance measurement for test number 4.

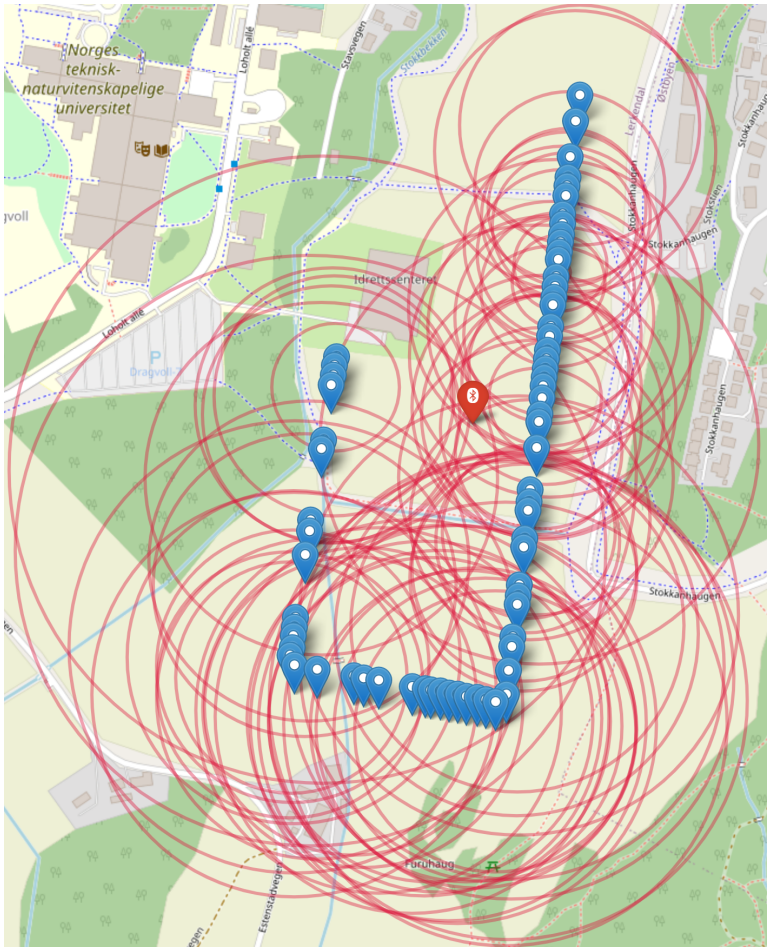

Figure C.6: Multilateration using RSSI-based distance measurement for test number 5.

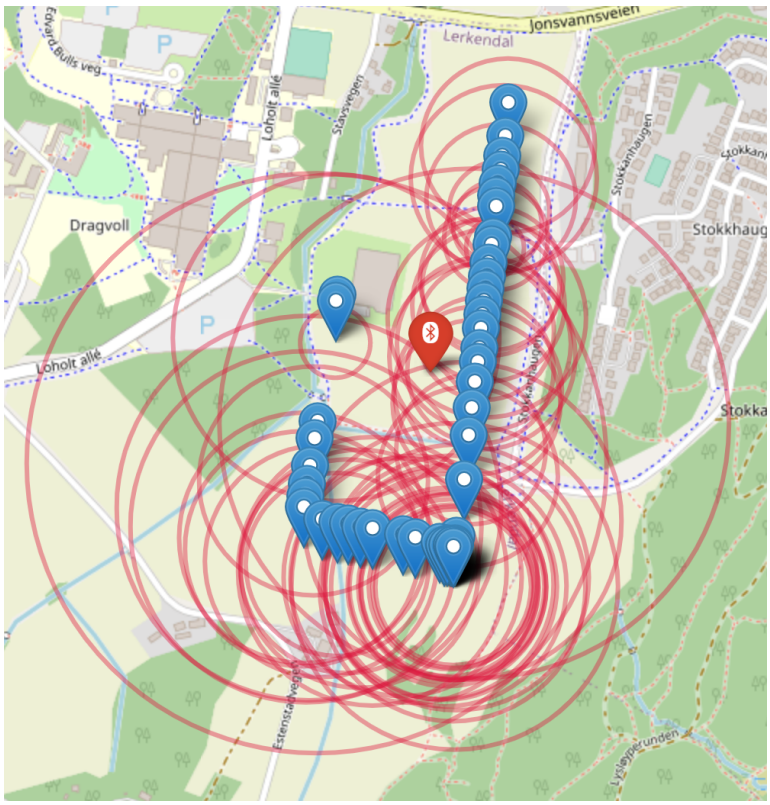

Figure C.7: Multilateration using RSSI-based distance measurement for test number 6.

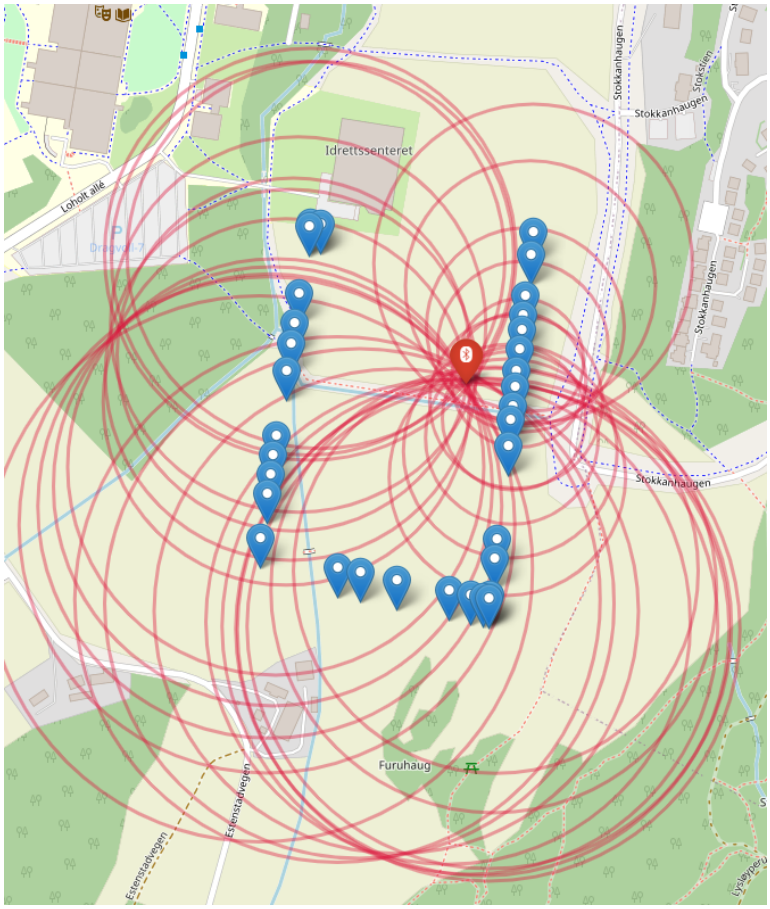

Figure C.8: Multilateration using RTT-based distance measurement for test number 1.

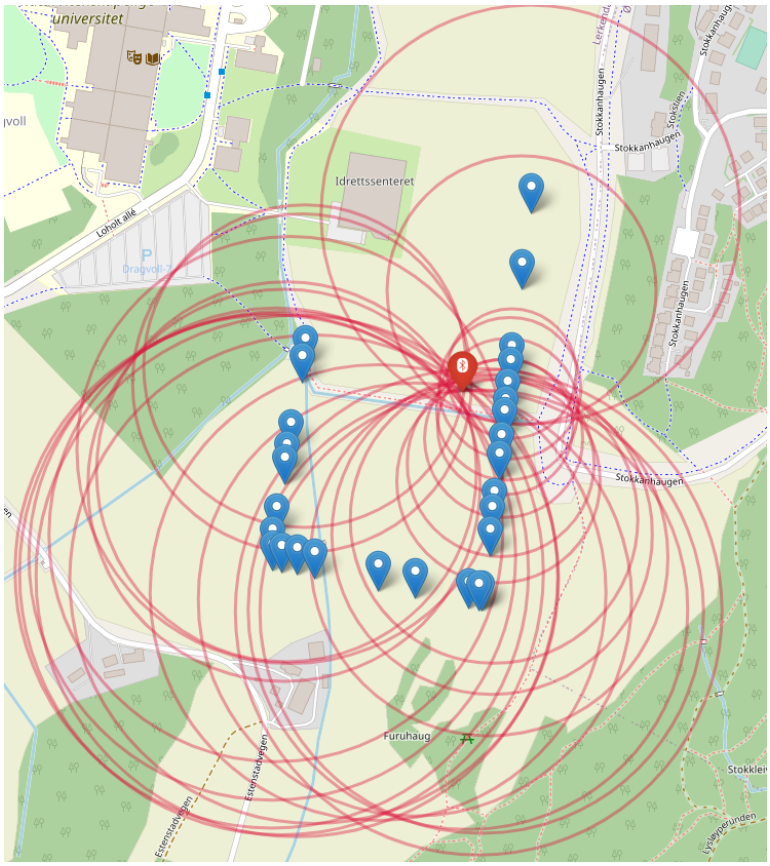

Figure C.9: Multilateration using RTT-based distance measurement for test number 2.

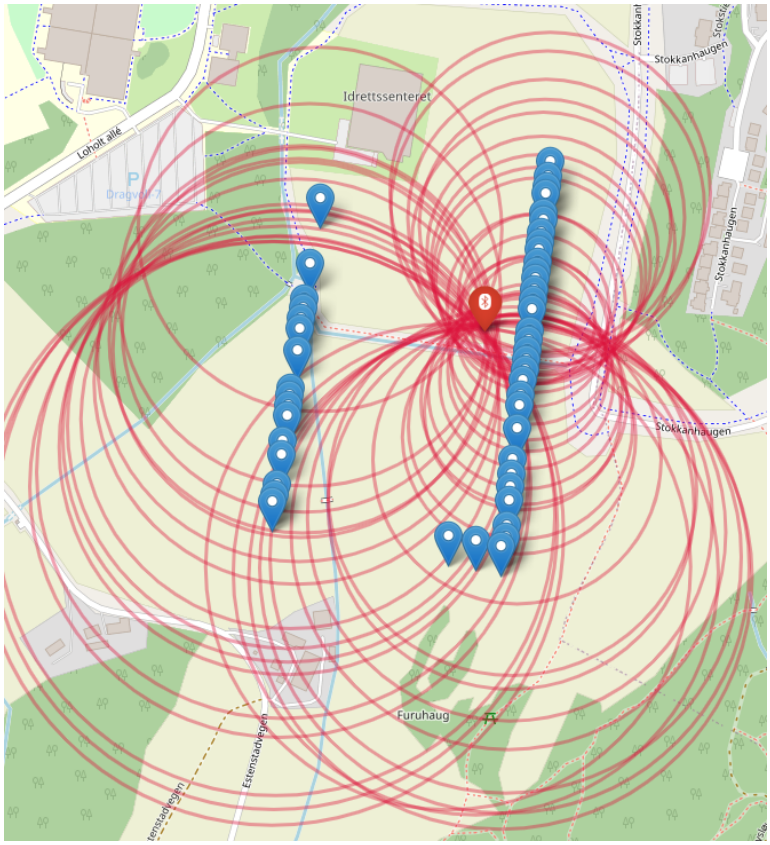

Figure C.10: Multilateration using RTT-based distance measurement for test number 3.

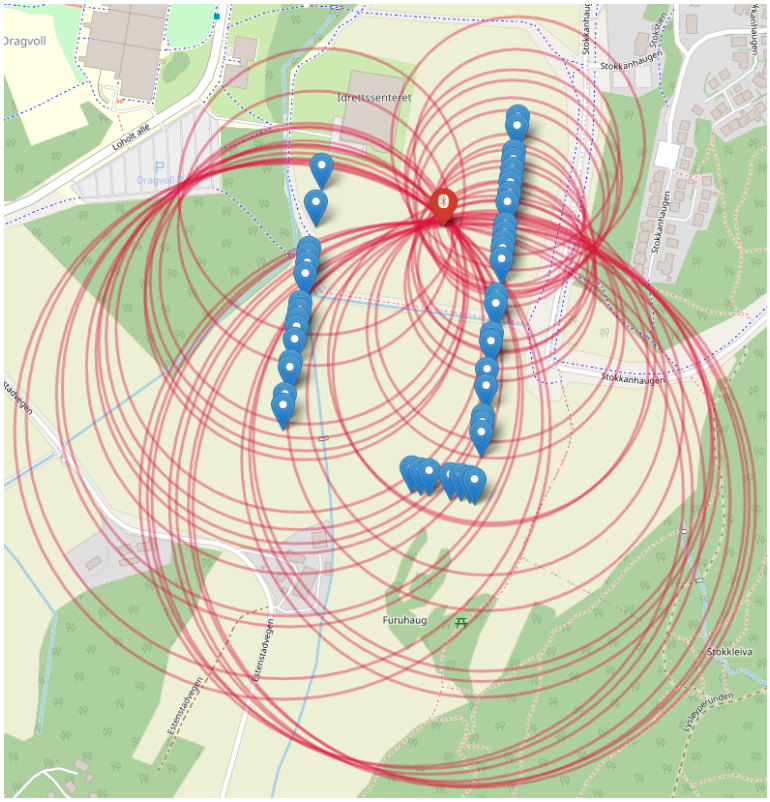

Figure C.11: Multilateration using RTT-based distance measurement for test number 4.

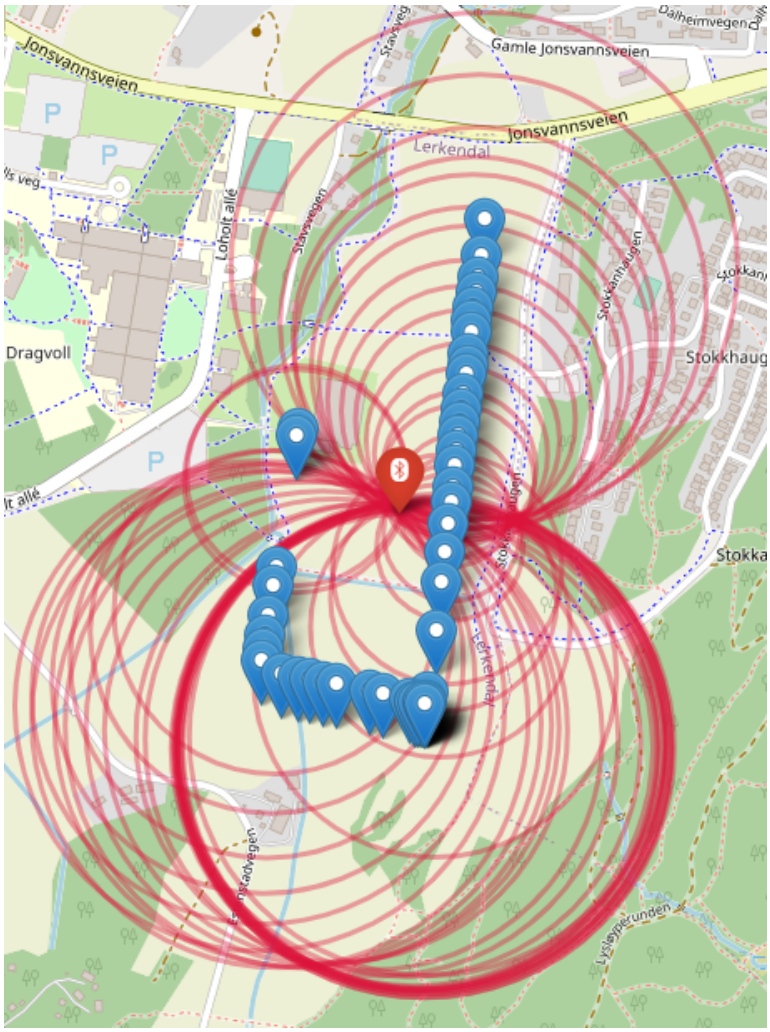

Figure C.12: Multilateration using RTT-based distance measurement for test number 6.